Karlsruhe Institute of Technology

Institute of Mechanics

Prof. Dr.-Ing. habil. Peter Betsch
Prof. Dr.-Ing. habil. Thomas Seelig

BACHELOR THESIS

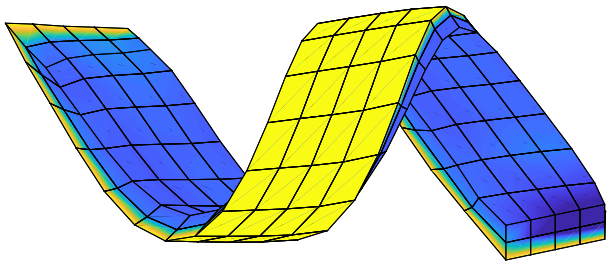

Theory and Numerical Methods for Transversely Isotropic Materials in Large Strain Electromechanics

Philipp Lothar Kinon

December 2017, Karlsruhe

First examiner: Prof. Dr.-Ing. habil. Peter Betsch
Supervisors: Dr.-Ing. Marlon Franke,
M. Sc. Alexander Janz

Karlsruher Institut für Technologie

Institut für Mechanik
Prof. Dr.-Ing. habil. Peter Betsch
Prof. Dr.-Ing. habil. Thomas Seelig

Bachelorarbeit:
„Theorie und Numerik transversal isotropen Materials für elektromechanische Probleme unter großen Deformationen“

‘Theory and Numerical Methods for Transversely Isotropic Materials in Large Strain Electromechanics’

Im Rahmen dieser Bachelor-Arbeit soll die numerische Simulation von elektromechanisch gekoppelten Randwertproblemen (RWP) untersucht werden. Mit elektromechanisch gekoppelten RWPen können z.B. elektroaktive Polymeren (EAP) modelliert werden (siehe z.B. [1, 2, 3]). Mit EAPen, welche Gegenstand aktueller Forschung in der Biomechanik sind, können Muskeln nachgebildet werden so dass Roboter mit diesen künstlichen Muskeln ausgestattet werden können. Muskeln wiederum können als faserartiges, anisotropes Material modelliert werden. Für die Modellierung soll von einem polykonvexen Ansatz nach [4, 5, 2, 3] ausgegangen werden. Die anschließende numerische Modellierung soll mit Hilfe der finiten Elemente Methode umgesetzt werden. Neben der numerischen Modellierung stehen auch konkrete numerische Simulationen sowie Benchmark-Beispiele im Fokus der Arbeit. Im Rahmen der Bachelorarbeit ist die Einarbeitung geplant in

1) die nichtlineare Kontinuumsmechanik und FEM nach [6, 7] sowie in den vom Institut bereitgestellten Forschungscode *esra*,
2) die rein mechanische polykonvexe Formulierungen unter Verwendung des äußeren Tensorprodukts nach [5, 8],
3) die polykonvexe elektromechanisch gekoppelte, statische Formulierung nach [2, 3],
4) sowie die polykonvex basierte symmetrische 3-Feld Formulierung nach [9].

Die polykonvex basierte symmetrische 3-Feld Formulierung in Punkt 4) bietet die Basis für die Bachelorarbeit und soll ausführlich dokumentiert werden. Auf dieser Grundlage ist dann die Modellierung von anistropen EAPen möglich. Konkret soll ein transversal-isotropes Materialgesetz implementiert werden. Das numerische Modell soll in zahlreichen Beispielen untersucht werden. Die Ergebnisse der Arbeit sollen in LaTeX dokumentiert werden.

Voraussetzungen

Kontinuumsmechanik, Finite-Elemente-Methode, Programmierkenntnisse in *MATLAB*.

Ansprechpartner

Alexander Janz (alexander.janz@kit.edu) und Marlon Franke (marlon.franke@kit.edu)

Bearbeiter
Name: Philipp Kinon
Matr.-Nr.: 1801150

Termine
Ausgabedatum: 16.10.2017
Soll-Abgabedatum: 16.01.2018
Ist-Abgabedatum:
Vortrag gehalten am:

Literatur

[1] T. Schlögl and S. Leyendecker. Electrostatic-viscoelastic finite element model of dielectric actuators. *Computer Methods in Applied Mechanics and Engineering*, 299:421 – 439, 2016.

[2] Rogelio Ortigosa and Antonio J. Gil. A new framework for large strain electromechanics based on convex multi-variable strain energies: Finite element discretisation and computational implementation. *Computer Methods in Applied Mechanics and Engineering*, 302:329 – 360, 2016.

[3] Antonio J. Gil and Rogelio Ortigosa. A new framework for large strain electromechanics based on convex multi-variable strain energies: Variational formulation and material characterisation. *Computer Methods in Applied Mechanics and Engineering*, 302:293 – 328, 2016.

[4] J. Bonet, A.J. Gil, and R. Ortigosa. On a tensor cross product based formulation of large strain solid mechanics. *Int. J. Solids Structures*, 84:49–63, 2016.

[5] J. Bonet, A. Gil, and R. Ortigosa. A computational framework for polyconvex large strain elasticity. *Comput. Methods Appl. Mech. Engrg.*, 283:1061–1094, 2015.

[6] GA Holzapfel. *Nonlinear solid mechanics. A continuum approach for engineering*. John Wiley & Sons, Ltd, 2000.

[7] P. Wriggers. *Nichtlineare Finite-Element-Methoden*. Springer-Verlag, 2001.

[8] P. Betsch, A. Janz, and C. Hesch. A mixed variational framework for the design of energy-momentum schemes relying on polyconvex stored energy functions. *Submitted for publication in Comput. Methods Appl. Mech. Engrg.*, 2017.

[9] R. Ortigosa. Report on Energy-momentum preserving time integrators in elasto-dynamics. *Report*, 2017.

Preface

This thesis would not have been possible without all those who supported me professionally and personally.

First of all, I would like to show my gratitude to Dr.-Ing. Marlon Franke and M.Sc. Alexander Janz for supervising this work with all their knowledge and experience. I owe my gratitude especially to Mr. Janz, who engaged me as a student assistant two years ago and guided me ever since. It is a pleasure to thank Prof. Dr.-Ing. Thomas Seelig to arouse my interest in mechanics and to encourage me to maintain this study programme after the second semester. Moreover, it is an honour to thank Prof. Dr.-Ing. Peter Betsch, who gave me an understanding of finite element methods throughout his lectures in the previous year. Furthermore, I would like to thank Johanna Ruge, my former office neighbour, for her suggestions and proofreading this thesis.

Most notably, I am eminently grateful for the relentless support by Lorena Krames. Eventually, I would like to show my gratitude to my parents Regina Mannheim and Lothar Kinon.

Declaration of Authorship

I hereby declare that the thesis submitted is my own unaided work. All direct or indirect sources used are acknowledged as references.

I am aware that the thesis in digital form can be examined for the use of unauthorised aid and in order to determine whether the thesis as a whole or parts incorporated in it may be deemed as plagiarism. For the comparison of my work with existing sources I agree that it shall be entered in a database where it shall also remain after examination, to enable comparison with future theses submitted. Further rights of reproduction and usage, however, are not granted here. This paper was not previously presented to another examination board and has not been published.

Furthermore I ensure that I considered the *'Regeln zur Sicherung guter wissenschaftlicher Praxis im Karlsruher Institut für Technologie (KIT)'* in their legal version.

Eidesstattliche Erklärung

Ich erkläre hiermit an Eides statt, dass ich die vorliegende Arbeit selbstständig angefertigt habe. Die aus fremden Quellen direkt und indirekt übernommenen Inhalte sind als solche kenntlich gemacht.

Ich weiß, dass die Arbeit in digitalisierter Form daraufhin überprüft werden kann, ob unerlaubte Hilfsmittel verwendet wurden und ob es sich insgesamt oder in Teilen um ein Plagiat handelt. Zum Vergleich meiner Arbeit mit existierenden Quellen darf sie in eine Datenbank eingestellt werden und nach der Überprüfung zum Vergleich mit künftig eingehenden Arbeiten dort verbleiben. Weitere Vervielfältigungs und Verwertungsrechte werden dadurch nicht eingeräumt. Die Arbeit wurde weder einer anderen Prüfungsbehörde vorgelegt noch veröffentlicht.

Darüber hinaus versichere ich, dass ich die *„Regeln zur Sicherung guter wissenschaftlicher Praxis im Karlsruher Institut für Technologie (KIT)"* in der gültigen Fassung beachtet habe.

December 21, 2017

Contents

1 Introduction and Motivation

In the past few years, there has been a spate of interest in multiphysical enhancements in the field of computational mechanics. Multiple other quantities from physical disciplines which effect the mechanical behaviour of solid bodies has been included into the theories such as thermal fields (see, e.g. [FJSB]) , the phase field (see, e.g. [HGO+17] or acoustic influences. Particularly electromechanical investigations have been carried out as of late (see e.g. [DO05, VSP07, BDO09, OFJ+]), as they require the numerical solution techniques to be even more stable and robust, due to the large scale of the order of magnitude of the regarded variables. Furthermore, numerical models are crucial in order to understand and to make reliable predictions about the behaviour of electroactive polymers (EAPs), which are considered in most cases. These kind of polymers react to applied electric fields with deformation and do not have insulating properties as common plastics do. Unlike piezoelectric metals, these types of plastics act hyperelastically, so that a nonlinear description is urgently necessary.

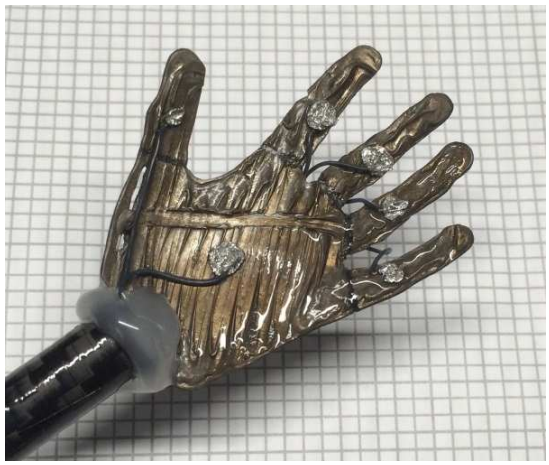

Figure 1: 3D printed hand model using artificial muscle structures made of EAPs, found in [www16]

Combined with metallic electrodes, that prescribe electric fields caused by their inherited electric charges, such EAPs can easily be controlled via the voltage applied on the electrodes. On that account, electric charges within the molecules polarise which leads to stresses within the material. Most often, these systems are implemented using a sandwich structure consisting of two capacitor plates and the dielectric in between ([SL16], see also Figure 2). Hence, this actuator can be compressed or elongated respectively. One further possible purpose is the construction of artificial muscles in the field of robotics, as this new actuation technique achieves higher efficiencies than its mechanical or pneumatic counterparts ([SL16]). Moreover, the capabilities to perform are broadend as these muscle structures are able to perform bending procedures and thereby move multidimensionally.

As the technical realisation of EAPs has not been investigated in its entirety, pioneering is contemporarily happening. Supported by novel 3D-printing techniques researchers succeeded in creating a replica of the human hand, which is able to imitate the natural motion patterns such as grasping, due to the integration of thin electrodes to prescribe electric fields (see Figure 1).

Furthermore, as muscles are fibroid structures they represent a material, which is highly anisotropic. Due to the direction of its fibres, it is crucial to model the material behaviour as transversely isotropic in order to achieve similarity to the biological tissues. This provides advantages concerning the energy-efficiency of the actuators as well, as desired deformations can be amplified without enlarging external influences. The impact of fibre reinforcement on the electroactuation of EAPs has been lately investigated by [SSG17]. However, the previous works in compuatational electromechanics either fail to take account of anisotropic material properties (see, e.g. [SL16]) in spite of their aim to describe artificial muscle models or the respective models are implemented and used without investigating the effects in more detail (as in [SWB11, OG16]).

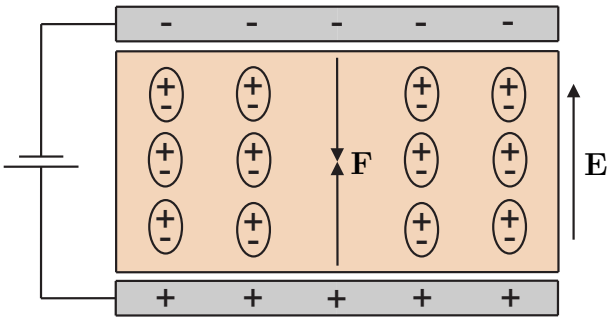

Figure 2: Scheme of a dieletric actuator

Hence, this thesis attempts to fill this gap by including the theory of transversal isotropy into the framework of electromechanics. To solve the resulting boundary value problems (BVPs) the finite element method (FEM) is employed. Thus, an existing element routine of the finite element research code *'ESRA'* is extended with the transversely isotropic material model presented in [SWB11]. *ESRA* was developed at the Institute of Mechanics (Karlsruhe Institute of Technology (KIT)) and the Chair of Computational Mechanics (University of Siegen) and is implemented in the environment of *MATLAB*®.

Initially, nonlinear continuum mechanics is being considered and its fundamentals are presented in Chapter 2. A new formulation, already presented in [BJH17], introduces a cascade-like structure which takes account of the tensor cross product for the definition of the strain quantities. At this point the basic electric field theory is presented as well. In

Chapter 3 material models are considered which are given by the so-called strain energy functions that thereby profit from the tensor cross product formulation due to the concept of polyconvexity. In Chapter 4 the resulting BVP is presented in differential and weak form, respectively. Corresponding variational principles are introduced and are based on a three-field formulation. The FEM - together with related mathematical methods - is carried out in Chapter 4.3. The newly gained finite element (FE) formulation makes it furthermore possible to conduct specific examples in Chapter 5. The computational results are presented and evaluated with respect to specific consequences of the transversely isotropic model extension. Finally, conclusional remarks are given in Chapter 6.

2 Basics and Fundamentals

2.1 Continuum Mechanics for Large Deformations

The following preliminary fundamentals of continuum mechanics are essential to work with the subsequent variational principles used to simulate electromechanically coupled problems. These descriptions are mainly taken from the well written work [Hol00] and have already been pointed out in several other works before. Initially, the kinematic relations are described. Herein, a strict distinction between reference and current configuration is essential. Hence, nonlinear strain measures and on therefore also nonlinear stress quantities are introduced. Eventually, conservation principles need to be considered in order to derive formulations of the mechanical BVP.

2.1.1 Kinematics

Let us consider a three dimensional continuum body which is comprised of an amount of particles before and after a specific motion. The whole domain of the continuum is denoted as $\mathcal{B}_0$ in the so-called reference configuration and $\mathcal{B}$ in the current configuration. The boundaries of the continuum are referred to as $\partial\mathcal{B}$ and $\partial\mathcal{B}_0$ respectively. We describe both states with individual coordinates, such as the material coordinates $\mathbf{X} = X_A\mathbf{E}_A$ with respect to the reference configuration ('Lagrangian description') and the spatial coordinates $\mathbf{x}_a = x_a\mathbf{e}_a$ with respect to the current configuration ('Eulerian description'). Thereby the body's motion can be described as a mapping in the form of

$$\mathbf{x} = \boldsymbol{\varphi}(\mathbf{X}) \tag{2.1}$$

Because of large deformations the two configurations do not coincide as it is assumed in the linear theory. Moreover, in the present work most quantities are written in dependence of material coordinates. Furthermore, the displacements of each point in material coordinates are given as

$$\mathbf{U}(\mathbf{X}) = \boldsymbol{\varphi}(\mathbf{X}) - \mathbf{X} \tag{2.2}$$

Both, the position vectors and the displacement field can be expressed in Cartesian coordinates within the right-handed orthonormal coordinate system which applies both for material and spatial coordinates ($\mathbf{e}_a = \mathbf{E}_A$), described by its basis vectors $\mathbf{e}_1$, $\mathbf{e}_2$ and $\mathbf{e}_3$ as

$$\mathbf{X} = X_1\,\mathbf{E}_1 + X_2\,\mathbf{E}_2 + X_3\,\mathbf{E}_3 = X_A\mathbf{E}_A \tag{2.3}$$

$$\mathbf{U} = U_1\,\mathbf{E}_1 + U_2\,\mathbf{E}_2 + U_3\,\mathbf{E}_3 = U_A\mathbf{E}_A \tag{2.4}$$

The scalars X_A and U_A herein denote the vector's component of the corresponding unit

vector. Note that the above relation make use of the Einstein notation which applies throughout the entire thesis.

If we now want to characterize the deformation of the body we need to introduce strain measures, which transform infinitesimal elements, e.g. lines, areas and volumes, from the reference to the current configuration. We achieve that by employing a Taylor series expansion of $\boldsymbol{\varphi}$ at a point $\mathbf{X}_0$ as

$$\boldsymbol{\varphi}(\mathbf{X}_0 + \mathrm{d}\mathbf{X}) = \boldsymbol{\varphi}(\mathbf{X}_0) + \frac{\partial \boldsymbol{\varphi}}{\partial \mathbf{X}}(\mathbf{X}_0) \cdot \mathrm{d}\mathbf{X} + \mathcal{O}(\mathrm{d}\mathbf{X}^2) \tag{2.5}$$

By neglecting higher order terms the deformation gradient is obtained as

$$\mathrm{d}\mathbf{x} = \mathbf{F}(\mathbf{X})\,\mathrm{d}\mathbf{X} \tag{2.6}$$

which is a quantity of deformation for infinitesimal line elements $\mathrm{d}\mathbf{x}$ and $\mathrm{d}\mathbf{X}$. This partial derivative with respect to the material coordinates can be expressed in serveral ways as

$$\mathbf{F}(\mathbf{X}) = \mathrm{D}\boldsymbol{\varphi}(\mathbf{X}) = \frac{\partial \boldsymbol{\varphi}(\mathbf{X})}{\partial \mathbf{X}} \tag{2.7}$$

where the Gateaux operator $\mathrm{D}(\bullet)$ is defined as the partial derivative with respect to the only argument. A general definition of the gradient $\partial/\partial\mathbf{X}$ can be found in (A.2). On that account the deformation gradient can be recasted as

$$\mathbf{F}(\mathbf{X}) = \mathrm{Grad}(\boldsymbol{\varphi}) = \frac{\partial x_a}{\partial X_A}\mathbf{e}_a \otimes \mathbf{e}_A \tag{2.8}$$

As it can be easily seen the deformation gradient is a tensor of order two which contains material as well as spatial coordinates and is thereby a two-point tensor that is in general not symmetric and accordingly has nine independent components F_{aA}. The mathematically aesthetical taylor series approach has been nicely presented in [Fra14] and [Rug17].

Mapping infinitesimal volume elements $\mathrm{d}\upsilon$, which can be described by their corresponding line elements $\mathrm{d}\mathbf{x}_1$,$\mathrm{d}\mathbf{x}_2$ and $\mathrm{d}\mathbf{x}_3$, is achieved using the determinant of the deformation gradient. It is called the Jacobi determinant or Jacobian $J(\mathbf{X})$

$$\mathrm{d}\upsilon = (\mathrm{d}\mathbf{x}_1 \times \mathrm{d}\mathbf{x}_2) \cdot \mathrm{d}\mathbf{x}_3 = \det(\mathbf{F}(\mathbf{X}))\,\mathrm{d}V = J(\mathbf{X})\,\mathrm{d}V \tag{2.9}$$

Eventually, infinitesimal oriented area elements $\mathrm{d}\mathbf{a}$ transform as follows

$$\mathrm{d}\mathbf{a} = \mathrm{d}\mathbf{x}_1 \times \mathrm{d}\mathbf{x}_2 = J(\mathbf{X})\,\mathbf{F}(\mathbf{X})^{-\mathrm{T}}\,\mathrm{d}\mathbf{A} = \mathbf{H}(\mathbf{X})\,\mathrm{d}\mathbf{A} \tag{2.10}$$

The last equation is often referred to as "Nanson's formula" and makes use of the so-called

cofactor of the deformation gradient:

$$\mathbf{H} = \mathrm{cof}(\mathbf{F}) = \det(\mathbf{F})\,\mathbf{F}^{-\mathrm{T}} \tag{2.11}$$

For the sake of readability, the dependence of $\mathbf{X}$ was omitted. As far as not mentioned differently, this will have to be taken into account in the rest of this thesis. A concise depiction of the deformation mapping can be found in Figure 3.

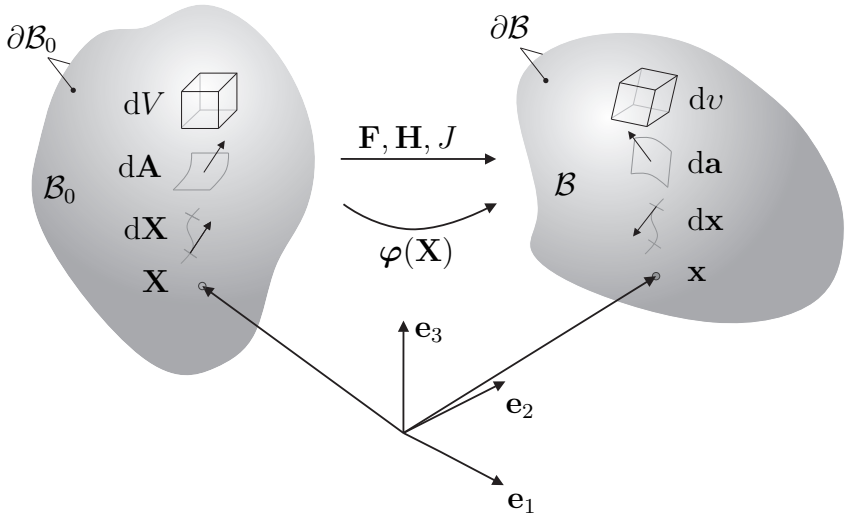

Figure 3: Deformation mapping of a continuum

2.1.2 Symmetric Strain Measures

There are several other strain measures that can be found in the literature. For the purpose of this work it is helpful to use symmetric strain tensors, such as the right Cauchy-Green strain tensor

$$\mathbf{C} = \mathbf{F}^{\mathrm{T}}\mathbf{F} = (\mathbf{F}^{\mathrm{T}}\mathbf{F})^{\mathrm{T}} = \mathbf{C}^{\mathrm{T}} \tag{2.12}$$

or the Green-Lagrange strain tensor

$$\mathbf{E} = \frac{1}{2}\left(\mathbf{F}^{\mathrm{T}}\mathbf{F} - \mathbf{I}\right) = \frac{1}{2}\left(\mathbf{C} - \mathbf{I}\right) = \mathbf{E}^{\mathrm{T}} \tag{2.13}$$

In the last equation $\mathbf{I}$ denotes the second order unit tensor. These symmetric strain measures quantify the change of squared lengths and possess just six independent components C_{AB} and E_{AB}.

Instead of using $\mathbf{F}, \mathbf{H}$ and J for describing the deformation of a flexible body one can now benefit from the knowledge of the right Cauchy-Green strain tensor and use its

determinant and cofactor

$$\mathbf{G} = \operatorname{cof}(\mathbf{C}) = \det(C)\,\mathbf{C}^{-\mathrm{T}} = \mathbf{H}^{\mathrm{T}}\,\mathbf{H} \tag{2.14}$$

$$C = \det(\mathbf{C}) = J^2 \tag{2.15}$$

The tensor cross product has been introduced by [dB82] and was used in the context of continuum mechanics for the first time by [BGO16]. It has been marvellously explained in [BJH17]. The tensor cross product between two tensors of order two $\mathbf{A}$ and $\mathbf{B}$ can be computed via

$$(\mathbf{A}\boldsymbol{\diamond}\mathbf{B})_{ij} = \varepsilon_{i\alpha\beta}\,\varepsilon_{jab}\,(\mathbf{A})_{\alpha a}\,(\mathbf{B})_{\beta b} \tag{2.16}$$

where ε_{ijk} denotes the well-known permutation symbol. By making use of the tensor cross product the cofactor and determinant of a tensor can be reexpressed. A cascade formulation is achieved, which facilitates later computations with

$$\mathbf{H} = \frac{1}{2}\,\mathbf{F}\boldsymbol{\diamond}\mathbf{F} \tag{2.17}$$

$$J = \frac{1}{3}\,\mathbf{H} : \mathbf{F} = \frac{1}{6}\,(\mathbf{F}\boldsymbol{\diamond}\mathbf{F}) : \mathbf{F} \tag{2.18}$$

and

$$\mathbf{G} = \frac{1}{2}\,\mathbf{C}\boldsymbol{\diamond}\mathbf{C} \tag{2.19}$$

$$C = \frac{1}{3}\,\mathbf{G} : \mathbf{C} = \frac{1}{6}\,(\mathbf{C}\boldsymbol{\diamond}\mathbf{C}) : \mathbf{C} \tag{2.20}$$

The tremendous analogy between the geometrical and kinematical structure can be seen and is given in the following Table:

geometric elements	non-symmetric kinematics	symmetric kinematics
$\mathrm{d}\mathbf{x}$	$\mathbf{F}$	$\mathbf{C}$
$\mathrm{d}\mathbf{a} = \mathrm{d}\mathbf{x}_1 \times \mathrm{d}\mathbf{x}_2$	$\mathbf{H} = \frac{1}{2}\,\mathbf{F}\boldsymbol{\diamond}\mathbf{F}$	$\mathbf{G} = \frac{1}{2}\,\mathbf{C}\boldsymbol{\diamond}\mathbf{C}$
$\mathrm{d}v = (\mathrm{d}\mathbf{x}_1 \times \mathrm{d}\mathbf{x}_2) \cdot \mathrm{d}\mathbf{x}_3$	$J = \frac{1}{6}\,(\mathbf{F}\boldsymbol{\diamond}\mathbf{F}) : \mathbf{F}$	$C = \frac{1}{6}\,(\mathbf{C}\boldsymbol{\diamond}\mathbf{C}) : \mathbf{C}$

Table 1: Analogy of geometric elements and the corresponding symmetric strain measures

2.1.3 Concept of Stress

Deformations as they can be described now, give always rise to interactions inside a continuum. These interactions cause stress, which has the physical dimension of force per unit of area. There exist multiple stress values, that have been introduced over time. A fine overview has been presented in [Hol00] and will be the basis of this section.

Let us consider an arbitrary incremental area element ΔA inside a continuum body that is subjected to a force increment. Hence, a traction vector in the Eulerian description $\mathbf{t}$ to describe stress is defined via Cauchy's postulate ([GHW11]) as

$$\mathbf{t} = \lim_{\Delta A \to 0} \frac{\Delta \mathbf{F}}{\Delta \mathrm{A}} \tag{2.21}$$

where $\Delta \mathbf{F}$ denotes the force acting on the area ΔA. If we recast this equation in terms of infinitesimal quantities Cauchy's postulate reads

$$\mathrm{d}\mathbf{f} = \mathbf{t}\,\mathrm{da} = \mathbf{T}\,\mathrm{dA} = \mathrm{d}\mathbf{F} \tag{2.22}$$

where $\mathbf{T}$ represents the equivalent of $\mathbf{t}$ with respect to the reference configuration and is called the first Piola-Kirchhoff traction vector. The area element in material coordinates is symbolised as dA. A visualisation of Cauchy's postulate is given in Figure 4.

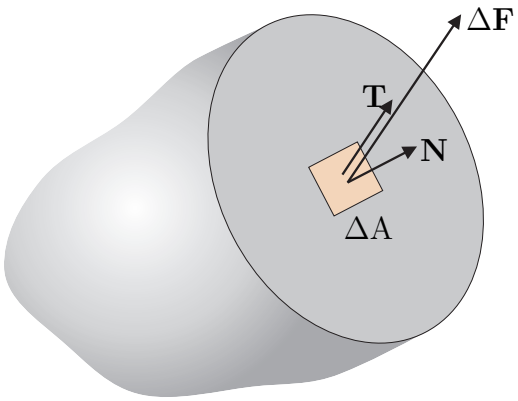

Figure 4: Visualisation of Cauchy's postulate

Moreover, Cauchy's stress theorem introduces stress tensors as follows

$$\mathbf{t} = \boldsymbol{\sigma} \cdot \mathbf{n} \tag{2.23}$$

$$\mathbf{T} = \mathbf{P} \cdot \mathbf{N} \tag{2.24}$$

where $\mathbf{n}$ and $\mathbf{N}$ denote the outward normal unit vectors perpendicular to the surface. The stress tensors $\boldsymbol{\sigma}$ and $\mathbf{P}$ are the commonly known Cauchy stress tensor and the first Piola-Kirchhoff stress tensor (1st PK), respectively. Basically (2.24) states that the traction vectors are linear in the outward unit normals. It is straightforward that due to this

linearity the following relations hold:

$$\mathbf{t}(\mathbf{x}, \mathbf{n}) = -\mathbf{t}(\mathbf{x}, -\mathbf{n}) \tag{2.25}$$

$$\mathbf{T}(\mathbf{X}, \mathbf{N}) = -\mathbf{T}(\mathbf{X}, -\mathbf{N}) \tag{2.26}$$

These are also referred to as Newton's (third) law of action and reaction.

To achieve a relation between the two stress tensors $\boldsymbol{\sigma}$ and $\mathbf{P}$, (2.22) can be recasted under the incorporation of (2.24) as

$$\boldsymbol{\sigma} \cdot \mathbf{n}\, \mathrm{da} = \mathbf{P} \cdot \mathbf{N}\, \mathrm{dA} \tag{2.27}$$

Taking into account Nanson's formula (2.10) and the knowledge that $\mathrm{d}\mathbf{a} = \mathbf{n}\mathrm{da}$ and $\mathrm{d}\mathbf{A} = \mathbf{N}\mathrm{dA}$ the so-called Piola transformation is completed as

$$\mathbf{P} = \boldsymbol{\sigma}\, \mathbf{H} \tag{2.28}$$

A prescription for the Cauchy stress is therefore given as

$$\boldsymbol{\sigma} = \mathbf{P}\, \mathbf{H}^{-1} = \frac{1}{J} \mathbf{P}\, \mathbf{F}^{\mathrm{T}} = \boldsymbol{\sigma}^{\mathrm{T}} \tag{2.29}$$

As the Cauchy stress tensor is known to be symmetric - this can be obtained by applying the angular momentum equilibirum on an infinitesimal volume element - the relation

$$\mathbf{P}\, \mathbf{F}^{\mathrm{T}} = \mathbf{F}\, \mathbf{P}^{\mathrm{T}} \tag{2.30}$$

emerges. Consequently, the 1st PK is in general not symmetric and thereby comprises nine independent entries. Here again it is target-aimed to work with a symmetric stress measure. The most popular one is the so-called second Piola-Kirchhoff stress tensor (2nd PK). It is defined as

$$\mathbf{S} = \mathbf{F}^{-1}\, \mathbf{P} \tag{2.31}$$

The symmetry can be proven easily as it is recasted using (2.28) and (2.11) as

$$\mathbf{S} = J\, \mathbf{F}^{-1}\, \boldsymbol{\sigma}\, \mathbf{F}^{-\mathrm{T}} = \mathbf{S}^{\mathrm{T}} \tag{2.32}$$

This means that there are are only six independent components. Moreover, subsequent numerical implementations are facilitated by taking this symmetry into account. Even-

tually, the Cauchy stress tensor can be rewritten in the form

$$\boldsymbol{\sigma} = \frac{1}{J}\,\mathbf{F}\,\mathbf{S}\,\mathbf{F}^{\mathrm{T}} \tag{2.33}$$

2.1.4 Conservation Principles for Continua

Mechanical systems can be described in their entirety by conservation principles. They lead either to governing differential equations or to further important and useful properties of some of the incorporated quantities. As they hold also for dynamic approaches, the time-dependence is stated at this point.

The most known principle is the conservation of mass. It tells that the mass of a body m is neither increased nor decreased during a deformation process

$$m = \int_{\mathcal{B}_0} \rho_0(\mathbf{X})\,\mathrm{d}V = \int_{\mathcal{B}} \rho(\mathbf{x},t)\,\mathrm{d}v = \text{const.} > 0 \tag{2.34}$$

ρ and ρ_0 denote the mass densities in mass per unit current volume and undeformed volume, respectively. Because the integration is a linear operator, the arguments need to satisfy the equations themselves. Hence, the local form reads

$$\rho_0(\mathbf{X})\,\mathrm{d}V = \rho(\mathbf{x},t)\,\mathrm{d}v > 0 \tag{2.35}$$

or under the use of the Jacobian as defined in equation (2.9)

$$\rho_0(\mathbf{X}) = \rho(\mathbf{x},t)\,J \tag{2.36}$$

In the last equation it becomes apparent that the Jacobian strictly needs to be greater than zero because the mass densities ρ and ρ_0 are always greater than zero.

Another value to be conservated is the translational momentum $\mathbf{L}$

$$\mathbf{L}(t) = \int_{\mathcal{B}} \rho\,\mathbf{v}\,\mathrm{d}v = \int_{\mathcal{B}_0} \rho_0\,\mathbf{V}\,\mathrm{d}V \tag{2.37}$$

where $\mathbf{v} = \mathbf{v}(\mathbf{x},t)$ and $\mathbf{V} = \mathbf{V}(\mathbf{X},t)$ denote the velocity fields in Eulerian and Lagrangian description, respectively. Material time differentiation yields

$$\dot{\mathbf{L}}(t) = \frac{\mathrm{D}}{\mathrm{D}t}\int_{\mathcal{B}_0} \rho_0\,\mathbf{V}\,\mathrm{d}V = \int_{\mathcal{B}_0} \rho_0\,\dot{\mathbf{V}}\,\mathrm{d}V = \mathbf{F}^{ext}(t) \tag{2.38}$$

In the last equation $\mathbf{F}^{ext}$ characterises the resultant external force which can also be written in terms of external impacts, such as forces per unit volume $\mathbf{B}$ or traction vectors $\mathbf{T}$, as

$$\mathbf{F}^{ext}(t) = \int_{\partial\mathcal{B}_0} \mathbf{T}\,\mathrm{d}\mathbf{A} + \int_{\mathcal{B}_0} \mathbf{B}\,\mathrm{d}V \tag{2.39}$$

Inserting (2.39) into (2.38), taking into account the divergence theorem (A.7) and Cauchy's theorem (2.24) we obtain the local form of equilibrium

$$\mathrm{Div}(\mathbf{P}) + \mathbf{B} = \rho_0\,\dot{\mathbf{V}}_0 \tag{2.40}$$

where the divergence of a tensor of order two is defined by (A.4).

Furthermore, as also rotational motions are to be regarded the angular momentum $\mathbf{J}$ with respect to a reference point $\mathbf{x}_0$ needs to be introduced as

$$\mathbf{J}(t) = \int_{\mathcal{B}} \mathbf{r} \times \rho\,\mathbf{v}\,\mathrm{d}v = \int_{\mathcal{B}_0} \mathbf{r} \times \rho_0\,\mathbf{V}\,\mathrm{d}V \tag{2.41}$$

where $\mathbf{r}$ denotes the distance to a reference point $\mathbf{x}_0$ as

$$\mathbf{r}(\mathbf{x}(\mathbf{X},t)) = \mathbf{x}(\mathbf{X},t) - \mathbf{x}_0 \tag{2.42}$$

Again the time derivative can be written as

$$\dot{\mathbf{J}}(t) = \frac{\mathrm{D}}{\mathrm{Dt}} \int_{\mathcal{B}_0} \mathbf{r} \times \rho_0\,\mathbf{V}\,\mathrm{d}V = \mathbf{M}^{ext}(t) \tag{2.43}$$

and it represents the resultant moment which can be recasted similar to the resultant force as

$$\mathbf{M}^{ext}(t) = \int_{\partial\mathcal{B}_0} \mathbf{r} \times \mathbf{T}\,\mathrm{d}\mathbf{A} + \int_{\mathcal{B}_0} \mathbf{r} \times \mathbf{B}\,\mathrm{d}V \tag{2.44}$$

By deploying Cauchy's theorem (2.24), the divergence theorem and the local equilibrium of angular momentum (2.40) we can derive a proof that the 2nd PK is symmetric (cf. (2.32))

$$\mathbf{S} = \mathbf{S}^{\mathrm{T}} \tag{2.45}$$

Therefore the arbitrariness of the regarded volume is taken into account. Moreover, the same conclusion can be drawn for the Cauchy stresses $\boldsymbol{\sigma}$ (cf. (2.33))

$$\boldsymbol{\sigma} = \boldsymbol{\sigma}^{\mathrm{T}} \tag{2.46}$$

if one works with quantities in the Eulerian description. Therefore, (2.29) can be proven.

Finally, the well known energy conservation is an essential principle. It states that the total energy E_{tot}, which in elasto-statics can be expressed as the sum of the potential Π and the kinetic energy $\mathcal{K}$, needs to be constant during the deformation. The potential function can be additively split into the external and internal parts:

$$E_{tot} = \Pi + \mathcal{K} = \text{const.} \tag{2.47}$$

$$\Pi = \Pi_{ext} + \Pi_{int} \tag{2.48}$$

The kinetic energy $\mathcal{K}$ which is defined as

$$\mathcal{K} = \int_{\partial\mathcal{B}_0} \frac{1}{2}\,\rho_0\,\mathbf{V}\cdot\mathbf{V}\,\mathrm{d}V \tag{2.49}$$

vanishes for static problems as $\mathbf{V} = \mathbf{0}$. Π_{ext} contains any mechanical forces. Hence it derives from the scalar product of applied traction vectors and body forces with the displacement of their working points.

$$\Pi_{ext} = \int_{\partial\mathcal{B}_0} \mathbf{T}\cdot\mathbf{U}\,\mathrm{dA} + \int_{\mathcal{B}_0} \mathbf{B}\cdot\mathbf{U}\,\mathrm{d}V \tag{2.50}$$

The internal energy comes from the deformation of the material itself and can be expressed as the integral over the whole body of the internal energy per unit undeformed volume.

$$\Pi_{int} = \int_{\mathcal{B}_0} e(\mathbf{X})\,\mathrm{d}V \tag{2.51}$$

The form of this internal energy changes with the kind of problem investigated and can be described via so-called strain energy functions. This will be considered subsequently in Chapter 3.

2.2 Electrostatic Field Theory

As this work aims to couple mechanical with electric theories, it is necessary to introduce the governing equations in order to evoke basic knowledge of electric fields. The description of the equations presented in this first section is based on [DO14]. As electric field

theories are widely carried out with respect the current configurations it is necessary here to show the transition to Lagrangian forms.

2.2.1 Full Set of Maxwell's Equations

The most important equations for electromechanical coupling come from the well-known Maxwell's equations. They describe the behaviour of electric and magnetic fields entirely. There are four equations in total. The first two make statements concerning the origins to cause two vector fields, the electric field and the magnetic field. The electric field $\mathbf{E}_E$, which shall be considered in Eulerian description, is caused by an electric charge which is represented by charge density ρ^e per unit current volume. Thus, Maxwell's first equation, also referred to as Gauss' law, reads

$$\operatorname{div}(\mathbf{E}_E) = \frac{\rho^e}{\varepsilon_0} \tag{2.52}$$

In this equation the physical constant ε_0 is used. It is called vacuum permittivity and has a value of $8.854 \cdot 10^{-12} Fm^{-1}$. The definition of the divergence of a vector valued quantity can be found in (A.3). The second equation, due to the similarity to the first one called Gauss' law for magnetism, is fundamental for magnetostatic. It states, "that magnetic poles cannot be isolated, i.e. there is no counterpart in magnetostatics of the electrostatic point charge."([DO14]) Hence, the magnetic field $\mathbf{B}_E$ is divergence free:

$$\operatorname{div}(\mathbf{B}_E) = 0 \tag{2.53}$$

Maxwell's third and fourth equation cover the fact that the two field variables are directly effected by another. Faraday's law of induction in the form of

$$\operatorname{curl}(\mathbf{E}_E) = -\frac{\mathrm{D}}{\mathrm{D}t}(\mathbf{B}_E) \tag{2.54}$$

gives evidence about the rotation of $\mathbf{E}_E$ around a time-dependent magnetic field. The Curl operator can be looked up in the Appendix equation (A.5). In the analogy vice versa, Ampere's circuital law is given as

$$\operatorname{curl}(\mathbf{B}_E) = \mu_0 \, \mathbf{J}_E^e + \mu_0 \, \varepsilon_0 \, \frac{\mathrm{D}}{\mathrm{D}t}(\mathbf{E}_E) \tag{2.55}$$

It states, that magnetic fields rotate around time depending electric fields. In this equation μ_0 represents the physical constant of vacuum permeability. $\mathbf{J}_E^e$ denotes the current density and describes at which rate electric charges pass a unit surface of arbitrary orientation.

2.2.2 Electrostatic Approach

As the focus of this work shall not lie on sophisticated electric relations, time depending values and the occurance of magnetic fields are neglected in this work:

$$\frac{\mathrm{D}}{\mathrm{D}t}(\bullet) = 0 \qquad\qquad \mathbf{B}_0 = 0 \tag{2.56}$$

Hence, the introduced equations either simplify or even become obsolete. Gauss' law of magnetism and Ampere's circuital law can be omitted due to the conditions made. Hereby, the electric current density in (2.55) vanishes as it is defined via the velocity at which charges move

$$\mathbf{J}_E^e = \rho^e \, \mathbf{v} = \mathbf{0} \tag{2.57}$$

Gauss' law can be recasted for our purposes due to the relation

$$\mathbf{D}_E = \varepsilon_0 \, \mathbf{E}_E \tag{2.58}$$

where the introduced $\mathbf{D}_E$ denotes the so-called electric displacement field. Hence, a new differential form of Gauss' law, which is more suitable for our aims, reads

$$\mathrm{div}(\mathbf{D}_E) = \rho^e \tag{2.59}$$

By making use of (2.56) Faraday's law of induction gives

$$\mathrm{curl}(\mathbf{E}_E) = \mathbf{0} \tag{2.60}$$

and is therefore in this form referred to as static Faraday's law.

The field variables $\mathbf{E}_E$ and $\mathbf{D}_E$ imply an Eulerian description which is indicated by the subscripted E. As we want to consider the Langrangian description, indicated by a subscripted 0 ($\mathbf{E}_0$, $\mathbf{D}_0$), the two equations (2.59) and (2.60) can be transformed into their Lagrangian equivalents by applying the divergence theorem and Stokes' theorem respectively together with some kinematic relations (for the detailed derivation see [DO05],[DO14]). On that account Gauss' law can be recasted in the Langrangian form as

$$\mathrm{Div}(\mathbf{D}_0) = \rho_0^e \tag{2.61}$$

where ρ_0^e symbolises an electric charge density per unit undeformed volume. Moreover Faraday's law of induction (2.60) gives

$$\mathrm{Curl}(\mathbf{E}_0) = \mathbf{0} \tag{2.62}$$

The above two equations (2.61) and (2.62) remain to be included into the electromechanical framework. This has already been completed by [OG16] and [GO16]. The applied transformations between spatial and material coordinates evoke direct relations between the equivalent vector fields as

$$\mathbf{E}_0(\mathbf{X}) = \mathbf{F}^{\mathrm{T}}\,\mathbf{E}_E(\mathbf{x}) \tag{2.63}$$

$$\mathbf{D}_0(\mathbf{X}) = \mathbf{H}^{\mathrm{T}}\,\mathbf{D}_E(\mathbf{x}) \tag{2.64}$$

These kind of relations are referred to as 'pull-back' operations. Moreover, electric charge densities can be expressed per unit undeformed volume by making use of the Jacobian as

$$\rho_0^e = J\rho^e \tag{2.65}$$

We are moreover also interested in integral forms of the two gouverning equations. Making use of the divergence theorem and defining an electric charge per unit undeformed area

$$\omega_0^e = -\mathbf{D}_0 \cdot \mathbf{N} \tag{2.66}$$

an integral form of (2.61) is given as

$$\int\limits_{\partial\mathcal{B}_0^\omega} \omega_0^e \,\mathrm{dA} + \int\limits_{\mathcal{B}_0} \rho_0^e \,\mathrm{d}V = 0 \tag{2.67}$$

where $\mathbf{N}$ denotes the outer unit normal vector of the boundary area, on which the flux-like quantity ω_0^e is applied, labelled as $\partial\mathcal{B}_0^\omega$. Moreover, this equation yields the external potential energy due to electric impacts. Therefore, in analogy to (2.50), it can be derived by multiplication with the electric potential, such that

$$\Pi_{ext}^e = \int\limits_{\partial\mathcal{B}_0^\omega} \omega_0^e\phi \,\mathrm{dA} + \int\limits_{\mathcal{B}_0} \rho_0^e\phi \,\mathrm{d}V \tag{2.68}$$

The dimension of ω_0 is electric charge per unit area, thus the physical unit is

$$[\omega_0^e] = \frac{C}{m^2} = \frac{A\,s}{m^2} \tag{2.69}$$

Furthermore, Faraday's law of induction (2.62) can be recasted due to the fact, that the electric field is a gradient field (see,e.g. [DO14]). Therefore it reads

$$\mathbf{E}_0 = -\mathrm{Grad}(\phi) = -\mathrm{D}\phi \tag{2.70}$$

From a mathematical point of view, the standard vector identity $\mathrm{Curl}(\mathrm{Grad}(a)) = \mathbf{0}$ with $a \in \mathbb{R}$ is stated. The minus sign is obtained due to canonical conventions which state

that electric fields always point from positive into the direction of negative charges. In (2.70) $\phi = \phi(\mathbf{X})$ is a scalar valued quantity. It denotes the electric potential and has the same physical unit as voltage

$$[\phi] = \frac{kg\,m^2}{A\,s^3} = V \tag{2.71}$$

Therefore, the electric potential of an electrode equals the applied voltage on it. An integral form of (2.70) is given by

$$\oint_{\mathcal{C}} \mathbf{E}_0 \cdot \mathrm{d}\mathbf{X} = 0 \tag{2.72}$$

which means, that the integral of the electric field on an arbitrary closed curve $\mathcal{C}$ vanishes. It can be derived by applying Stokes' theorem, as defined in (A.9), on (2.62).

2.2.3 Electric Field Energy

Every electric field obviously possesses a certain amount of energy. Eventually, for the case of free space its Eulerian form reads [GK11]

$$e_c = \frac{1}{2}\varepsilon_0\,\mathbf{E}_E \cdot \mathbf{E}_E \tag{2.73}$$

The dimension is energy per unit current volume. Together with (2.58) it becomes

$$e_c = \frac{1}{2\varepsilon_0}\,\mathbf{D}_E \cdot \mathbf{D}_E \tag{2.74}$$

By taking into account the Jacobian (2.9) and using (2.64) one obtains a Lagrangian recast with respect to the undeformed volume

$$e_0 = J\,e_c = \frac{1}{2\varepsilon_0 J}\,\mathbf{F}\,\mathbf{D}_0 \cdot \mathbf{F}\,\mathbf{D}_0 \tag{2.75}$$

Finally, for the case of solid continua the so-called relative permittivity has to be introduced. It is defined as the ratio of the absolute permittivity of a solid body in an electric field ε and the vacuum permittivity, e.g.

$$\varepsilon_r = \frac{\varepsilon}{\varepsilon_0} \tag{2.76}$$

Eventually, the internal energy of a solid body exposed to an electric field is given as

$$e_0 = \frac{1}{2\varepsilon_0\varepsilon_r J}\,\mathbf{F}\,\mathbf{D}_0 \cdot \mathbf{F}\,\mathbf{D}_0 \tag{2.77}$$

or in terms of the symmetric right Cauchy-Green strain tensor (2.12) and its determinant (2.15)

$$e_0 = \frac{1}{2\varepsilon_0\varepsilon_r C^{1/2}}\,\mathbf{D}_0 \cdot \mathbf{C}\,\mathbf{D}_0 \tag{2.78}$$

2.3 Mathematical Preliminaries

As the presented quantities and equations are nonlinear in most cases, analytical solutions can only be gained for few exceptions. Therefore numerical methods are to be carried out in order to solve the problems approximately. The knowledge which is provided has been gained by the the textbook [Wri01].

2.3.1 Linearisation

The linearisation of a non scalar valued function $\mathbf{G}(\mathbf{w})$ mainly follows the idea of employing a Taylor series expansion up to the linear term in the operating point $\overline{\mathbf{w}}$ into the direction of a vector $\Delta\mathbf{w}$ as

$$\mathbf{G}(\overline{\mathbf{w}} + \Delta\mathbf{w}) = \overline{\mathbf{G}} + \overline{\mathrm{D}}\mathbf{G} \cdot \Delta\mathbf{w} + \mathbf{R} \tag{2.79}$$

where the notation $\overline{(\bullet)}$ is defined as evaluated at the point $\overline{\mathbf{w}}$. Hence,

$$\overline{\mathbf{G}} = \mathbf{G}(\overline{\mathbf{w}}) \tag{2.80}$$

and the partial differentiation which is symbolised by the Gateaux operator $\mathrm{D}(\bullet)$ reads

$$\overline{\mathrm{D}}\mathbf{G} = \mathrm{D}\mathbf{G}(\overline{\mathbf{w}}) = \left.\frac{\partial \mathbf{G}(\mathbf{w})}{\partial \mathbf{w}}\right|_{\mathbf{w}=\overline{\mathbf{w}}} \tag{2.81}$$

If the function depends on multiple variables, the partial derivative with respect to the i-th argument is denoted by

$$\mathrm{D}_i\mathbf{G}(\mathbf{w}_1, \ldots, \mathbf{w}_n) = \frac{\partial \mathbf{G}(\mathbf{w}_1, \ldots, \mathbf{w}_n)}{\partial \mathbf{w}_i} \tag{2.82}$$

The tangential part of (2.79) can be interpreted as the Gateaux differential of $\mathbf{G}$ into the direction of $\Delta\mathbf{w}$. Therefore we obtain a recast as

$$\overline{\mathrm{D}}\mathbf{G} \cdot \Delta\mathbf{w} = \mathrm{D}\mathbf{G}(\overline{\mathbf{w}}) \cdot \Delta\mathbf{w} = \frac{\mathrm{d}}{\mathrm{d}\varepsilon}\left[\mathbf{G}(\overline{\mathbf{w}} + \varepsilon\,\Delta\mathbf{w})\right]\Big|_{\varepsilon=0} \tag{2.83}$$

Eventually, the linearisation neglects the terms of higher order and is defined as

$$\mathbf{L}[\mathbf{G}]_{\mathbf{w}=\overline{\mathbf{w}}} := \overline{\mathbf{G}} + \overline{\mathrm{D}}\mathbf{G} \cdot \Delta\mathbf{w} = \overline{\mathbf{G}} + \Delta\overline{\mathbf{G}} \tag{2.84}$$

where the point of linearisation is denoted in subscripts and $\Delta(\bullet)$ symbolises the tangential part.

The linearisation of a scalar valued function $g(w)$ with $w \in \mathbb{R}$ can derived as

$$L[g]_{w=\overline{w}} = \overline{g} + \Delta\overline{g} = \overline{g} + \overline{\mathrm{D}}g \cdot \Delta w \tag{2.85}$$

where

$$\overline{\mathrm{D}}g = \mathrm{D}g(\overline{w}) = \frac{\partial g}{\partial w}\Big|_{w=\overline{w}} \tag{2.86}$$

and $w \in \mathbb{R}$. The corresponding visualisation can be found in Figure 5.

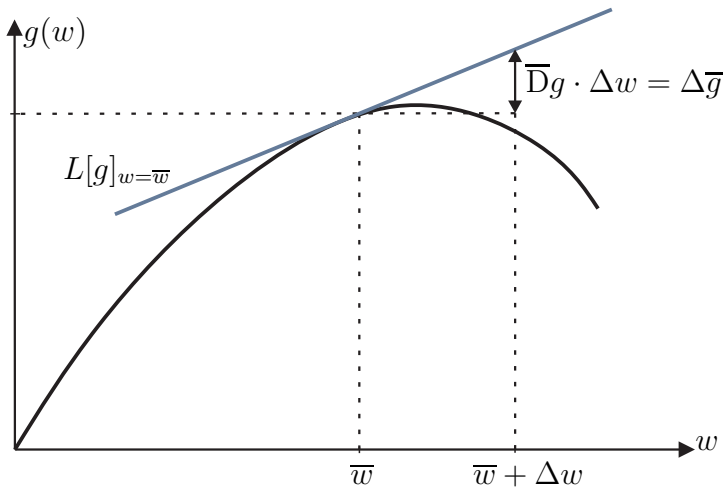

Figure 5: Visualisation of the linearisation of a scalar valued function $g(w)$

In the following two linearisations of quantities depending on the deformation $\boldsymbol{\varphi}$ are presented. In this case, $\mathbf{w}$ represents the material displacement vector $\mathbf{U}$. Thus, it is worth noting that the following relation holds:

$$\Delta\boldsymbol{\varphi} = \mathrm{D}\boldsymbol{\varphi} \cdot \Delta\mathbf{U} = \frac{\mathrm{d}}{\mathrm{d}\varepsilon}\left(\boldsymbol{\varphi} + \varepsilon\,\Delta\mathbf{U}\right)\Big|_{\varepsilon=0} = \Delta\mathbf{U} \tag{2.87}$$

For example the right Cauchy-Green strain tensor can be linearised as

$$\mathbf{L}[\mathbf{C}]_{\boldsymbol{\varphi}=\overline{\boldsymbol{\varphi}}} = \overline{\mathbf{C}} + \Delta\overline{\mathbf{C}} \tag{2.88}$$

and the Gateaux differential can be executed via (2.83) as

$$\Delta\overline{\mathbf{C}} = \overline{\mathrm{D}}\mathbf{C}\cdot\Delta\mathbf{U} = \frac{\mathrm{d}}{\mathrm{d}\varepsilon}\mathbf{C}(\overline{\boldsymbol{\varphi}} + \varepsilon\,\Delta\mathbf{U})\Big|_{\varepsilon=0} \tag{2.89}$$

$$= \frac{\mathrm{d}}{\mathrm{d}\varepsilon}\left[\frac{\partial}{\partial\mathbf{X}}(\overline{\boldsymbol{\varphi}} + \varepsilon\,\Delta\mathbf{U})\right]^{\mathrm{T}}\left[\frac{\partial}{\partial\mathbf{X}}(\overline{\boldsymbol{\varphi}} + \varepsilon\,\Delta\mathbf{U})\right]\Big|_{\varepsilon=0} \tag{2.90}$$

$$= \frac{\mathrm{d}}{\mathrm{d}\varepsilon}\left[\overline{\mathbf{F}}^{\mathrm{T}} + \varepsilon\,\mathrm{Grad}(\Delta\mathbf{U})^{\mathrm{T}}\right]\left[\overline{\mathbf{F}} + \varepsilon\,\mathrm{Grad}(\Delta\mathbf{U})\right]\Big|_{\varepsilon=0} \tag{2.91}$$

$$= \overline{\mathbf{F}}^{\mathrm{T}}\,\mathrm{Grad}(\Delta\mathbf{U}) + \mathrm{Grad}(\Delta\mathbf{U})^{\mathrm{T}}\,\overline{\mathbf{F}} \tag{2.92}$$

Thus, the final linearisation reads

$$\mathbf{L}[\mathbf{C}]_{\boldsymbol{\varphi}=\overline{\boldsymbol{\varphi}}} = \overline{\mathbf{C}} + \overline{\mathbf{F}}^{\mathrm{T}}\,\mathrm{Grad}(\Delta\mathbf{U}) + \mathrm{Grad}(\Delta\mathbf{U})^{\mathrm{T}}\,\overline{\mathbf{F}} \tag{2.93}$$

and if this is done with respect to the reference configuration we obtain under the use of the property (2.87)

$$\mathbf{L}[\mathbf{C}]_{\boldsymbol{\varphi}=\mathbf{X}} = \mathbf{I} + \mathrm{Grad}(\Delta\boldsymbol{\varphi}) + \mathrm{Grad}(\Delta\boldsymbol{\varphi})^{\mathrm{T}} \tag{2.94}$$

The Jacobi-determinant can be linearised as

$$L[J]_{\boldsymbol{\varphi}=\overline{\boldsymbol{\varphi}}} = \overline{J} + \overline{J}\,\overline{\mathrm{div}}(\boldsymbol{\varphi}) \tag{2.95}$$

$$L[J]_{\boldsymbol{\varphi}=\mathbf{X}} = 1 + \mathrm{Div}(\boldsymbol{\varphi}) \tag{2.96}$$

2.3.2 Variations

As we want to make use of variational principles in order to obtain a certain formulation for the BVP, it is essential to briefly introduce variations. The variation of a vector-valued variable $\mathbf{w}$ is defined as the deviation to a possible slightly different vector field $\tilde{\mathbf{w}}$ as

$$\delta\mathbf{w} = \tilde{\mathbf{w}} - \mathbf{w} \tag{2.97}$$

This difference is considered to be arbitrary. Moreover, $\delta\mathbf{w}$ is said to be a virtual change. Due to its arbitrariness, the variation can be employed to determine the stationarity of a given function $\mathbf{G}(\mathbf{w})$. On that account, similar to the procedure of linearisation, the Gateaux differential (2.83) is employed in order to define the variation of $\mathbf{G}$ in the direction of $\delta\mathbf{w}$ as

$$\delta_{\mathbf{w}}\mathbf{G}(\mathbf{w}) = \mathrm{D}\mathbf{G}(\mathbf{w})\cdot\delta\mathbf{w} = \frac{\mathrm{d}}{\mathrm{d}\varepsilon}\left[\mathbf{G}(\mathbf{w} + \varepsilon\,\delta\mathbf{w})\right]\Big|_{\varepsilon=0} \tag{2.98}$$

The stationarity of $\mathbf{G}$ can be expressed by a vanishing variation

$$\delta_{\mathbf{w}}\mathbf{G}(\mathbf{w}) = \mathbf{0} \tag{2.99}$$

The solution of this conditional equation represents the stationary point. If the varied quantity depends on multiple arguments, the direction of variation is denoted in the subscript and the Gateaux differential is executed with respect to one argument, according to (2.82), e.g.

$$\delta_{\mathbf{v}}\mathbf{G}(\mathbf{u}, \mathbf{v}, \mathbf{w}) = \mathrm{D}_2\mathbf{G}(\mathbf{u}, \mathbf{v}, \mathbf{w}) \cdot \delta\mathbf{v} \tag{2.100}$$

Note that the variation as well as the linearisation are linear operations. Hence, usual properties of differentiation and integration still hold.

If $\mathbf{w}$ characterises the mechanical displacement field $\mathbf{U}$, its variation is given as

$$\delta\mathbf{U}(\mathbf{X}) = \delta\boldsymbol{\varphi}(\mathbf{X}) - \delta\mathbf{X} \tag{2.101}$$

As the reference position vector is fixed, its variation vanishes and hence, analogously to (2.87),

$$\delta\mathbf{U} = \delta\boldsymbol{\varphi}(\mathbf{X}) \tag{2.102}$$

2.3.3 Newton's Method

Newton's method or to be more precise the Newton-Raphson-method is a commonly employed way to solve nonlinear equations or set of equations. Consider the following structure

$$\mathbf{G}(\mathbf{w}, \lambda) = \mathbf{R}(\mathbf{w}) - \lambda\,\mathbf{P} = \mathbf{0} \tag{2.103}$$

with $\mathbf{w} \in \mathbb{R}^n$. $\mathbf{P}$ denotes a load term and can be weighted with the loading parameter λ. The aim is to find a solution for any λ up to $\lambda = 1$. In doing so, the loading parameter is enlarged in $N \in \mathbb{N}^+$ steps as

$$\lambda_k = k\,\frac{1}{N} \tag{2.104}$$

with $k \in \{1, ..., N\}$. As often deployed, linearisation of $\mathbf{G}$ yields

$$\mathbf{G}(\mathbf{w}_k + \Delta\mathbf{w}, \lambda_k) = \mathbf{G}(\mathbf{w}_k, \lambda_k) + \mathrm{D}\mathbf{G}(\mathbf{w}_k, \lambda_k) \cdot \Delta\mathbf{w} \tag{2.105}$$

where $\mathbf{w}_k$ denotes an approximation of the solution for λ_k and $\mathrm{D}\mathbf{G}(\mathbf{w}_k, \lambda_k) = \mathbf{K}_T$ is called tangential matrix. To find this approximated solution an iterational procedure is given as

1. The residual und tangential matrix are computed.

2. An increment is computed via: $\Delta\mathbf{w}_{i+1} = -\mathbf{K}_T(\mathbf{w}_i)^{-1}\,\mathbf{G}(\mathbf{w}_i, \lambda)$.

3. The unknown is updated as $\mathbf{w}_{i+1} = \mathbf{w}_i + \Delta\mathbf{w}_{i+1}$.

4. Comparing the new norm $||\mathbf{G}(\mathbf{w}_{i+1}, \lambda_k)||$ with a demanded tolerance: If it is less or equal than the accepted imprecision a solution has been found: $\mathbf{w}_{k+1} \leftarrow \mathbf{w}_{i+1}$.
   If $||\mathbf{G}(\mathbf{w}_{i+1}, \lambda_k)||$ is greater than the tolerance the iteration starts from the beginning with: $i \leftarrow i + 1$

If the solution has been found, the load factor is increased and the above iteration is executed for $k = k + 1$. This procedure continues until $\lambda = 1$ and $\mathbf{w}_k$ solves the regarded system (2.103).

Due to the structure of this technique, it converges quadratically towards the exact solution $\mathbf{w}^*$ and

$$||\mathbf{w}_{i+1} - \mathbf{w}^*|| \leq C\,||\mathbf{w}_i - \mathbf{w}^*||^2 \tag{2.106}$$

with $C \in \mathbb{R}$ holds.

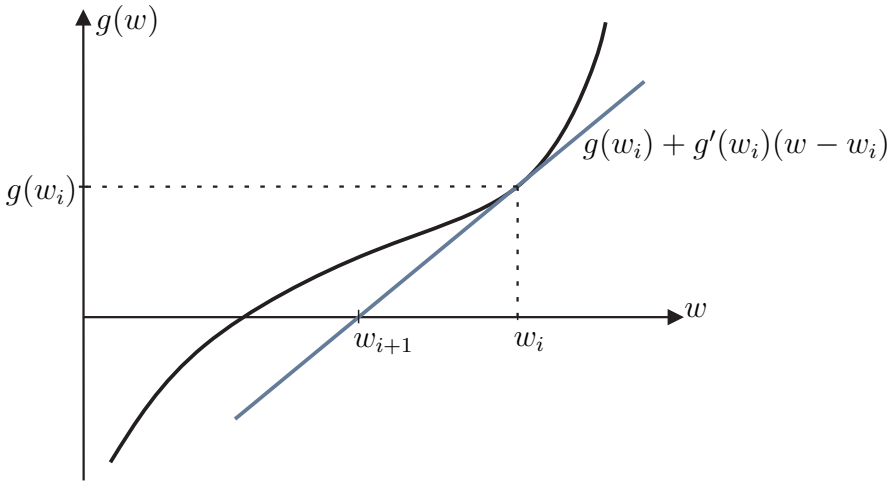

Figure 6: Visualisation of Newton's method for a scalar valued function $g(w)$

To get a deeper understanding of the presented method, the special case of a scalar fvalued function $g(w)$ with $w \in \mathbb{R}$ can be adduced. In doing so, the tangential part gives

$$\mathrm{D}g(w_i) = \frac{\partial g}{\partial w}\Big|_{w=w_i} =: g'(w) \tag{2.107}$$

and the increment Δw_{i+1} can be computed as

$$\Delta w_{i+1} = -\frac{g(w_i)}{g'(w_i)} \tag{2.108}$$

A depiction can be found in Figure 6.

2.3.4 Gauss Integration

Gauss integration pursues the idea of solving integrals in a standardised domain by evaluating the integrand function $g(\xi, \eta, \zeta)$ at the so-called Gauss integration points with the coordinates ξ_p, η_p, ζ_p as

$$\int_{-1}^{1}\int_{-1}^{1}\int_{-1}^{1} g(\xi,\eta,\zeta)\ \mathrm{d}\xi\mathrm{d}\eta\mathrm{d}\zeta = \sum_{p=1}^{n_p} g(\xi_p,\eta_p,\zeta_p)\cdot w_p \tag{2.109}$$

Thereby, the n_p discrete values of the function g are weighted with specific factors w_p and summed up. The Gauss coordinates and weights for the three dimensional case with $n_p = 2$ are given in the following Table 2.

p	ξ_p	η_p	ζ_p	w_p
1	$-1/\sqrt{3}$	$-1/\sqrt{3}$	$-1/\sqrt{3}$	1
2	$1/\sqrt{3}$	$-1/\sqrt{3}$	$-1/\sqrt{3}$	1
3	$-1/\sqrt{3}$	$1/\sqrt{3}$	$-1/\sqrt{3}$	1
4	$1/\sqrt{3}$	$1/\sqrt{3}$	$-1/\sqrt{3}$	1
5	$-1/\sqrt{3}$	$-1/\sqrt{3}$	$1/\sqrt{3}$	1
6	$1/\sqrt{3}$	$-1/\sqrt{3}$	$1/\sqrt{3}$	1
7	$-1/\sqrt{3}$	$1/\sqrt{3}$	$1/\sqrt{3}$	1
8	$1/\sqrt{3}$	$1/\sqrt{3}$	$1/\sqrt{3}$	1

Table 2: Gauss integration points and weights

Others can be found in standard FE books, such as [Hug00, Wri01].

3 Constitutive Equations and Stored Energy Functions

To solve BVPs it is now necessary to link the strain with the stress measures via constitutive equations. This is often done by deploying functions for the definition of the internal energy in (2.51). Eventually, considering the equilibrium of total energy (2.47) leads to a description of the BVP in an integral form. But first, strain energy functions in the sense of

$$e(\mathbf{X}) = \tilde{\Psi}(\mathbf{F}) \tag{3.1}$$

are used to formulate the internal energy. These functions are also referred to as stored energy functions. They can be formulated in dependence of arbitrary strain measures, such as $\mathbf{F}, \mathbf{C}$ or $\mathbf{E}$

$$\tilde{\Psi}(\mathbf{F}) = \Psi(\mathbf{C}) = \hat{\Psi}(\mathbf{E}) \tag{3.2}$$

and the idea was well presented in [Hol00]. The following descriptions have been taken from this recapitulatory work.

3.1 General Remarks on Stored Energy Functions

However, there are two main conditions for stored energy functions. First, it is necessary that Ψ finds its global minimum in the reference configuration. Therefore, it should fulfill the normalisation condition and become zero. For all other configurations the stored energy must be non-negative:

$$\tilde{\Psi}(\mathbf{F} = \mathbf{I}) = \min(\tilde{\Psi}) = 0 \qquad \text{in } \mathcal{B}_0 \tag{3.3}$$

$$\tilde{\Psi}(\mathbf{F} \neq \mathbf{I}) > 0 \qquad \text{in } \mathcal{B} \tag{3.4}$$

The above relations ensure the stress in the reference configuration to vanish. Second, the growth condition states, that for deformations, for which the volume is close to zero or infinity, the stored energy function has to tend to infinity.

$$\left\{ \begin{matrix} \det(\mathbf{F}) \to +\infty \\ \det(\mathbf{F}) \to 0^{+} \end{matrix} \right\} \Rightarrow \tilde{\Psi}(\mathbf{F}) \to +\infty \tag{3.5}$$

For purely mechanical problems the differentiation of Ψ with respect to the strain measures yields the stress tensors. If the strain energy function depends on the non-symmetric

deformation gradient, the 1st PK is obtained

$$\mathbf{P} = \frac{\partial \tilde{\Psi}(\mathbf{F})}{\partial \mathbf{F}} \tag{3.6}$$

If symmetric quantities are considered, the relations

$$\mathbf{S} = 2\,\frac{\partial \Psi(\mathbf{C})}{\partial \mathbf{C}} = \frac{\partial \hat{\Psi}(\mathbf{E})}{\partial \mathbf{E}} \tag{3.7}$$

hold. $\mathbf{F}$ and $\mathbf{P}$ as well as $\mathbf{C}$ or $\mathbf{E}$ and $\mathbf{S}$ respectively are referred to as work conjugated quantities.

For the mathematical sake of polyconvexity it can be useful to enhance the arguments of Ψ, as it is presented in [BJH17]. In doing so, each and every argument is considered to be independent. Hence, the strain energy function is defined as

$$\Psi = \Psi(\mathbf{C}, \mathbf{G}, C) \tag{3.8}$$

if symmetric strain measures are considered.

3.2 Isotropic Mechanical Material Models

Isotropic material models are used quite frequently. This property is defined by stating that the material behaviour is the same into every direction in space. One way to characterise these models is to investigate whether or not they are invariant of rigid body motions before deformation. A rigid body motion can be expressed via an offset vector $\mathbf{c}$ and a rotation tensor $\mathbf{Q}$, so that the body occupies a modified reference configuration as

$$\mathbf{X}^* = \mathbf{c} + \mathbf{Q}\,\mathbf{X} \tag{3.9}$$

Thus, the deformation gradient can be recasted as

$$\mathbf{F} = \frac{\partial \mathbf{x}}{\partial \mathbf{X}} = \frac{\partial \mathbf{x}}{\partial \mathbf{X}^*}\,\mathbf{Q} = \mathbf{F}^*\,\mathbf{Q} \tag{3.10}$$

If the material model is isotropic the stored energy function has the same value for the usual and the modified reference configuration

$$\tilde{\Psi}(\mathbf{F}) = \tilde{\Psi}(\mathbf{F}^*) = \tilde{\Psi}(\mathbf{F}\,\mathbf{Q}^{\mathrm{T}}) \tag{3.11}$$

3.2.1 Saint-Venant Kirchhoff Material Model

One material model to satisfy the condition of isotropy is the Saint-Venant Kirchhoff material model. It has already been presented in several works, e.g. [Fra14]. In contrast

to most other models it is indeed geometrical nonlinear but still materially linear. Thereby it is often used for metallic materials. One common formulation reads

$$\hat{\Psi}(\mathbf{E}) = \frac{\lambda}{2}\left[\mathrm{tr}(\mathbf{E})\right]^2 + \mu\,\mathrm{tr}(\mathbf{E}^2) \tag{3.12}$$
$$\lambda, \mu : \text{Lamé constants}$$

As expected, the 2nd PK emerges as a linear function of the Green-Lagrange strain tensor by derivation of (3.12) with respect to $\mathbf{E}$

$$\mathbf{S} = \frac{\partial \hat{\Psi}(\mathbf{E})}{\partial \mathbf{E}} = \lambda\left[\mathrm{tr}(\mathbf{E})\right]\mathbf{I} + 2\mu\,\mathbf{E} \tag{3.13}$$

where the linear relation between strain and stress measure becomes obvious. The analogy to the linear elastic model (broadly known as Hooke's law) is unmissable. This is evident as the linear elastic theory can be derived by linearising the Saint-Venant Kirchhoff model (as described in Section 2.3.1). The linear elastic Hooke's law gives a prescription for Cauchy stresses as

$$\boldsymbol{\sigma} = \lambda\left[\mathrm{tr}(\boldsymbol{\varepsilon})\right]\mathbf{I} + 2\mu\,\boldsymbol{\varepsilon} \tag{3.14}$$

It is worth noting, that the linear elastic strain tensor $\boldsymbol{\varepsilon}$ represents the linearisation of the Green-Lagrange strain tensor $\mathbf{E}$ with respect to the reference configuration for the derivation see (2.93)) as

$$\mathbf{L}[\mathbf{E}]_{\boldsymbol{\varphi}=\mathbf{X}} = \frac{1}{2}\left[\mathrm{Grad}(\mathbf{u}_{lin}) + \mathrm{Grad}(\mathbf{u}_{lin})^{\mathrm{T}}\right] = \nabla^{\mathrm{sym}}(\mathbf{u}_{lin}) = \boldsymbol{\varepsilon} \tag{3.15}$$

Note, that in the last equation, $\mathbf{u}_{lin} = \Delta\mathbf{U}$ represents the displacement field of the linear theory, where there is no distinction between spatial and material coordinates.

Moreover, the material constants λ and μ are the two Lamé parameters and the well known one dimensional Young's modulus E and Poisson's ratio υ can be expressed as

$$E = \frac{(3\lambda + 2\mu)}{\lambda + \mu}\,, \quad \upsilon = \frac{\lambda}{2\,(\lambda + \mu)} \tag{3.16}$$

3.2.2 Mooney-Rivlin Material Model

A second more frequently used isotropic hyperelastic material model, which is in fact also nonlinear in its prescription, is the so-called Mooney-Rivlin material model. It is predominantly used to describe rubber and rubber-like materials. A formulation in terms

of the invariants of a strain tensor is common. For example,

$$\Psi(J, I_{\mathbf{C}}, II_{\mathbf{C}}) = a\,(I_{\mathbf{C}} - 3) + b\,(II_{\mathbf{C}} - 3) + c\,(J-1)^2 - d\ln(J) \tag{3.17}$$

works with the invariants of the right Cauchy-Green strain tensor $\mathbf{C}$, given by

$$I_{\mathbf{C}} = \mathrm{tr}(\mathbf{C}) \tag{3.18}$$

$$II_{\mathbf{C}} = \frac{1}{2}\left[(\mathrm{tr}(\mathbf{C}))^2 - \mathrm{tr}(\mathbf{C}^2)\right] \tag{3.19}$$

$$III_{\mathbf{C}} = \det(\mathbf{C}) \tag{3.20}$$

Invariants of a tensor are independent of the coordinate system in which the tensor is formulated. The Jacobian represents a recast of the third invariant as it is shown in (2.15). To get further knowledge of the incorporated material parameters, linearisation allows us to compare a, b, c and d with the Lamé parameters λ and μ as it has been done in [Gov07] in more detail. At first, the 2nd PK is derived via (3.7) as

$$\mathbf{S} = 2\left[\frac{\partial\Psi}{\partial I_{\mathbf{C}}}\frac{\partial I_{\mathbf{C}}}{\partial\mathbf{C}} + \frac{\partial\Psi}{\partial II_{\mathbf{C}}}\frac{\partial II_{\mathbf{C}}}{\partial\mathbf{C}} + \frac{\partial\Psi}{\partial J}\frac{\partial J}{\partial\mathbf{C}}\right] \tag{3.21}$$

Taking note of the differentiations

$$\frac{\partial\Psi}{\partial I_{\mathbf{C}}} = a \qquad \frac{\partial\Psi}{\partial II_{\mathbf{C}}} = b \qquad \frac{\partial\Psi}{\partial J} = 2c\,(J-1) - \frac{d}{J} \tag{3.22}$$

$$\frac{\partial I_{\mathbf{C}}}{\partial\mathbf{C}} = \mathbf{I} \qquad \frac{\partial II_{\mathbf{C}}}{\partial\mathbf{C}} = I_{\mathbf{C}}\,\mathbf{I} - \mathbf{C} \qquad \frac{\partial J}{\partial\mathbf{C}} = \frac{1}{2}J\,\mathbf{C}^{-1} \tag{3.23}$$

the 2nd PK can be recasted as

$$\mathbf{S} = 2a\,\mathbf{I} + 2b\,(I_{\mathbf{C}}\,\mathbf{I} - \mathbf{C}) + J\,\mathbf{C}^{-1}\left[2c\,(J-1) - \frac{d}{J}\right] \tag{3.24}$$

By making use of (2.33) the resulting prescription for the Cauchy stresses $\boldsymbol{\sigma}$ can be linearised according to Chapter 2.3.1 and compared to the linear theory (3.14) as

$$2a + 4b - d = 0 \tag{3.25}$$

$$-2a + 2c + d = \lambda \tag{3.26}$$

$$4a + 4b = 2\mu \tag{3.27}$$

$$\tag{3.28}$$

A stress free reference configuration can only be provided if the scalar valued parameters satisfy the first equation as

$$d = 2\,(a + 2b) \tag{3.29}$$

The two next equations allow us to compute the Lamé parameters for given constants in the Mooney-Rivlin model. It is worth noting that we are even able to determine Young's modulus E and Poisson's ratio υ by making use of (3.16). It is common to choose $b = 2a$ (see [BJH17],[BGO15],[OG16]). On that account we gain the concise relations

$$E = \frac{6a\,(36a + 6c)}{14a + 2c} \qquad\qquad \upsilon = \frac{8a + 2c}{28a + 4c} \tag{3.30}$$

3.2.3 Elasticity Tensors

One slightly different possibility to map the strain on the stress variables is to incorporate fourth order tensors. They emerge from differentiation of the stress values with respect to the strain values. Derived by using the total differential (A.6) of the 2nd PK

$$\mathrm{d}\mathbf{S} = \frac{\partial \mathbf{S}(\mathbf{C})}{\partial \mathbf{C}} : \mathrm{d}\mathbf{C} = \mathbb{C} : \frac{1}{2}\,\mathrm{d}\mathbf{C} \tag{3.31}$$

an elasticity tensor turns out to be

$$\mathbb{C} = 2\,\frac{\partial \mathbf{S}(\mathbf{C})}{\partial \mathbf{C}} \tag{3.32}$$

or if there is a given stored energy function

$$\mathbb{C} = 4\,\frac{\partial^2 \Psi(\mathbf{C})}{\partial \mathbf{C}\,\partial \mathbf{C}} \tag{3.33}$$

In this last case, the elasticity tensor is globally symmetric due to the symmetry of $\mathbf{C}$. Of the $3 \times 3 \times 3 \times 3 = 81$ components remain just 21 independent. This becomes useful when it comes to the computational implementation.

3.3 Electric Constitutive Equations

Furthermore we need to introduce constituve equations regarding the electric fields. A first one has already been presented in (2.58). However, this does not take account of solids and is only valid in vacuo. In order to overcome this condition, the relative permittivity ε_r has to be included. Thus, (2.58) has to be rewritten in the form of

$$\mathbf{D}_E = \varepsilon_0 \varepsilon_r\, \mathbf{E}_E \tag{3.34}$$

By taking into account the transformation rules (2.63) and (2.64) the above equations can be rewritten with respect to material coordinates as

$$\mathbf{D}_0 = \varepsilon_0 \varepsilon_r C^{1/2}\, \mathbf{C}^{-1} \mathbf{E}_0 \tag{3.35}$$

In analogy to the mechanical constitutive equation (3.7), this electric constitutive equation can also be gained by differentiation of the electric field energy. Hence,

$$\mathbf{E}_0 = \frac{\partial e_0(\mathbf{C}, \mathbf{D}_0)}{\partial \mathbf{D}_0} = \frac{1}{\varepsilon_0 \varepsilon_r C^{1/2}}\, \mathbf{C}\mathbf{D}_0 \tag{3.36}$$

If the considered strain energy function Ψ is eletromechanically coupled, as presented in the subsequent section, it also comprises the Lagrangian eletric field energy and therefore

$$\mathbf{E}_0 = \frac{\partial e_0(\mathbf{C}, \mathbf{D}_0)}{\partial \mathbf{D}_0} = \frac{\partial \Psi}{\partial \mathbf{D}_0} \tag{3.37}$$

This constitutive equation is an isotropic relation. Making use if it is reasonable, as fibre reinforcement of EAPs only evokes mechanical anisotropy and not electric [SSG17].

However for different types of material, there are other possibilities to formulate the material's reaction on evoked electric fields which are stated here. One anisotropic approach is to incorporate a tensorial value for the relative permittivity $\boldsymbol{\varepsilon}_r \in \mathbb{R}^{3\times 3}$ [LL60]. Hence, a recast of the constitutive equation (3.35) in the form of

$$\mathbf{D}_0 = \varepsilon_0 C^{1/2}\, \boldsymbol{\varepsilon}_r\, \mathbf{C}^{-1}\, \mathbf{E}_0 \tag{3.38}$$

with the matrix representation of $\boldsymbol{\varepsilon}_r$ as

$$[\boldsymbol{\varepsilon}_\mathbf{r}] = \begin{bmatrix} \varepsilon_{r11} & \varepsilon_{r12} & \varepsilon_{r13} \\ \varepsilon_{r21} & \varepsilon_{r22} & \varepsilon_{r23} \\ \varepsilon_{r31} & \varepsilon_{r32} & \varepsilon_{r33} \end{bmatrix} \tag{3.39}$$

would emerge.

Another possible way to define an anisotropic constitutive equation for dielectrics would be to consider the so-called polarisation density $\mathbf{P}_0$ [DO14]. Thus, the electric displacement in an electroactive material would be defined as

$$\mathbf{D}_0 = \varepsilon_0\, C^{1/2}\, \mathbf{C}^{-1}\, \mathbf{E}_0 + \mathbf{P}_0 \tag{3.40}$$

On that account, anisotropy would be comprised within $\mathbf{P}_0$ and (3.35) would therefore be replaced.

3.4 Transversely Isotropic Electromechanically Coupled Material Model

As it is the aim of this work to take account of transversely isotropic material descriptions, a new material model is proposed in the following. The complete strain energy function in terms of the symmetric strain measures can be formulated as the summation of three individual parts

$$\Psi(\mathbf{C}, \mathbf{G}, C, \mathbf{D}_0) = \Psi^{MR}(\mathbf{C}, \mathbf{G}, C) + \Psi^{TI}(\mathbf{C}, \mathbf{G}, C) + \Psi^{EL}(\mathbf{C}, C, \mathbf{D}_0) \tag{3.41}$$

The first part is one possible recast of the isotropic Mooney-Rivlin model in the form of

$$\Psi^{MR}(\mathbf{C}, \mathbf{G}, C) = a\,[\mathrm{tr}(\mathbf{C}) - 3] + b\,[\mathrm{tr}(\mathbf{G}) - 3] + c\,[C^{1/2} - 1]^2 - d\ln(C^{1/2}) \tag{3.42}$$

It vanishes in the reference configuration, meaning $\mathbf{C} = \mathbf{I}$, $\mathbf{G} = \mathbf{I}$ and $C = 1$, due to its build up automatically, as constant parts are incorporated. This is a rather theoretical property, as the deformations are gouverned by the derivatives of the strain energy function. To give a stress free reference configuration the condition (3.29) is inevitable. The fact that the second invariant of a tensor equals the first invariant of the tensors cofactor

$$II_{\mathbf{C}} = I_{\mathbf{G}} = \mathrm{tr}(\mathbf{G}) \tag{3.43}$$

has been taken into account. To achieve multi-variable convexity, or also called polyconvexity, the material constants a, b and c need to be strictly positive [BJH17]. This concept was introduced particularly for coupled problems with several independent arguments.

The second term enhances the mechanical part with transversely isotropic terms including a structural tensor $\mathbf{M}$ which is an even function of an unit orientation vector $\mathbf{a}_0$ for the preferred direction in the material, e.g. the one of reinforcement fibres

$$\mathbf{M} = \mathbf{a}_0 \otimes \mathbf{a}_0 \tag{3.44}$$

Thus, the transversely isotropic part of (3.41) reads

$$\Psi^{TI}(\mathbf{C}, \mathbf{G}, C) = g_0 \left[\frac{1}{g_{\mathbf{C}} + 1} \mathrm{tr}(\mathbf{C}\,\mathbf{M})^{g_{\mathbf{C}}+1} + \frac{1}{g_{\mathbf{G}} + 1} \mathrm{tr}(\mathbf{G}\,\mathbf{M})^{g_{\mathbf{G}}+1} + \frac{1}{g_C}\, C^{-g_C} \right] - \Psi_0^{TI} \tag{3.45}$$

where the constant part Ψ_0^{TI} is proposed for the purpose of a vanishing strain energy in the reference confifguration. For $\Psi_0^{TI} = 0$ the transversely isotropic model introduced by [SWB11] is achieved. In order to fulfill the conditions (3.3) and (3.4) an appropriate form

would be given as

$$\Psi_0^{TI} = g_0 \left[\frac{1}{g_{\mathbf{C}} + 1} + \frac{1}{g_{\mathbf{G}} + 1} + \frac{1}{g_C} \right] \tag{3.46}$$

where use has been made of the property $\mathrm{tr}(\mathbf{M}) = 1$ which comes from $\mathbf{a}_0$ being an unit vector. To achieve a stress-free reference configuration and the mathematical property of polyconvexity the scalar valued material parameters need to satisfy the conditions

$$g_0 > 0 \ , \ g_{\mathbf{C}} > 0 \ , \ g_{\mathbf{G}} > 0 \ , \ g_C > 1 \tag{3.47}$$

Note, that if the strain energy function is written as a function of the invariants (3.18)-(3.20), the terms $\mathrm{tr}(\mathbf{CM})$ and $\mathrm{tr}(\mathbf{GM})$ can be rewritten by making use of (3.44). Therefore, they form additional invariants as

$$\mathrm{tr}(\mathbf{C}\,\mathbf{M}) = \mathbf{a}_0 \cdot \mathbf{C}\,\mathbf{a}_0, =: I_4(\mathbf{C}, \mathbf{a}_0) \qquad \mathrm{tr}(\mathbf{G}\,\mathbf{M}) = \mathbf{a}_0 \cdot \mathbf{G}\,\mathbf{a}_0 =: I_5(\mathbf{G}, \mathbf{a}_0) \tag{3.48}$$

On that account, (3.45) could also be formulated entirely in terms of invariants.

The last part of (3.41), which aims to take account of electroactivity, refers to the internal energy of solids in electric fields (2.78) and is given as

$$\Psi^{EL}(\mathbf{C}, C, \mathbf{D}_0) = \frac{1}{2\varepsilon_0 \varepsilon_r C^{1/2}}\, \mathbf{D}_0 \cdot \mathbf{C}\,\mathbf{D}_0 \tag{3.49}$$

For the subsequent implementations the derivatives with respect to $\mathbf{C}, \mathbf{G}, C$ and $\mathbf{D}_0$ respectively are needed. They can be found in Appendix A.3.

4 Boundary Value Problem and Numerical Treatment

In this section the BVP is formulated in its entirety pointing out the two possible approaches. At first, equations are considered to be locally defined. As continuity conditions are very strong for this case, this approach is referred to as "strong form" of the BVP. In a next step, the same fundamental equations are recasted as integral formulations. As they are considered globally, continuity conditions are rather weak, which leads to the terminology "weak form" of the problem. By making use of variational calculus, stationarity conditions are derived, which can be discretised in the next step. This numerical discretisation takes place within the frame of the FEM. It is state of the art for solving BVPs in the field of compuational mechanics numerically. In the end, an algebraic set of equations is generated.

4.1 Differential Form of the Problem

The coupled local form of the BVP of large strain static electromechanics comes in its Lagrangian description and with symmetric quantities. The equilibrium equations consist of the equilibrium of linear momentum (2.40) for statics and the electric Gauss' law (2.59)

$$\mathrm{Div}(\mathbf{F}\,\mathbf{S}) + \mathbf{B} = 0 \qquad \forall\ \mathbf{X} \in \mathcal{B}_0 \tag{4.1}$$

$$\mathrm{Div}(\mathbf{D}_0) = \rho_0^e \qquad \forall\ \mathbf{X} \in \mathcal{B}_0 \tag{4.2}$$

The above equations describe the material's reaction in the terms of the 2nd PK and the electric displacement. Deformation and the electric potential, are described via the kinematical symmetric measures (2.12),(2.19),(2.20) and the static Faraday's law (2.70).

Constitutive equations are relations between strain and stress tensors as well as electric field and electric displacement field. They have already been introduced in the previous chapter as

$$\mathbf{S} = 2\,\frac{\partial \Psi}{\partial \mathbf{C}} \tag{4.3}$$

$$\mathbf{E}_0 = \frac{\partial \Psi}{\partial \mathbf{D}_0} \tag{4.4}$$

In order to guarantee the uniqueness of the problem boundary conditions (BCs) have to be included. We consider two different types of BCs. The so-called Dirichlet BCs

$$\boldsymbol{\varphi}(\mathbf{X}) = \overline{\boldsymbol{\varphi}}(\mathbf{X}) \qquad \forall\ \mathbf{X} \in \partial\mathcal{B}_0^{\boldsymbol{\varphi}} \tag{4.5}$$

$$\phi(\mathbf{X}) = \overline{\phi}(\mathbf{X}) \qquad \forall\ \mathbf{X} \in \partial\mathcal{B}_0^{\phi} \tag{4.6}$$

set precise values for the unknowns at certain points on the boundary. The domains $\mathcal{B}_0^{\varphi}$ and $\mathcal{B}_0^{\phi}$ denote the boundaries on which specific values of $\boldsymbol{\varphi}$ and ϕ are given. Therefore, given quantities are from now on denoted as $\overline{(\bullet)}$. And then there are Neumann BCs which are expressions of Cauchy's theorem (2.24) and the electric quantity ω_0^e (2.66)

$$(\mathbf{F}\,\mathbf{S}) \cdot \mathbf{N} = \overline{\mathbf{T}} \qquad \forall\ \mathbf{X} \in \partial\mathcal{B}_0^{\sigma} \tag{4.7}$$

$$(\mathbf{F}\,\mathbf{S}) \cdot \mathbf{N} = \mathbf{0} \qquad \forall\ \mathbf{X} \in \partial\mathcal{B}_0^{\varphi} \tag{4.8}$$

$$-\mathbf{D}_0 \cdot \mathbf{N} = \overline{\omega}_0^e \qquad \forall\ \mathbf{X} \in \partial\mathcal{B}_0^{\omega} \tag{4.9}$$

$$-\mathbf{D}_0 \cdot \mathbf{N} = 0 \qquad \forall\ \mathbf{X} \in \partial\mathcal{B}_0^{\phi} \tag{4.10}$$

The domains $\mathcal{B}_0^{\sigma}$ and $\mathcal{B}_0^{\omega}$ denote the boundaries on which specific values of $\boldsymbol{\sigma}$ and ω are given. The following relations between the particular boundaries hold:

$$\partial\mathcal{B}_0^{\varphi} \subset \partial\mathcal{B}_0 \qquad \partial\mathcal{B}_0^{\varphi} \cup \partial\mathcal{B}_0^{\sigma} = \partial\mathcal{B}_0 \tag{4.11}$$

$$\partial\mathcal{B}_0^{\sigma} \subset \partial\mathcal{B}_0 \qquad \partial\mathcal{B}_0^{\varphi} \cap \partial\mathcal{B}_0^{\sigma} = \varnothing \tag{4.12}$$

And the electric boundaries fulfill the conditions

$$\partial\mathcal{B}_0^{\omega} \subset \partial\mathcal{B}_0 \qquad \partial\mathcal{B}_0^{\omega} \cup \partial\mathcal{B}_0^{\phi} = \partial\mathcal{B}_0 \tag{4.13}$$

$$\partial\mathcal{B}_0^{\phi} \subset \partial\mathcal{B}_0 \qquad \partial\mathcal{B}_0^{\omega} \cap \partial\mathcal{B}_0^{\phi} = \varnothing \tag{4.14}$$

Neumann BCs determine the problem indirectly by giving values for the derivated quantities of the unknowns.

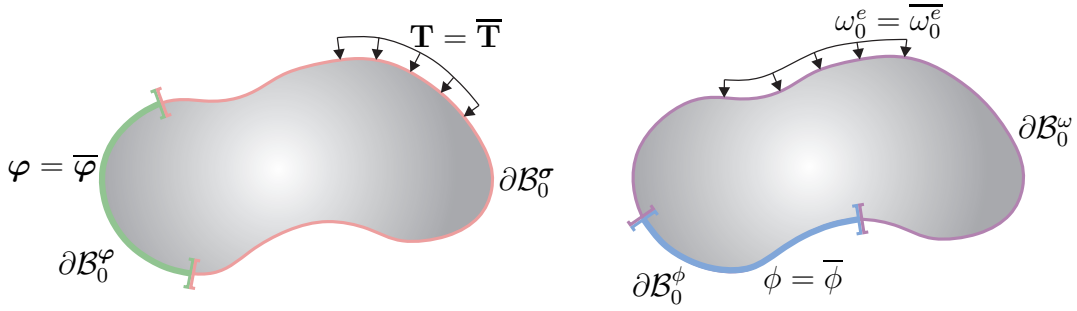

Figure 7: Mechanical (left) and electric (right) boundaries of the BVP

4.2 Weak Form and Variational Approach

Another possibility to describe a BVP is the weak formulation. Herein, an integral description which has inferior continuity requirements for the solution of the problem evokes. There a two ways to do so.

First, one can derive a weak form by considering the differential equations, which are

scalar multiplied with test functions for the unknowns, e.g. $\delta\boldsymbol{\varphi}$, and integrated over the whole domain $\mathcal{B}_0$. By taking account of mathematical laws, commonly the divergence theorem (A.7), the final weak form is achieved and Neumann BCs can be included herein. This procedure poses strictly mathematical and is for the sake of conciseness not presented at this point. It can be looked up in [Wri01] or [Bet13].

The second and rather physically insightful way is to work with the equilibrium of total potential (2.47) and hence incorporate the formerly introduced strain energy function in the sense of (2.51) and (3.1). The principle of the stationarity is used to claim that total potential is constant.

The simplest form of the total elastic potential in analogy to purely mechanical forms reads as

$$\hat{\Pi}(\boldsymbol{\varphi}, \mathbf{D}_0) = \int_{\mathcal{B}_0} e(\boldsymbol{\varphi}, \mathbf{D}_0)\,\mathrm{d}V + \Pi_m^{ext}(\boldsymbol{\varphi}) \tag{4.15}$$

Therefore, all electric impacts are comprised within the internal energy which is extended in the sense of (3.41). The external potential represents the external mechanical energy (2.50) and is shown here again for the sake of completeness

$$\Pi_m^{ext}(\boldsymbol{\varphi}) = -\int_{\mathcal{B}_0} \overline{\mathbf{B}} \cdot \mathbf{U}\,\mathrm{d}V - \int_{\partial\mathcal{B}_0^\sigma} \overline{\mathbf{T}} \cdot \mathbf{U}\,\mathrm{dA} \tag{4.16}$$

Moreover, the electric conditions

$$\mathrm{Div}(\mathbf{D}_0) = \overline{\rho}_0^e \qquad \text{in } \mathcal{B}_0 \tag{4.17}$$

$$-\mathbf{D}_0 \cdot \mathbf{N} = \overline{\omega}_0^e \qquad \text{on } \partial\mathcal{B}_0^\omega \tag{4.18}$$

need to be enforced. This formulation has been presented by [GO16]. This work also provided a second formulation which can be derived under the use of the electric potential which acts as a Langrange multiplier (see, e.g. [GO16]) and enforces the conditions (4.17),(4.18) as

$$\begin{aligned}\Pi(\boldsymbol{\varphi}, \phi, \mathbf{D}_0) = &\int_{\mathcal{B}_0} e(\boldsymbol{\varphi}, \mathbf{D}_0)\,\mathrm{d}V + \int_{\mathcal{B}_0} \phi\,(\overline{\rho}_0^e - \mathrm{Div}(\mathbf{D}_0))\,\mathrm{d}V \\ &+ \int_{\partial\mathcal{B}_0^\omega} \phi\,(\overline{\omega}_0^e + \mathbf{D}_0 \cdot \mathbf{N})\,\mathrm{dA} + \Pi_m^{ext}(\boldsymbol{\varphi})\end{aligned} \tag{4.19}$$

Considering the divergence theorem in the special form of (A.8) we obtain the recast

$$\Pi(\boldsymbol{\varphi}, \phi, \mathbf{D}_0) = \int_{\mathcal{B}_0} e(\boldsymbol{\varphi}, \mathbf{D}_0) + \mathrm{D}\phi \cdot \mathbf{D}_0 + \phi \left[-\mathrm{Div}(\mathbf{D}_0) + \mathrm{Div}(\mathbf{D}_0) + \overline{\rho}_0^e\right] \mathrm{d}V \tag{4.20}$$

$$+ \int_{\partial\mathcal{B}_0^\omega} \phi \overline{\omega}_0^e \, \mathrm{dA} + \Pi_m^{ext}(\boldsymbol{\varphi}) \tag{4.21}$$

Making use of the definition of a Helmholtz-like energy density Υ [GO16] as

$$\Upsilon(\boldsymbol{\varphi}, \phi, \mathbf{D}_0) = e(\boldsymbol{\varphi}, \mathbf{D}_0) + \mathrm{D}\phi \cdot \mathbf{D}_0 \tag{4.22}$$

we can formulate the final potential function in the form of

$$\Pi(\boldsymbol{\varphi}, \phi, \mathbf{D}_0) = \int_{\mathcal{B}_0} \Upsilon(\boldsymbol{\varphi}, \phi, \mathbf{D}_0) \, \mathrm{d}V + \Pi^{ext}(\boldsymbol{\varphi}, \phi) \tag{4.23}$$

Hereby, the electric displacement $\mathbf{D}_0$ and the electric potential ϕ will be regarded as independent variables as well as $\boldsymbol{\varphi}$. This variational principle was already included in [GO16, OFJ+]. The external potential is split into mechanical and electric parts as

$$\Pi^{ext} = \Pi_m^{ext}(\boldsymbol{\varphi}) + \Pi_e^{ext}(\phi) \tag{4.24}$$

$$\Pi_m^{ext}(\boldsymbol{\varphi}) = -\int_{\mathcal{B}_0} \overline{\mathbf{B}} \cdot \mathbf{U} \, \mathrm{d}V - \int_{\partial\mathcal{B}_0^\sigma} \overline{\mathbf{T}} \cdot \mathbf{U} \, \mathrm{dA} \tag{4.25}$$

$$\Pi_e^{ext}(\phi) = \int_{\mathcal{B}} \overline{\rho}_0^e \phi \, \mathrm{d}V + \int_{\partial\mathcal{B}_0^\omega} \overline{\omega}_0^e \phi \, \mathrm{dA} \tag{4.26}$$

As we want to make use of symmetric strain measures the internal energy is formulated as a strain energy function W_{sym}, which is inspired by the concept of polyconvexity. It represents the transversely isotropic, electromechanically coupled function Ψ which was derived in section 3.4 and is given in (3.41) as

$$e(\boldsymbol{\varphi}, \mathbf{D}_0) = \Psi(\mathbf{C}(\boldsymbol{\varphi}), \mathbf{G}(\boldsymbol{\varphi}), C(\boldsymbol{\varphi}), \mathbf{D}_0) =: W_{sym}(\boldsymbol{\varphi}, \mathbf{D}_0) \tag{4.27}$$

Hence, the final potential function reads

$$\Pi(\boldsymbol{\varphi}, \phi, \mathbf{D}_0) = \int_{\mathcal{B}_0} \left[W_{sym}(\boldsymbol{\varphi}, \mathbf{D}_0) + \mathrm{D}\phi \cdot \mathbf{D}_0\right] \mathrm{d}V + \Pi^{ext}(\boldsymbol{\varphi}, \phi) \tag{4.28}$$

To achieve the weak form of the BVP the stationarity condition is applied. On that account, the variations (see Chapter 2.3.2 for an introduction) of the potential function with respect to the three individual unknowns $\{\boldsymbol{\varphi}, \phi, \mathbf{D}_0\}$ yield the weak forms of the

problem as

$$\mathcal{W}_{\boldsymbol{\varphi}} = \delta_{\boldsymbol{\varphi}}\Pi = \mathrm{D}_1\Pi(\boldsymbol{\varphi}, \phi, \mathbf{D}_0) \cdot \delta\boldsymbol{\varphi} \qquad = \int_{\mathcal{B}_0} \mathbf{S} : \frac{1}{2}\,\delta\mathbf{C}\,\mathrm{d}V + \delta_{\boldsymbol{\varphi}}\Pi_m^{ext} = 0 \tag{4.29}$$

$$\mathcal{W}_{\phi} = \delta_{\phi}\Pi = \mathrm{D}_2\Pi(\boldsymbol{\varphi}, \phi, \mathbf{D}_0)\,\delta\phi \qquad = \int_{\mathcal{B}_0} \mathrm{D}\delta\phi \cdot \mathbf{D}_0\,\mathrm{d}V + \delta_{\phi}\Pi_e^{ext} = 0 \tag{4.30}$$

$$\mathcal{W}_{\mathbf{D}_0} = \delta_{\mathbf{D}_0}\Pi = \mathrm{D}_3\Pi(\boldsymbol{\varphi}, \phi, \mathbf{D}_0) \cdot \delta\mathbf{D}_0 \qquad = \int_{\mathcal{B}_0} \delta\mathbf{D}_0 \cdot \left(\frac{\partial W_{sym}}{\partial \mathbf{D}_0} + \mathrm{D}\phi\right)\mathrm{d}V = 0 \tag{4.31}$$

Due to claiming stationarity, the above equations strictly need to vanish. Hence, equations (4.29)-(4.31) represent the weak formulation of our BVP. The variations of the external potential which represents the external impacts therefore read

$$\delta_{\boldsymbol{\varphi}}\Pi_m^{ext} = -\int_{\mathcal{B}_0} \overline{\mathbf{B}} \cdot \delta\boldsymbol{\varphi}\,\mathrm{d}V - \int_{\partial\mathcal{B}_0^{\sigma}} \overline{\mathbf{T}} \cdot \delta\boldsymbol{\varphi}\,\mathrm{d}\mathrm{A} \tag{4.32}$$

$$\delta_{\phi}\Pi_e^{ext} = \int_{\mathcal{B}} \overline{\rho}_0^e \delta\phi\,\mathrm{d}V + \int_{\partial\mathcal{B}_0^{\omega}} \overline{\omega}_0^e \delta\phi\,\mathrm{d}\mathrm{A} \tag{4.33}$$

Moreover, as we want to take account of the cascade-shaped formulation (2.12),(2.19),(2.20) use has been made of the virtual symmetric kinematic measures which can be expressed as

$$\delta\mathbf{C} = \frac{\mathrm{d}}{\mathrm{d}\varepsilon}(\mathrm{D}\boldsymbol{\varphi}_{\varepsilon})^{\mathrm{T}}\mathrm{D}\boldsymbol{\varphi}_{\varepsilon}\Big|_{\varepsilon=0} = (\mathrm{D}\delta\boldsymbol{\varphi})^{\mathrm{T}}\mathrm{D}\boldsymbol{\varphi} + (\mathrm{D}\boldsymbol{\varphi})^{\mathrm{T}}\mathrm{D}\delta\boldsymbol{\varphi} \tag{4.34}$$

$$\delta\mathbf{G} = \frac{\mathrm{d}}{\mathrm{d}\varepsilon}\frac{1}{2}\,\mathbf{C}_{\varepsilon} \barwedge \mathbf{C}_{\varepsilon}\Big|_{\varepsilon=0} = \mathbf{C} \barwedge \delta\mathbf{C} \tag{4.35}$$

$$\delta C = \frac{\mathrm{d}}{\mathrm{d}\varepsilon}\det(\mathbf{C}_{\varepsilon})\Big|_{\varepsilon=0} = \mathrm{cof}(\mathbf{C}) : \frac{\mathrm{d}}{\mathrm{d}\varepsilon}\mathbf{C}_{\varepsilon}\Big|_{\varepsilon=0} = \mathbf{G} : \delta\mathbf{C} \tag{4.36}$$

where the subscript $(\bullet)_{\varepsilon}$ denotes that the respective quantity is evaluated at the point $(\boldsymbol{\varphi} + \varepsilon\,\delta\boldsymbol{\varphi})$. Thus, the 2nd PK unlike the formulation (4.3) in this case is extended as

$$\mathbf{S} = 2\Big(\boldsymbol{\Sigma}_{\mathbf{C}} + \boldsymbol{\Sigma}_{\mathbf{G}} \barwedge \mathbf{C} + \Sigma_C \mathbf{G}\Big) \tag{4.37}$$

and depends on the symmetric strain measures introduced (2.12),(2.19) and (2.20). Their work conjugated stresses are achieved via differentiation of the strain energy function

$$\boldsymbol{\Sigma}_{\mathbf{C}} = \frac{\partial W_{sym}}{\partial \mathbf{C}}\ ,\ \boldsymbol{\Sigma}_{\mathbf{G}} = \frac{\partial W_{sym}}{\partial \mathbf{G}}\ ,\ \Sigma_C = \frac{\partial W_{sym}}{\partial C} \tag{4.38}$$

4.3 Finite Element Method

For applying the FEM the considered body $\mathcal{B}_0$ is approximated by dividing it into n_e finite elements with the domains Ω_e, such that

$$\mathcal{B}_0 \approx \mathcal{B}_0^h = \bigcup_{e=1}^{n_e} \Omega_e \tag{4.39}$$

For the boundary $\partial\mathcal{B}_0$ of the body we similarly have

$$\partial\mathcal{B}_0 \approx \partial\mathcal{B}_0^h = \bigcup_{e=1}^{n_e} \partial\Omega_e \tag{4.40}$$

The finite elements are neither allowed to overlap nor to occupy gaps in between. The shape of the elements is determined by its so-called nodes and the surrounding elements have to share the same nodes. On that account a node must not be situated on the surface or the edge of another element.

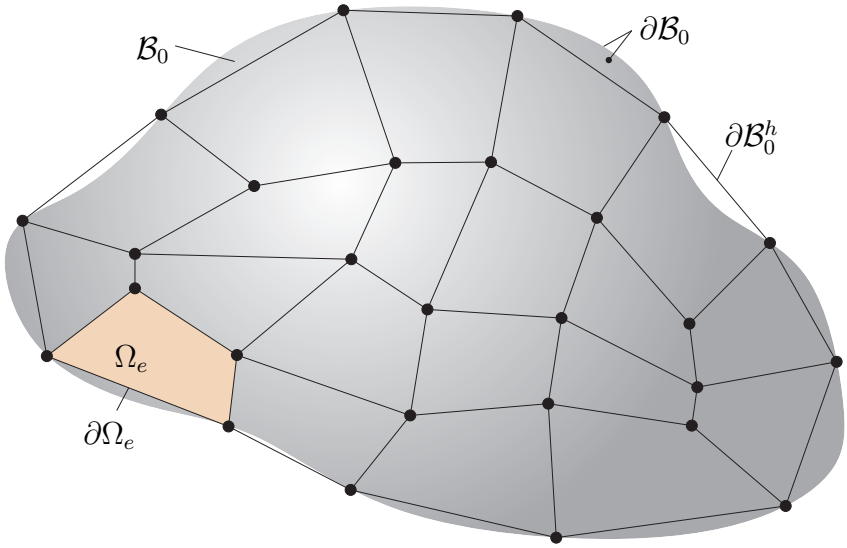

Figure 8: FE discretisation of a continuum

4.3.1 Isoparametric Concept

The individual unknowns are approximated individually as well as the bodies geometry

$$\boldsymbol{\varphi}(\mathbf{X}) \approx \boldsymbol{\varphi}^h(\mathbf{X}) \tag{4.41}$$

$$\phi(\mathbf{X}) \approx \phi^h(\mathbf{X}) \tag{4.42}$$

$$\mathbf{D}_0(\mathbf{X}) \approx \mathbf{D}_0^h(\mathbf{X}) \tag{4.43}$$

$$\mathbf{X} \approx \mathbf{X}^h \tag{4.44}$$

The isoparametric concept states, that the geometry is approximated with the same type of shape functions as the unknowns of the problem. Here we use standard Lagrange shape function polynomials $N_I(\mathbf{X})$

$$\boldsymbol{\varphi}^h(\mathbf{X}) = \sum_{A=1}^{n} N_A^{\boldsymbol{\varphi}}(\mathbf{X})\, \boldsymbol{\varphi}_A \qquad \delta\boldsymbol{\varphi}^h(\mathbf{X}) = \sum_{A=1}^{n} N_A^{\boldsymbol{\varphi}}(\mathbf{X})\, \delta\boldsymbol{\varphi}_A \tag{4.45}$$

$$\phi^h(\mathbf{X}) = \sum_{A=1}^{n} N_A^{\phi}(\mathbf{X})\, \phi_A \qquad \delta\phi^h(\mathbf{X}) = \sum_{A=1}^{n} N_A^{\phi}(\mathbf{X})\, \delta\phi_A \tag{4.46}$$

$$\mathbf{D}_0^h(\mathbf{X}) = \sum_{A=1}^{n} N_A^{\mathbf{D}_0}(\mathbf{X})\, (\mathbf{D}_0)_A \qquad \delta\mathbf{D}_0^h(\mathbf{X}) = \sum_{A=1}^{n} N_A^{\mathbf{D}_0}(\mathbf{X})\, (\delta\mathbf{D}_0)_A \tag{4.47}$$

where n denotes the total amount of nodes considered in the FE model. Taking account of the isoparametric concept, the order of interpolation also determines the approximation of geometry and hence the finite elements' shape

$$\mathbf{X}^h = \sum_{A=1}^{n} N_A^{\mathbf{X}}(\mathbf{X})\, \mathbf{X}_A \tag{4.48}$$

For example, for the case of linear shape functions and $n = 8$ nodes, elements are hexahedrons with one node at each corner and have surfaces and edges that can be described by linear polynomials.

In equation (4.48), N_A are the global Langrange shape functions for the approximation of $\mathbf{X}$. Moreover, $N_A^{\mathbf{X}}(\mathbf{X}) = N_A^{\boldsymbol{\varphi}}(\mathbf{X})$. The superscript h symbolises the approximative nature and can be omitted for the sake of clearness. $\mathbf{X}_A, \boldsymbol{\varphi}_A, \phi_A$ and $(\mathbf{D}_0)_A$ and their corresponding variational unknowns are the unknown nodal quantities - scalar or tensor valued - at the node A. Moreover, the global shape functions are build up in such a way, that they become 1 at one specific node and vanish at all the other nodes. Hence, the approximated quantities attain the nodal values at the nodes and are interpolated in between depending on the chosen order of interpolation, e.g. linearly or quadratically.

Considering the above approximations, the sets of all admissible solutions can be defined as

$$\boldsymbol{\varphi}^h \in \mathcal{C}_{\boldsymbol{\varphi}} = \{\boldsymbol{\varphi}^h : \mathcal{B}_0^h \to \mathbb{R}^3 \,|\, \boldsymbol{\varphi}^h \in H^1(\mathcal{B}_0^h),\, \boldsymbol{\varphi}^h(\mathbf{X}) = \overline{\boldsymbol{\varphi}}(\mathbf{X}) \,\forall\, \mathbf{X} \in \partial\mathcal{B}_0^{\boldsymbol{\varphi}}\} \tag{4.49}$$

$$\phi^h \in \mathcal{C}_{\phi} = \{\phi^h : \mathcal{B}_0^h \to \mathbb{R} \,|\, \phi^h \in H^1(\mathcal{B}_0^h),\, \phi^h(\mathbf{X}) = \overline{\phi}(\mathbf{X}) \,\forall\, \mathbf{X} \in \partial\mathcal{B}_0^{\phi}\} \tag{4.50}$$

$$\mathbf{D}_0^h \in \mathcal{C}_{\mathbf{D}_0} = \{\mathbf{D}_0^h : \mathcal{B}_0^h \to \mathbb{R}^3 \,|\, \mathbf{D}_0^h \in \mathbb{L}_2(\mathcal{B}_0^h)\} \tag{4.51}$$

where H^1 denotes a H^1 Sobolev space, which means that the all contained functions and any derivative of them until the i-th have to be square integrable functions. That

corresponds to C^0 continuity of the related variable. Hence, $\boldsymbol{\varphi}$ and ϕ are approximated continuously beyond the element borders but do not necessarily need to be continuously differentiable. $\mathbf{D}_0$ is, as already pointed out, discontinuously approximated beyond the element borders. It only needs to be square integrable and therefore comes out of the $\mathbb{L}_2$ space. This makes the inferior continuity requirements due to the weak formulation of the BVP obvious. The variational unknown need to vanish where Dirichlet BCs apply. This fact is referred to as essential BC. The corresponding sets of all admissible variations therefore read

$$\delta\boldsymbol{\varphi}^h \in \mathcal{V}_{\boldsymbol{\varphi}} = \{\delta\boldsymbol{\varphi}^h : \mathcal{B}_0^h \to \mathbb{R}^3 \,|\, \delta\boldsymbol{\varphi}^h \in H^1(\mathcal{B}_0^h),\, \delta\boldsymbol{\varphi}^h(\mathbf{X}) = \mathbf{0}\,\forall\,\mathbf{X} \in \partial\mathcal{B}_0^{\boldsymbol{\varphi}}\} \tag{4.52}$$

$$\delta\phi^h \in \mathcal{V}_{\phi} = \{\delta\phi^h : \mathcal{B}_0^h \to \mathbb{R} \,|\, \delta\phi^h \in H^1(\mathcal{B}_0^h),\, \delta\phi^h(\mathbf{X}) = 0\,\forall\,\mathbf{X} \in \partial\mathcal{B}_0^{\phi}\} \tag{4.53}$$

$$\delta\mathbf{D}_0^h \in \mathcal{V}_{\mathbf{D}_0} = \{\mathbf{D}_0^h : \mathcal{B}_0^h \to \mathbb{R}^3 \,|\, \mathbf{D}_0^h \in \mathbb{L}_2(\mathcal{B}_0^h)\} \tag{4.54}$$

Furthermore, the quantities can be defined within the finite elements. As all the elements have a similar build-up on that account, it is expedient to work with a reference domain in which all the computations can be parallelized. The coordinates in the reference domain are changed to reference coordinates $\boldsymbol{\xi}$ with the basis vector $\mathbf{e}_\xi$ and thus also the shape functions are formulated in dependence of $\boldsymbol{\xi}$ so that the approximation of the material coordinates within an element can be expressed as

$$\mathbf{X}_e(\boldsymbol{\xi}) = \sum_{I=1}^{n^{(e)}} N_I^{\mathbf{X}}(\boldsymbol{\xi})\,\mathbf{X}_I \tag{4.55}$$

In this last equation $n^{(e)}$ denotes the amount of nodes with respect to one single element. Hence, there is one shape function for each node. The shape functions are now locally defined and depend on the reference coordinates. Similar to the global approach, $N_I(\boldsymbol{\xi})$ attains the value 1 at the node I and vanishes at all the other nodes. For an example see Appendix A.2. The similar local approximation is applied to the unknowns (4.45)-(4.47)

$$\boldsymbol{\varphi}_e(\boldsymbol{\xi}) = \sum_{I=1}^{n^{(e)}} N_I^{\boldsymbol{\varphi}}(\boldsymbol{\xi})\,\boldsymbol{\varphi}_I \qquad \delta\boldsymbol{\varphi}_e(\boldsymbol{\xi}) = \sum_{I=1}^{n^{(e)}} N_I^{\boldsymbol{\varphi}}(\boldsymbol{\xi})\,\delta\boldsymbol{\varphi}_I \tag{4.56}$$

$$\phi_e(\boldsymbol{\xi}) = \sum_{I=1}^{n^{(e)}} N_I^{\phi}(\boldsymbol{\xi})\,\phi_I \qquad \delta\phi_e(\boldsymbol{\xi}) = \sum_{I=1}^{n^{(e)}} N_I^{\phi}(\boldsymbol{\xi})\,\delta\phi_I \tag{4.57}$$

$$\mathbf{D}_{0,e}(\boldsymbol{\xi}) = \sum_{I=1}^{n^{(e)}} N_I^{\mathbf{D}_0}(\boldsymbol{\xi})\,(\mathbf{D}_0)_I \qquad \delta\mathbf{D}_{0,e}(\boldsymbol{\xi}) = \sum_{I=1}^{n^{(e)}} N_I^{\mathbf{D}_0}(\boldsymbol{\xi})\,(\delta\mathbf{D}_0)_I \tag{4.58}$$

Furthermore, the introduced mapping into and out of the reference domain require a recast of the deformation gradient as

$$\mathbf{F}_e = \mathrm{Grad}(\boldsymbol{\varphi}_e) = \sum_{I=1}^{n^{(e)}} \boldsymbol{\varphi}_I \otimes \mathrm{Grad}(N_I^{\boldsymbol{\varphi}}) \tag{4.59}$$

By applying the chainrule we obtain

$$\mathbf{F}_e = \frac{\partial \boldsymbol{\varphi}_e}{\partial \mathbf{X}} = \frac{\partial \boldsymbol{\varphi}_e}{\partial \boldsymbol{\xi}} \frac{\partial \boldsymbol{\xi}}{\partial \mathbf{X}} = \mathbf{j}_e \, \mathbf{J}_e^{-1} \tag{4.60}$$

where the element-related Jacobi-matrices are defined as

$$\mathbf{j}_e = \mathrm{Grad}_{\boldsymbol{\xi}}(\mathbf{x}_e) = \sum_{I=1}^{n^{(e)}} N_{I,\boldsymbol{\xi}}(\boldsymbol{\xi}) \, \mathbf{x}_I \otimes \mathbf{e}_\xi = \sum_{I=1}^{n^{(e)}} \mathbf{x}_I \otimes \mathrm{Grad}_{\boldsymbol{\xi}}[N_I(\boldsymbol{\xi})] \tag{4.61}$$

$$\mathbf{J}_e = \mathrm{Grad}_{\boldsymbol{\xi}}(\mathbf{X}_e) = \sum_{I=1}^{n^{(e)}} N_{I,\boldsymbol{\xi}}(\boldsymbol{\xi}) \, \mathbf{X}_I \otimes \mathbf{e}_\xi = \sum_{I=1}^{n^{(e)}} \mathbf{X}_I \otimes \mathrm{Grad}_{\boldsymbol{\xi}}[N_I(\boldsymbol{\xi})] \tag{4.62}$$

They map the reference onto spatial or material line elements. Therefore, analogously to the deformation formulation (2.6) we obtain

$$\mathrm{d}\boldsymbol{\xi}_e = \mathbf{J}_e^{-1} \mathrm{d}\mathbf{X}_e = \mathbf{j}_e \mathrm{d}\mathbf{x}_e \tag{4.63}$$

and for the mapping of infinitesimal volume elements in the reference domain $\mathrm{d}\square$ some tedious algebra yields

$$\mathrm{d}V = \det(\mathbf{J}_e) \mathrm{d}\square \tag{4.64}$$

A concise depiction in two dimensions is given in Figure 9. Consequently, any computations and integrations in particular which are defined globally at the first place can be executed in the reference domain sticking to the scheme

$$\int_{\mathcal{B}_0} g(\mathbf{X}) \, \mathrm{d}V \approx \int_{\mathcal{B}_0^h} g(\mathbf{X}^h) \, \mathrm{d}V_h = \mathop{\mathsf{A}}_{e=1}^{n_e} \int_{\Omega_e} g(\mathbf{X}_e) \, \mathrm{d}V = \mathop{\mathsf{A}}_{e=1}^{n_e} \int_{\Omega_\square} g(\boldsymbol{\xi}) \, \det[\mathbf{J}_e(\boldsymbol{\xi})] \, \mathrm{d}\square \tag{4.65}$$

The first relation states, that integrals are only solved approximately due to the discretisation of the continuum and the unknown vector fields. The second relation performs the transformation from a node-bound definition of the approximation to an approach on element level. Therefore, the shape functions stay the same, but are ordered with respect to node numbers on element level. The so-called "*assembly-operator*" A assembles the individual nodal components of the nodes defined in the multiple elements to achieve global nodal values. Therefore, allocation information about which elements belong to which

node and herein degrees of freedom (DOFs) has to be used. In the last transformation, the Jacobian determinant needs to be incorporated in order to change the integration variable when regarding the reference domain. If solved numerically Gauss integration as described in section 2.3.4 needs to be employed. Hence, the last integral reads

$$\int_{\Omega_\square} g(\boldsymbol{\xi})\, \det[\mathbf{J}_e(\boldsymbol{\xi})]\, \mathrm{d}\square = \int_{-1}^{1}\int_{-1}^{1}\int_{-1}^{1} g(\xi,\eta,\zeta)\, \det[\mathbf{J}_e(\xi,\eta,\zeta)]\, \mathrm{d}\xi\mathrm{d}\eta\mathrm{d}\zeta \tag{4.66}$$

Finally, this process (4.65) leads to an algebraic system of nonlinear equations with the nodal values as unknowns as it is shown later.

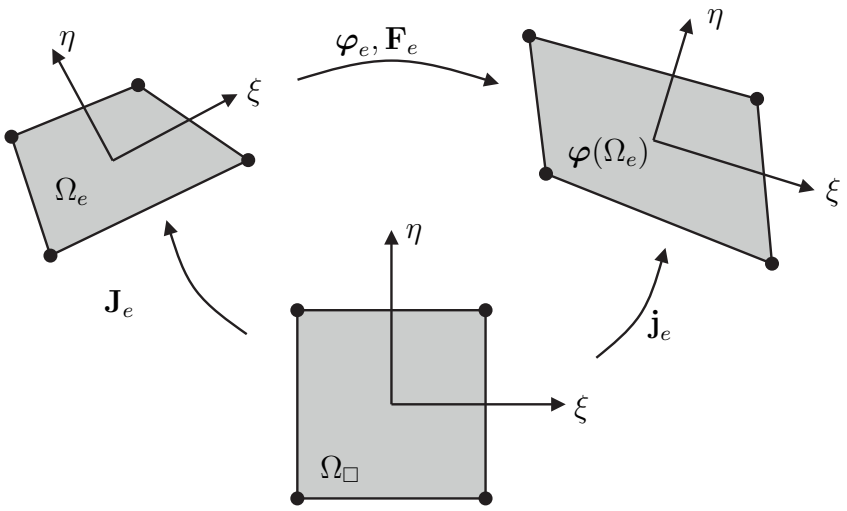

Figure 9: Isoparametric mapping of a finite element Ω_e

4.3.2 Discretization of the Weak Form

Plugging the local approximations (4.56)-(4.58) into the weak forms (4.29)-(4.31) and extracting the nodal unknowns yields the residual vectors which strictly need to vanish as follows:

$$\mathcal{W}^e_{\boldsymbol{\varphi}} = \delta\boldsymbol{\varphi}_I^{\mathrm{T}} \sum_{I=1}^{n^{(e)}} \mathbf{R}^{\boldsymbol{\varphi}}_{I,e} = 0 \tag{4.67}$$

$$\mathcal{W}^e_{\phi} = \delta\phi_I \sum_{I=1}^{n^{(e)}} R^{\phi}_{I,e} = 0 \tag{4.68}$$

$$\mathcal{W}^e_{\mathbf{D}_0} = \delta(\mathbf{D}_0)_I^{\mathrm{T}} \sum_{I=1}^{n^{(e)}} \mathbf{R}^{\mathbf{D}_0}_{I,e} = 0 \tag{4.69}$$

It is worth noting, that each node contributes to one entry of the residuals and that they are initially computed on element level

$$\mathbf{R}^{\boldsymbol{\varphi}}_{I,e} = \int\limits_{\Omega_e} \mathbf{B}_I^{\mathrm{T}}\, \mathbf{S}^{\mathrm{V}}\, \mathrm{d}V + \mathbf{R}^{m}_{I,e} \tag{4.70}$$

$$R^{\phi}_{I,e} = \int\limits_{\Omega_e} \mathrm{D}N_I^{\phi} \cdot \mathbf{D}_0\, \mathrm{d}V + R^{e}_{I,e} \tag{4.71}$$

$$\mathbf{R}^{\mathbf{D}_0}_{I,e} = \int\limits_{\Omega_e} N_I^{\mathbf{D}_0} \Big(\frac{\partial W_{sym}}{\partial \mathbf{D}_0} + \mathrm{D}\phi \Big)\, \mathrm{d}V \tag{4.72}$$

with the external residual parts concerning mechanical effects $\mathbf{R}^{m}_{I,e}$ and electric effects $R^{e}_{I,e}$ respectively, which read

$$\mathbf{R}^{m}_{I,e} = -\int\limits_{\Omega_e} N_I^{\boldsymbol{\varphi}}\, \overline{\mathbf{B}}\, \mathrm{d}V - \int\limits_{\partial\Omega_e} \tilde{N}_i^{\boldsymbol{\varphi}}\, \overline{\mathbf{T}}\, \mathrm{d}\mathrm{A} \tag{4.73}$$

$$R^{e}_{I,e} = \int\limits_{\Omega_e} N_I^{\phi} \overline{\rho}_0^{e}\, \mathrm{d}V + \int\limits_{\partial\Omega_e} \tilde{N}_I^{\phi} \overline{\omega}_0^{e}\, \mathrm{d}\mathrm{A} \tag{4.74}$$

where $\tilde{N}_i^{\boldsymbol{\varphi}}$ and $\tilde{N}_I^{\phi}$ denote Lagrange shape functions of the two-dimensional boundary area elements. The residuals are assembled later on. In the last equation the well known nodal operator matrix $\mathbf{B}$, also called B-matrix, with the components of the deformation gradient F_{ij} and partial derivatives of the displacement-related shape functions $N^{\boldsymbol{\varphi}}_{I,k}$

$$\mathbf{B}_I = \begin{bmatrix} F_{11}\, N^{\boldsymbol{\varphi}}_{I,1} & F_{21}\, N^{\boldsymbol{\varphi}}_{I,1} & F_{31}\, N^{\boldsymbol{\varphi}}_{I,1} \\ F_{12}\, N^{\boldsymbol{\varphi}}_{I,2} & F_{22}\, N^{\boldsymbol{\varphi}}_{I,2} & F_{32}\, N^{\boldsymbol{\varphi}}_{I,2} \\ F_{13}\, N^{\boldsymbol{\varphi}}_{I,3} & F_{23}\, N^{\boldsymbol{\varphi}}_{I,3} & F_{33}\, N^{\boldsymbol{\varphi}}_{I,3} \\ F_{11}\, N^{\boldsymbol{\varphi}}_{I,2} + F_{12}\, N^{\boldsymbol{\varphi}}_{I,1} & F_{21}\, N^{\boldsymbol{\varphi}}_{I,2} + F_{22}\, N^{\boldsymbol{\varphi}}_{I,1} & F_{31}\, N^{\boldsymbol{\varphi}}_{I,2} + F_{32}\, N^{\boldsymbol{\varphi}}_{I,1} \\ F_{12}\, N^{\boldsymbol{\varphi}}_{I,3} + F_{13}\, N^{\boldsymbol{\varphi}}_{I,2} & F_{22}\, N^{\boldsymbol{\varphi}}_{I,3} + F_{23}\, N^{\boldsymbol{\varphi}}_{I,2} & F_{32}\, N^{\boldsymbol{\varphi}}_{I,3} + F_{33}\, N^{\boldsymbol{\varphi}}_{I,2} \\ F_{11}\, N^{\boldsymbol{\varphi}}_{I,3} + F_{13}\, N^{\boldsymbol{\varphi}}_{I,1} & F_{21}\, N^{\boldsymbol{\varphi}}_{I,3} + F_{23}\, N^{\boldsymbol{\varphi}}_{I,1} & F_{31}\, N^{\boldsymbol{\varphi}}_{I,3} + F_{33}\, N^{\boldsymbol{\varphi}}_{I,1} \end{bmatrix} \tag{4.75}$$

that is used for incorporating Voigt notation (see Appendix A.4) has been introduced. Thus, the B-matrix is needed when it comes to the transformation of $\delta\mathbf{C}$

$$\delta\mathbf{E}^{\mathrm{V}} = \begin{bmatrix} \delta E_{11} \\ \delta E_{22} \\ \delta E_{33} \\ 2\delta E_{12} \\ 2\delta E_{23} \\ 2\delta E_{13} \end{bmatrix} = \frac{1}{2}\, \delta\mathbf{C}^{\mathrm{V}} = \sum_{I=1}^{n} \mathbf{B}_I\, \delta\boldsymbol{\varphi}_I \tag{4.76}$$

4.3.3 Derivation of an Algebraic Set of Equations

Eventually, equations (4.67) - (4.69) are to be solved by conducting Newton's method as presented in Chapter 2.3.3. On that account it is necessary to build up elementwise defined tangent matrices. Note that these matrices fulfill the purpose of elasticity tensors (see Chapter 3.2.3) presented in Voigt notation. They emerge during linearising the equations which is further explained in Chapter 2.3.1 with respect to each unknown. In the same step approximations for the linearised variables $\Delta\boldsymbol{\varphi}, \Delta\phi$ and $\Delta\mathbf{D}_0$ in sense of the isoparametric concept are incorporated, so that the tangential parts of the linearised residual vectors are as follows:

$$\mathrm{D}\mathbf{R}^{\boldsymbol{\varphi}}_{I,e} \cdot \Delta\boldsymbol{\varphi} = \sum_{J=1}^{n^{(e)}} (\mathbf{K}_{\boldsymbol{\varphi}\boldsymbol{\varphi}})^e_{IJ}\, \Delta\boldsymbol{\varphi}_J \tag{4.77}$$

$$\mathrm{D}\mathbf{R}^{\boldsymbol{\varphi}}_{I,e} \cdot \Delta\phi = \sum_{J=1}^{n^{(e)}} (\mathbf{K}_{\boldsymbol{\varphi}\phi})^e_{IJ}\, \Delta\phi_J \tag{4.78}$$

$$\mathrm{D}\mathbf{R}^{\boldsymbol{\varphi}}_{I,e} \cdot \Delta\mathbf{D}_0 = \sum_{J=1}^{n^{(e)}} (\mathbf{K}_{\boldsymbol{\varphi}\mathbf{D}_0})^e_{IJ}\, (\Delta\mathbf{D}_0)_J \tag{4.79}$$

$$\mathrm{D}R^{\phi}_{I,e}\, \Delta\boldsymbol{\varphi} = \sum_{J=1}^{n^{(e)}} (\mathbf{K}_{\phi\boldsymbol{\varphi}})^e_{IJ}\, \Delta\boldsymbol{\varphi}_J \tag{4.80}$$

$$\mathrm{D}R^{\phi}_{I,e}\, \Delta\phi = \sum_{J=1}^{n^{(e)}} (K_{\phi\phi})^e_{IJ}\, \Delta\phi_J \tag{4.81}$$

$$\mathrm{D}R^{\phi}_{I,e}\, \Delta\mathbf{D}_0 = \sum_{J=1}^{n^{(e)}} (\mathbf{K}_{\phi\mathbf{D}_0})^e_{IJ}\, (\Delta\mathbf{D}_0)_J \tag{4.82}$$

$$\mathrm{D}\mathbf{R}^{\mathbf{D}_0}_{I,e} \cdot \Delta\boldsymbol{\varphi} = \sum_{J=1}^{n^{(e)}} (\mathbf{K}_{\mathbf{D}_0\boldsymbol{\varphi}})^e_{IJ}\, \Delta\boldsymbol{\varphi}_J \tag{4.83}$$

$$\mathrm{D}\mathbf{R}^{\mathbf{D}_0}_{I,e} \cdot \Delta\phi = \sum_{J=1}^{n^{(e)}} (\mathbf{K}_{\mathbf{D}_0\phi})^e_{IJ}\, \Delta\phi_J \tag{4.84}$$

$$\mathrm{D}\mathbf{R}^{\mathbf{D}_0}_{I,e} \cdot \Delta\mathbf{D}_0 = \sum_{J=1}^{n^{(e)}} (\mathbf{K}_{\mathbf{D}_0\mathbf{D}_0})^e_{IJ}\, (\Delta\mathbf{D}_0)_J \tag{4.85}$$

The components of the tangential matrix related to $\boldsymbol{\varphi}$ have several parts and can thereby be split up into a geometrical part and several material ones as

$$(\mathbf{K}_{\boldsymbol{\varphi}\boldsymbol{\varphi}})^e_{IJ} = \mathbf{K}^{geo,e}_{IJ} + \sum_{i=1}^{7} \mathbf{K}^{mat,e,i}_{IJ} \tag{4.86}$$

The geometrical part of the stiffness matrix is the same as it is for variational principles purely formulated in the displacements

$$\mathbf{K}_{IJ}^{geo,e} = \int_{\Omega_e} (\mathrm{D}N_I^{\boldsymbol{\varphi}})^{\mathrm{T}}\, \mathbf{S}\, (\mathrm{D}N_J^{\boldsymbol{\varphi}})\, \mathrm{d}V \tag{4.87}$$

For the numerous material parts of $\mathbf{K}_{\varphi\varphi}$ please have a look at Appendix A.5. The other tangential matrices read

$$(\mathbf{K}_{\boldsymbol{\varphi}\phi})_{IJ}^e = (\mathbf{K}_{\phi\boldsymbol{\varphi}})_{IJ}^e = \mathbf{0} \tag{4.88}$$

$$(\mathbf{K}_{\phi\phi})_{IJ}^e = 0 \tag{4.89}$$

$$(\mathbf{K}_{\boldsymbol{\varphi}\mathbf{D}_0})_{IJ}^e = (\mathbf{K}_{\mathbf{D}_0\boldsymbol{\varphi}})_{IJ}^e = \int_{\Omega_e} \left[\mathbf{B}_I^{\mathrm{T}}\, \frac{1}{\varepsilon_0 \varepsilon_r C^{1/2}}\, \mathbf{B}_J^{el} + (\mathbf{B}_I^{\mathrm{T}}\, \mathbf{G}^{\mathrm{V}}) \otimes N_J^{\mathbf{D}_0}\, \frac{\partial W_{sym}}{\partial \mathbf{D}_0 \partial C} \right] \mathrm{d}V \tag{4.90}$$

$$(\mathbf{K}_{\phi\mathbf{D}_0})_{IJ}^e = (\mathbf{K}_{\mathbf{D}_0\phi}^{\mathrm{T}})_{IJ}^e = \int_{\Omega_e} N_I^{\mathbf{D}_0}\, \mathrm{D}N_J^{\phi}\, \mathrm{d}V \tag{4.91}$$

$$(\mathbf{K}_{\mathbf{D}_0\mathbf{D}_0})_{IJ}^e = \int_{\Omega_e} N_I^{\mathbf{D}_0}\, \frac{\partial^2 W_{sym}}{\partial \mathbf{D}_0^2}\, N_J^{\mathbf{D}_0}\, \mathrm{d}V \tag{4.92}$$

$$\tag{4.93}$$

The (6×3) operator matrix used in $\mathbf{K}_{\phi\mathbf{D}_0}^e$ conveys the third order tensor $(\mathbf{I} \otimes \mathbf{D}_0^h + \mathbf{D}_0^h \otimes \mathbf{I})$ into Voigt notation:

$$\mathbf{B}_I^{el} = \begin{bmatrix} 2N_I^{\mathbf{D}_0} D_{01} & 0 & 0 \\ 0 & 2N_I^{\mathbf{D}_0} D_{02} & 0 \\ 0 & 0 & 2N_I^{\mathbf{D}_0} D_{03} \\ N_I^{\mathbf{D}_0} D_{02} & N_I^{\mathbf{D}_0} D_{01} & 0 \\ 0 & N_I^{\mathbf{D}_0} D_{03} & N_I^{\mathbf{D}_0} D_{02} \\ N_I^{\mathbf{D}_0} D_{03} & 0 & N_I^{\mathbf{D}_0} D_{01} \end{bmatrix} \tag{4.94}$$

where D_{0i} denotes the i-th component of the nodal quantity $(\mathbf{D}_0)_I$. All integrals are solved on element level in the reference domain via Gauss' integration. Eventually, the application of Newton's method on the weak forms (4.67)-(4.69) yields

$$\delta\boldsymbol{\varphi}_I^{\mathrm{T}} \left(\mathbf{R}_{I,e}^{\boldsymbol{\varphi}} + ((\mathbf{K}_{\boldsymbol{\varphi}\boldsymbol{\varphi}})_{IJ}^e\, \Delta\boldsymbol{\varphi}_J + (\mathbf{K}_{\boldsymbol{\varphi}\phi})_{IJ}^e\, \Delta\phi_J + (\mathbf{K}_{\boldsymbol{\varphi}\mathbf{D}_0})_{IJ}^e\, (\Delta\mathbf{D}_0)_J] \right) = \mathbf{0} \tag{4.95}$$

$$\delta\phi_I \left(R_{I,e}^{\phi} + ((\mathbf{K}_{\phi\boldsymbol{\varphi}})_{IJ}^e\, \Delta\boldsymbol{\varphi}_J + (K_{\phi\phi})_{IJ}^e\, \Delta\phi_J + (\mathbf{K}_{\phi\mathbf{D}_0})_{IJ}^e\, (\Delta\mathbf{D}_0)_J] \right) = 0 \tag{4.96}$$

$$\delta(\mathbf{D}_0)_I^{\mathrm{T}} \left(\mathbf{R}_{I,e}^{\mathbf{D}_0} + [(\mathbf{K}_{\mathbf{D}_0\boldsymbol{\varphi}})_{IJ}^e\, \Delta\boldsymbol{\varphi}_J + (\mathbf{K}_{\mathbf{D}_0\phi})_{IJ}^e\, \Delta\phi_J + (\mathbf{K}_{\mathbf{D}_0\mathbf{D}_0})_{IJ}^e\, (\Delta\mathbf{D}_0)_J] \right) = \mathbf{0} \tag{4.97}$$

In the last equations, the fact that the variational nodal unknowns are arbitrary can be taken into account. Furthermore, the matrices and vectors are assembled as described in

(4.65) to regain globally defined variables, so that their entries are given as

$$\mathbf{K}_{AB} = \overset{n_e}{\underset{e=1}{\mathsf{A}}} \mathbf{K}^e_{IJ} \ , \quad \mathbf{R}_A = \overset{n_e}{\underset{e=1}{\mathsf{A}}} \mathbf{R}_{I,e} \tag{4.98}$$

Therefore, the final tangential matrices and residual vectors contain the information about all nodal information. Hence, one global system of equations emerges in the form of

$$\begin{bmatrix} \mathbf{K}_{\boldsymbol{\varphi}\boldsymbol{\varphi}} & \mathbf{0} & \mathbf{K}_{\boldsymbol{\varphi}\mathbf{D}_0} \\ \mathbf{0} & \mathbf{0} & \mathbf{K}_{\phi\mathbf{D}_0} \\ \mathbf{K}_{\mathbf{D}_0\boldsymbol{\varphi}} & \mathbf{K}_{\mathbf{D}_0\phi} & \mathbf{K}_{\mathbf{D}_0\mathbf{D}_0} \end{bmatrix} \begin{bmatrix} \Delta\boldsymbol{\varphi} \\ \Delta\phi \\ \Delta\mathbf{D}_0 \end{bmatrix} = - \begin{bmatrix} \mathbf{R}_{\boldsymbol{\varphi}} \\ \mathbf{R}_{\phi} \\ \mathbf{R}_{\mathbf{D}_0} \end{bmatrix} \tag{4.99}$$

4.3.4 Static Condensation

As this set of equations contains numerous entries that vanish, one possible way to reduce the computing effort is the so-called static condensation. For this procedure, the components of tangential matrices and residual vectors on element level are modified, so that only two variables are eventually brought to the global level again. Since we use discontinuous approximations of $\mathbf{D}_0$ over the element boundaries, it is target-aimed to choose $\boldsymbol{\varphi}$ and ϕ. On that account we rewrite the third row of the local set of equations as

$$(\Delta\mathbf{D}_0)_J = ((\mathbf{K}_{\mathbf{D}_0\mathbf{D}_0})^e_{IJ})^{-1} \left[-\mathbf{R}^{\mathbf{D}_0}_{I,e} - (\mathbf{K}_{\mathbf{D}_0\boldsymbol{\varphi}})^e_{IJ} \, \Delta\boldsymbol{\varphi}_J - (\mathbf{K}_{\mathbf{D}_0\phi})^e_{IJ} \, \Delta\phi_J \right] \tag{4.100}$$

Inserting them into the other rows, adding up and assembling again as it was similarly shown before, a new comparatively small set of equations pops out as

$$\begin{bmatrix} \tilde{\mathbf{K}}_{\boldsymbol{\varphi}\boldsymbol{\varphi}} & \tilde{\mathbf{K}}_{\phi\boldsymbol{\varphi}} \\ \tilde{\mathbf{K}}_{\phi\phi} & \tilde{\mathbf{K}}_{\phi\phi} \end{bmatrix} \begin{bmatrix} \Delta\boldsymbol{\varphi} \\ \Delta\phi \end{bmatrix} = - \begin{bmatrix} \tilde{\mathbf{R}}_{\boldsymbol{\varphi}} \\ \tilde{\mathbf{R}}_{\phi} \end{bmatrix} \tag{4.101}$$

with the definitions

$$\tilde{\mathbf{K}}_{\boldsymbol{\varphi}\boldsymbol{\varphi}} := \mathbf{K}_{\boldsymbol{\varphi}\boldsymbol{\varphi}} - \mathbf{K}_{\boldsymbol{\varphi}\mathbf{D}_0} \left(\mathbf{K}_{\mathbf{D}_0\mathbf{D}_0}\right)^{-1} \mathbf{K}_{\mathbf{D}_0\boldsymbol{\varphi}} \tag{4.102}$$

$$\tilde{\mathbf{K}}_{\boldsymbol{\varphi}\phi} := -\mathbf{K}_{\boldsymbol{\varphi}\mathbf{D}_0} \left(\mathbf{K}_{\mathbf{D}_0\mathbf{D}_0}\right)^{-1} \mathbf{K}_{\mathbf{D}_0\phi} \tag{4.103}$$

$$\tilde{\mathbf{K}}_{\phi\boldsymbol{\varphi}} := -\mathbf{K}_{\phi\mathbf{D}_0} \left(\mathbf{K}_{\mathbf{D}_0\mathbf{D}_0}\right)^{-1} \mathbf{K}_{\mathbf{D}_0\boldsymbol{\varphi}} \tag{4.104}$$

$$\tilde{\mathbf{K}}_{\phi\phi} := -\mathbf{K}_{\phi\mathbf{D}_0} \left(\mathbf{K}_{\mathbf{D}_0\mathbf{D}_0}\right)^{-1} \mathbf{K}_{\mathbf{D}_0\phi} \tag{4.105}$$

$$\tilde{\mathbf{R}}_{\boldsymbol{\varphi}} := \mathbf{R}_{\boldsymbol{\varphi}} - \mathbf{K}_{\boldsymbol{\varphi}\mathbf{D}_0} \left(\mathbf{K}_{\mathbf{D}_0\mathbf{D}_0}\right)^{-1} \mathbf{R}_{\mathbf{D}_0} \tag{4.106}$$

$$\tilde{\mathbf{R}}_{\phi} := \mathbf{R}_{\phi} - \mathbf{K}_{\varphi\mathbf{D}_0} \left(\mathbf{K}_{\mathbf{D}_0\mathbf{D}_0}\right)^{-1} \mathbf{R}_{\mathbf{D}_0} \tag{4.107}$$

Hence, $\mathbf{D}_0$ serves as an internal variable. The global number of DOFs is remarkably decreased.

5 Numerical Investigations

After these numerous deviations it is now possible to examine numerical examples which rely on the FE formulation probed in the previous chapter. As it is the main aim to investigate the impact of the transversely isotropic material model on the deformation behavior electric boundaries are ommited in the first place. Therefor, purely mechanical examples are shown in the section 5.1 and 5.2. The first one treats deformation mainly gouverned by bending impacts and the second one deals with tensile effects. To focus on the evoked displacements maximal simplicity is a main target. In the next investigation 5.3, the well-known Cook's membrane is loaded with purely electric conditions. Numerical properties of the FE-formulation are examined at this point. Transversal isotropy is subsidiary in this example. However, the two focussed issues of this work are combined in example 5.4. A clamped block undergoes large deformations due to electric BCs and the impact of transversal isotropy becomes obvious. Eventually, a simplified model of artificial muscles is considered with respect to the motivation of this work. Validation of the model based on the former work of [SL16] is attempted.

Throughout all the numerical investigations the transversely isotropic material model presented in (3.41) was employed. The isotropic parameters have been chosen as

$$a = 1/4 \cdot 10^5 \, Pa \tag{5.1}$$

$$b = 1/2 \cdot 10^5 \, Pa \tag{5.2}$$

$$c = 10^6 \, Pa \tag{5.3}$$

$$d = 2\,(a + 2b) \tag{5.4}$$

By making use of (3.30) the corresponding parameters of the linear theory can be computed

$$E \approx 4.403 \cdot 10^5 \, Pa \tag{5.5}$$

$$\upsilon \approx 0.468 \tag{5.6}$$

The discretisation has been done as explained in section 4.3 with trilinear isoparametric 8-node volume elements, so that $n = 8$ for each independent variable. The corresponding Lagrange shape functions can be found in Appendix A.2.

5.1 Cantilever Beam Exposed to Shear Force

The aim of this investigation is to understand the impact of transversal isotropy on the deformation behaviour of processes mainly gouverned by bending. In this case we are deploying an example in which a cantilever-typed beam is clamped on one side and undergoes a shear force on the other. Electric effects are ommited for the sake of simplicity. Its length is 25m and its cross-section is quadratic with an edge length of 5m. The beam is exposed to a mechanical Dirichlet BC, so that the displacement at the clamped side vanishes in all directions.

$$\mathbf{U}(X_1 = 0) = \mathbf{0} \tag{5.7}$$

On the opposite side a shear force is applied via a mechanical Neumann BC. Thereby it is distributed over the whole surface in equal magnitude for each finite element. The stress points in positive z-direction. Moreover, the resultant stress vector reads

$$\mathbf{p} = \begin{bmatrix} 0 \\ 0 \\ 0.4 \end{bmatrix} kPa \tag{5.8}$$

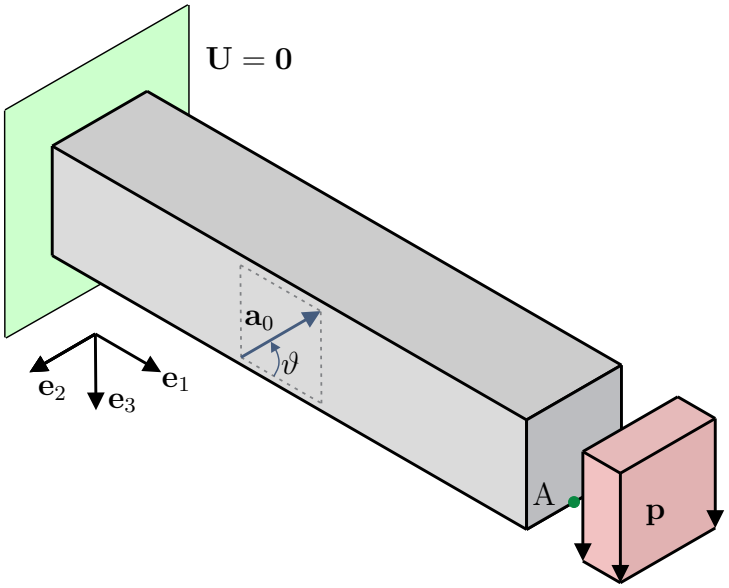

Figure 10: BCs of the cantilever beam test

The body is discretised with $20 \times 4 \times 4$ finite elements. The material parameters are depicted in Table 3.

The direction of fibre reinforcement is now varied within the $\mathbf{e}_1$-$\mathbf{e}_3$-plane by changing its angle ϑ to the $\mathbf{e}_1$-axis as it is shown in Figure 10. This yields the fibre direction vector

as

$$\mathbf{a}_0 = \begin{bmatrix} \cos(\vartheta) \\ 0 \\ -\sin(\vartheta) \end{bmatrix} \tag{5.9}$$

Several final configurations of the cantilever beam are presented in Figure 11. They differ with respect to the chosen direction of fibre reinforcement. It becomes obvious, that there is an immediate relation to the deflection of the body. The von Mises stress distribution is shown. It is computed with the components of the Cauchy stresses as [dSNPO08]

$$\sigma_{vM} = \sqrt{\frac{1}{2}\left[(\sigma_{11}-\sigma_{22})^2 + (\sigma_{22}-\sigma_{33})^2 + (\sigma_{33}-\sigma_{11})^2 + 6\left(\sigma_{23}^2+\sigma_{31}^2+\sigma_{12}^2\right)\right]} \tag{5.10}$$

and represents a general measure for the load a specific point of the body is subjected to. Several failure criteria base on this stress measure. The greatest stresses are located near the clamp as strains in all directions are prevented.

Anisotropic parameters:	g_0	$1.6 \cdot 10^5$	Pa	Geometry:
	$g_{\mathbf{C}}$	4		
	$g_{\mathbf{G}}$	8		
	g_C	1		

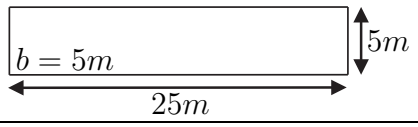

Table 3: Simulation parameters for the cantilever beam tests.

We can plot the displacement into the $\mathbf{e}_3$-direction of point A with $\mathbf{X}^A = [25\ 2.5\ 5]^{\mathrm{T}}$ in dependence of the corresponding fibre direction in terms of ϑ as it is done in Figure 12. First, we observe a nearly symmetric behaviour for angles greater and less than zero, respectively. Small differences are due to the evoked curvature of the beam. The maximal value of U_3^A occurs if fibres are positioned perpendicular to the beams longitudinal axis, which means $\vartheta = \pi/2$ or $\vartheta = -\pi/2$. The minimal displacement is situated at $\vartheta = 0$.

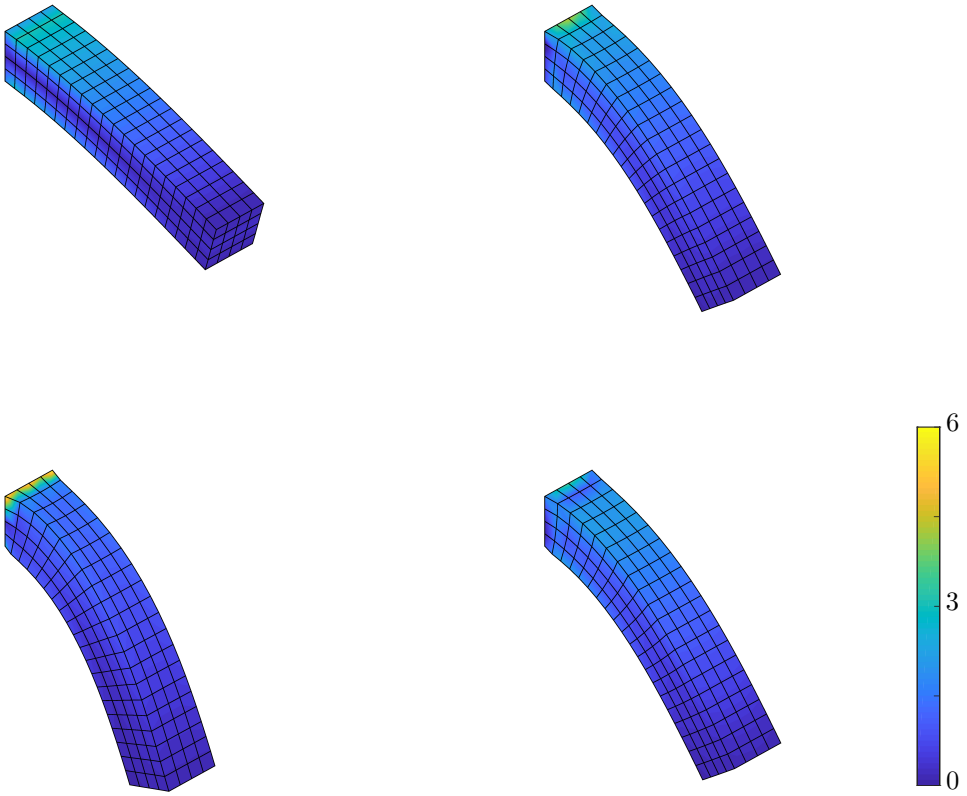

Figure 11: Final configurations for $\vartheta = 0$ (top left), $\vartheta = \pi/4$ (top right), $\vartheta = \pi/2$ (bottom left) and $\vartheta = -\pi/4$ (bottom right) with distribution of σ_{vM} $[10^5\, Pa]$

These observations are evident, as the bending and hence the deflection of the beam are mainly determined by the normal stresses. If the fibres are parallel to the x-axis their additional stiffness causes less strain than it would for an orientation perpendicular to the longitudinal axis of the beam. Effects due to shear stresses are negligibly small for this geometry and material model.

Furthermore, the impact of alternating stiffness of the fibres, expressed via the material parameter g_0, has to be investigated. If we choose a greater g_0 we observe the graph shown in Figure 13. Needless to say, the axis symmetry remains and any displacements are smaller than before. However, the range of values decreases, which means that the impact of transversal isotropy does as well. Moreover, the curve becomes more widespread. If the fibre direction angle is close to $\pm\pi/2$ differences in ϑ cause more differences in the displacement as it is for values close to zero. With the formerly regarded greater g_0 the behaviour is vice versa.

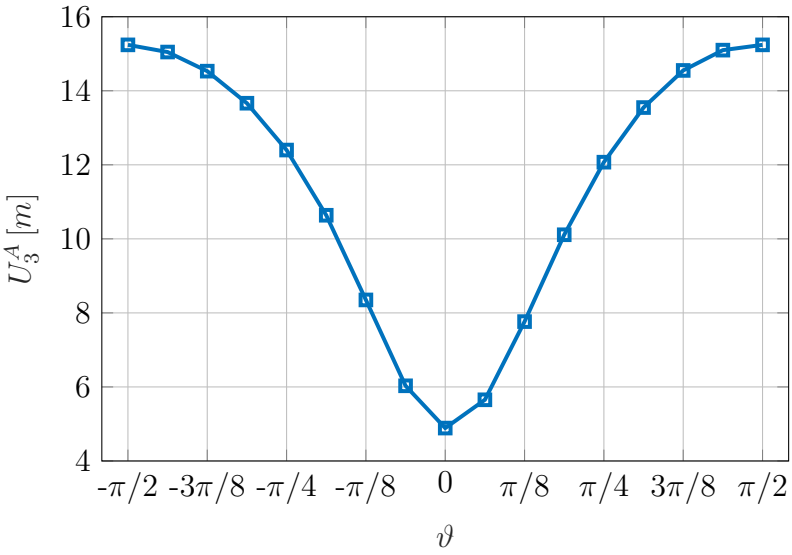

Figure 12: U_3^A over ϑ for $g_0 = 1.6 \cdot 10^5$

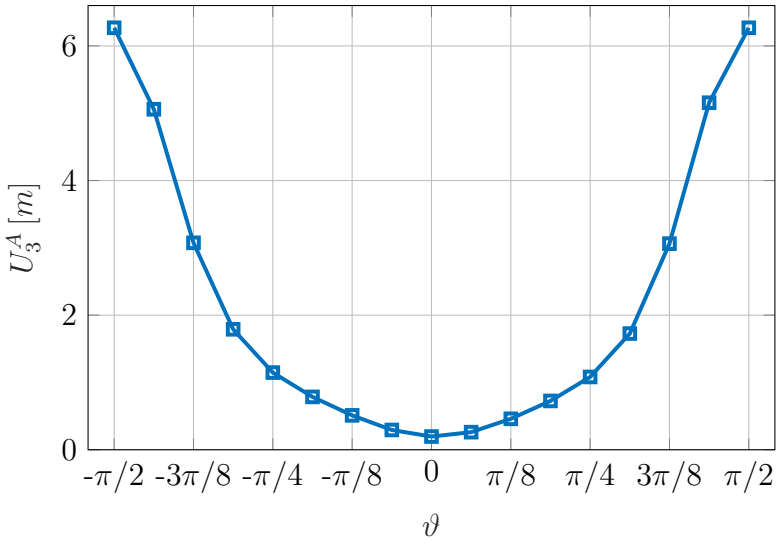

Figure 13: U_3^A over ϑ for $g_0 = 6 \cdot 10^6$

5.2 Plate Exposed to Traction Force

In this example the influence of transversal isotropy on the behaviour of solids exposed to tension stresses shall be examined. Again this investigation will be done with purely mechanical BCs.

Let us consider a very thin plate of dimensions $100m \times 50m \times 1m$. On the lower side, the displacement in $\mathbf{e}_2$-direction is prevented as well as the displacement of the centre points located at $\mathbf{X} = [50\ 0\ X_3]^{\mathrm{T}}$ into $\mathbf{e}_1$-direction in the form of mechanical Dirichlet BCs as

$$U_2(X_2 = 0) = 0 \tag{5.11}$$

$$U_1(X_1 = 50, X_2 = 0, X_3) = 0 \tag{5.12}$$

On the upper side the body is subjected to a tensile traction vector $\mathbf{p}$ whose resultant force vector reads

$$\mathbf{F}^{ext} = \begin{bmatrix} 0 \\ 2.5 \\ 0 \end{bmatrix} kPa \tag{5.13}$$

Here again, the load is distributed over the whole Neumann boundary side. The plate is discretized with just two finite elements in order to amplify numerical instabilities. The fibre reinforcement lies within the $\mathbf{e}_1$-$\mathbf{e}_2$-plane and is described by the angle ϑ with respect to the $\mathbf{e}_1$-axis. A comprehensive depiction can be seen in Figure 14 and the material parameters were chosen as shown in Table 4.

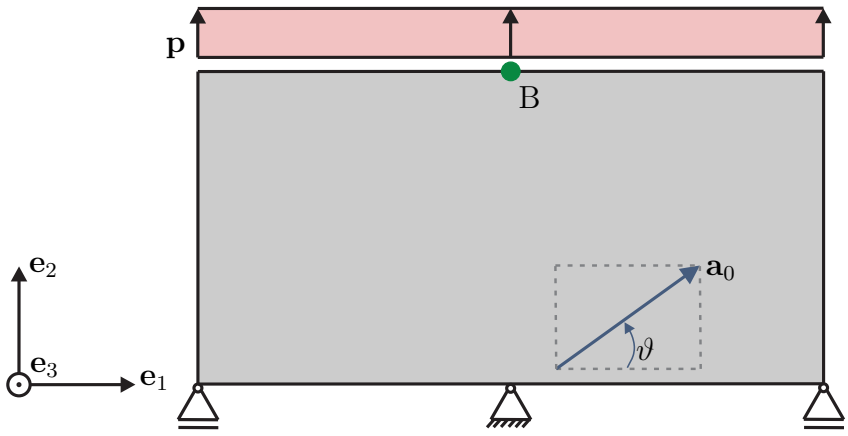

Figure 14: BCs for the plate tests

Anisotropic parameters:	g_0	10^5	Pa	Geometry:
	g_C	4		
	g_G	8		
	g_C	1		

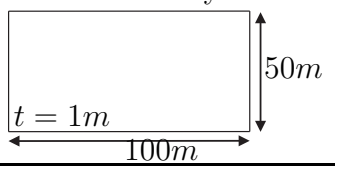

Table 4: Simulation parameters for the plate tests.

Moreover, the reinforcement direction is then varied between $\vartheta = 0$ and $\vartheta = \pi$. We observe different deformations in dependence of $\mathbf{a}_0$ as it becomes obvious in Figures 15 - 18 which also depict the distribution of the component of the Cauchy stress tensor in load direction σ_{22}.

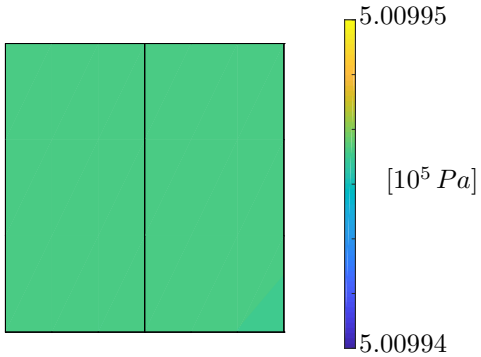

Figure 15: σ_{22} for $\vartheta = 0$

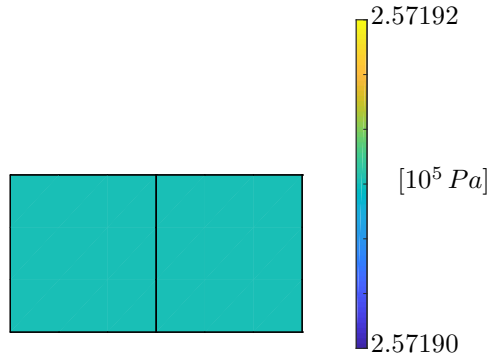

Figure 16: σ_{22} for $\vartheta = +\pi/2$

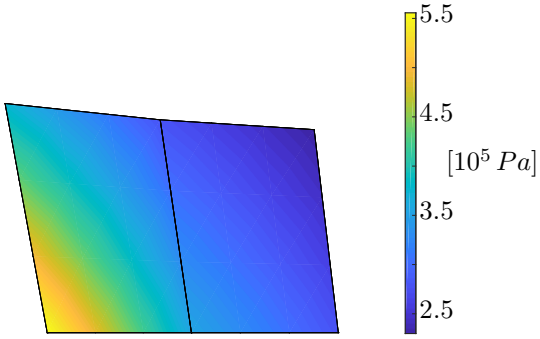

Figure 17: σ_{22} for $\vartheta = +\pi/4$

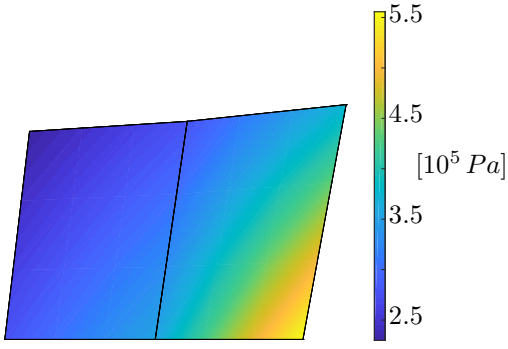

Figure 18: σ_{22} for $\vartheta = +3\pi/4$

We can observe, that in this plain stress state symmetric deformations are achieved if $\mathbf{a}_0$ is orthogonal or parallel to the principal axis in y-direction. Displacements are as expected larger if the fibres are perpendicular and smaller if the fibres are parallel to the $\mathbf{e}_2$-axis. For angles ϑ in between, strain orthogonal to $\mathbf{a}_0$ are amplified due to the lower stiffness within that direction.

Moreover, equal Cauchy stresses occur at each Gauss integration point (for explanation see Section 2.3.4) of this plate for the cases in which the fibre direction is parallel or perpendicular to the load. These Patch-Test-like homogenous stress distributions verify the developed element formulation with respect to numerical instabilities and the material model.

Furthermore the displacement components of Point B with $\mathbf{X}^B = [50\ 50\ 0]^{\mathrm{T}}$ are plotted over multiple angles in Figures 19 and 20 respectively to investigate the transversely isotropic behaviour in more detail.

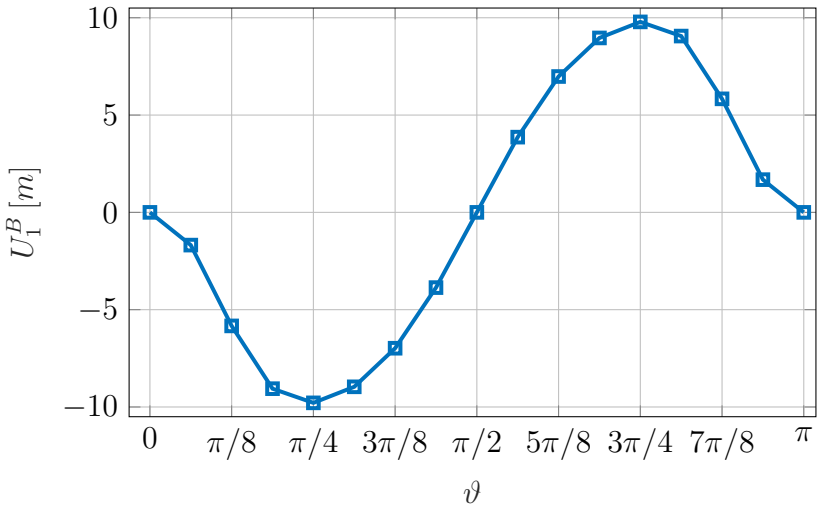

Figure 19: U_1^B over ϑ for $g_0 = 10^5 Pa$

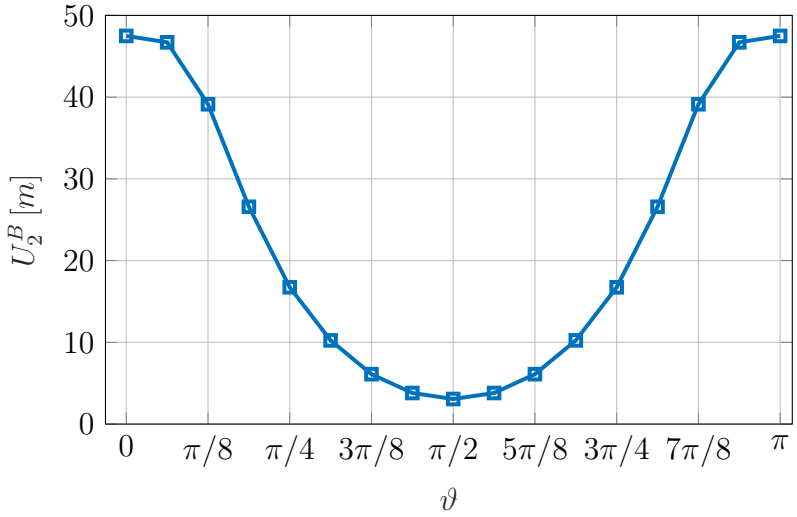

Figure 20: U_2^B over ϑ for $g_0 = 10^5 Pa$

U_1^B vanishes for $\vartheta = 0$ and for multiples of $\pi/2$. Its extrema occur for $\vartheta = \pi/4$ and $3\pi/4$. This observation conincides with the formerly gained information of the figures. It should be added, that there is no symmetry in the domain $\vartheta \in [0\ \pi/2]$. Angles close to $\pi/2$ evoke larger displacements than their equivalents close to zero. This might rest on the choice of g_0 and makes it inevitable to further investigate the impact of the reinforcements stiffness, as it has been already presented in the Cantilever beam example.
Needless to say that U_2^B is strictly symmetric with respect to $\vartheta = \pi/2$ (see Figure 20). The longitudinal displacement is maximal if the fibres are perpendicular to the direction of $\mathbf{F}^{ext}$ and minimal if the fibres lie within this direction ($\vartheta = \pi/2$).
What is striking is that for other values of g_0 the extrema of the plot change. As it is visible in Figure 21, for stiffer fibres the maximum occurs under smaller angles (curves with dashed lines). For softer fibres (which means smaller g_0) the maximum displacement occurs at higher angles (see black, red and blue line). The graph marked with green represents the formerly investigated choice of $g_0 = 10^5\ Pa$. The first guess has been confirmed.

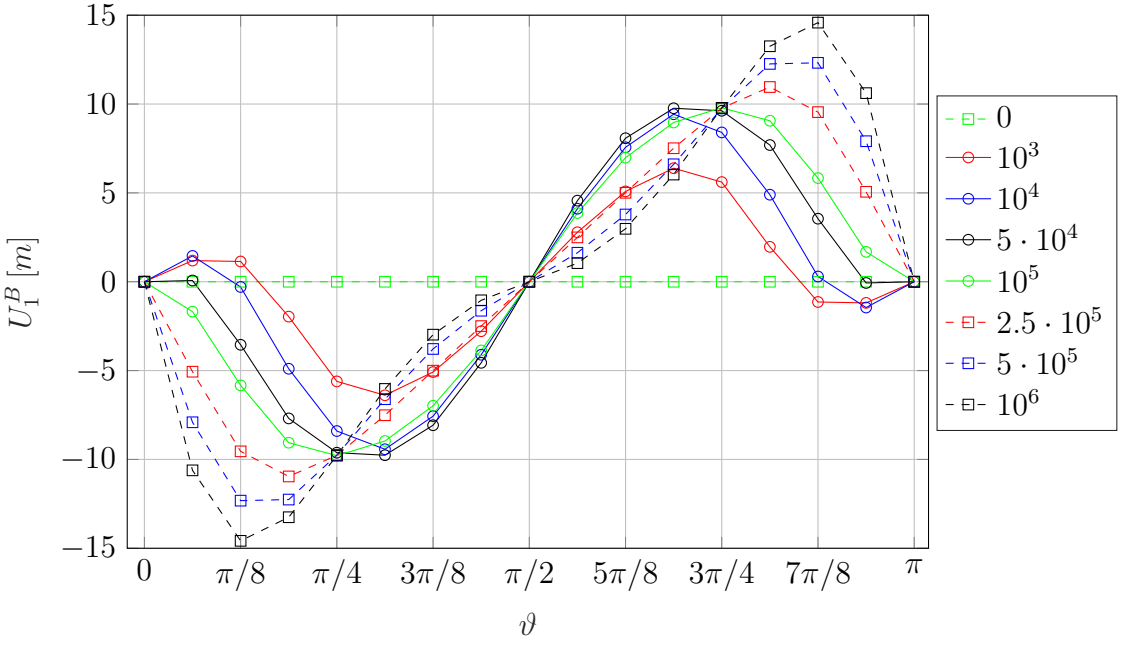

Figure 21: U_1^B over ϑ for various g_0 $[Pa]$

The stiffer the fibres are the more consequences are visible due to transversal isotropy. For ϑ close to $\pi/2$ the plate is a very stiff system with only few deformation. Deflections from that angle do not evoke large displacements either. By contrast, for angles close to zero we observe the inverted behaviour. For very small g_0 it happens to be vice versa.

If g_0 tends towards zero, the graph becomes invariant of the angle and hereby constant zero (see green dashed line).

Furthermore, there emerge two more maxima for angles close to zero. The impact of transverse deformation becomes obvious when investigating different choices of Poisson's ratio υ (see Figure 22). The displacement of the same point in $\mathbf{e}_1$-direction is investigated for different values of the material parameter c which is directly related to Poisson's ratio via (3.30). The other parameters were chosen as before. For smaller Poisson's ratios then before, the observed peaks remain but the displacements for small angles become less. However, the deformations for bigger ϑ are bigger. Thus, influences of transverse deformation cannot be denied and act contrary to the transversely isotropic displacements. Nevertheless, the reasons for this counter-intuitive behaviour are still to be researched in the future.

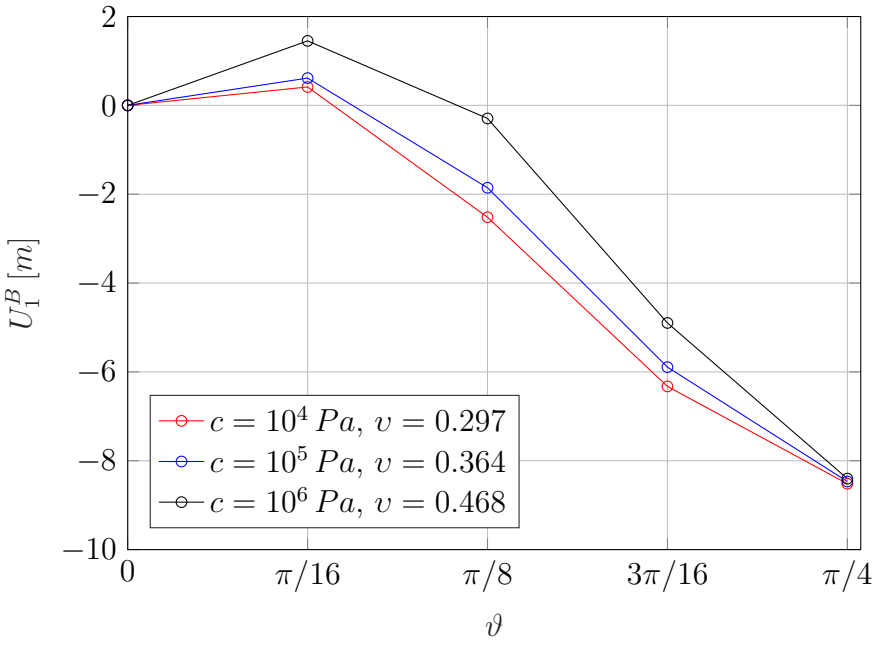

Figure 22: U_1^B over ϑ for $g_0 = 10^4\,Pa$ and three values of the parameter c

Similar peaks are also visible in the graphs of U_2^B (black, red and blue line, Figure 23). Higher displacements take place although the reinforcement fibres turn into the force direction. The standard behaviour however is as expected: Maximal displacement in $\mathbf{e}_1$-direction is achieved for fibres in $\mathbf{e}_2$-direction. Minimal displacements occur if the fibres are within direction of the load. For this component, total symmetry with regard to $\vartheta = \pi/2$ is observed.

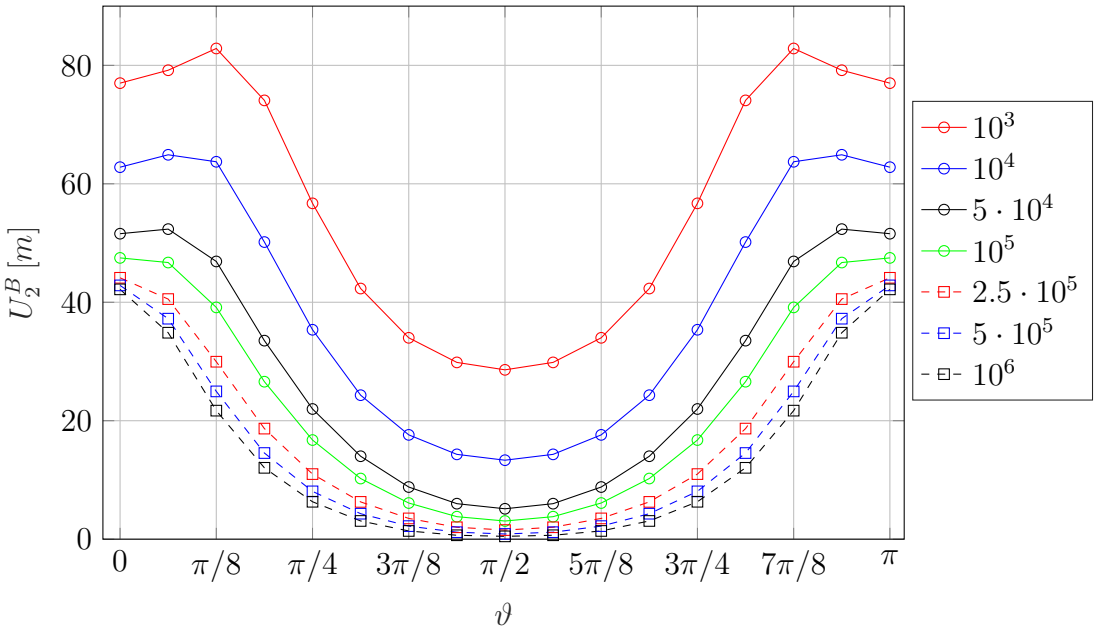

Figure 23: U_2^B over ϑ for various g_0 $[Pa]$

5.3 Cook's Membrane

In this well known example, firstly reported by Robert D. Cook [Coo74], several numerical features of the probed FE formulation are examined. For the first time in this chapter, electric BCs are applied. In general, the ability to perform with distorted elements from the reference configuration on is tested. Moreover the influence of the so called h-refinement, that means discretization with more and thereby smaller elements, shall be investigated. Incidentally, we show that locally quadratic convergence of Newton's method is given.

For the sake of completeness the setup of Cook's membrane is given in the following. A body with the geometry given in Table 5 is totally clamped on one surface as

$$\mathbf{U}(X_1 = 0) = \mathbf{0} \tag{5.14}$$

It is loaded with two electric Dirichlet BCs as

$$\phi(X_3 = 2) = 1.1 \cdot 10^8\, V \tag{5.15}$$

$$\phi(X_3 = 0) = 0 \tag{5.16}$$

The BCs are comprised in Fig. 24. By generating a gradient in the potential, see (2.70) and (3.35), an electric field and hence an electric displacement field evokes and causes compression between the Dirichlet boundaries. This causes transverse strain in the back layer of the membrane. As these effects are not taking place in the front layer, the membrane starts to bend into the positive $\mathbf{e}_3$-direction. Table 5 shows the material parameters which have been used during the tests.

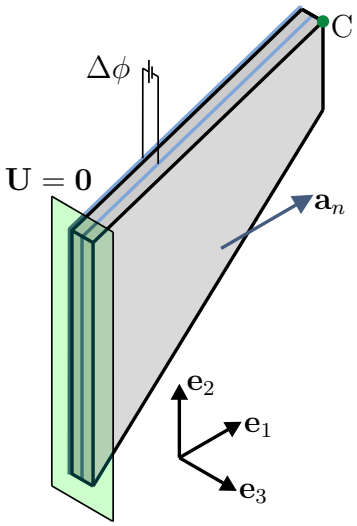

Figure 24: BCs for the Cook's membrane

Anisotropic parameters	g_0	$3 \cdot 10^4$	Pa	Geometry:
	$g_{\mathbf{C}}$	4		
	$g_{\mathbf{G}}$	8		
	g_C	1		
Electric parameters	ε_0	$8.854 \cdot 10^{-12}$	Pa	
	ε_r	4		

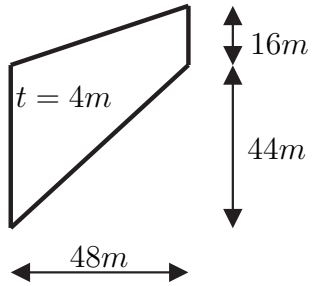

Table 5: Simulation parameters for the Cook's membrane tests.

First, the deformation behaviour for two choices of $\mathbf{a}_0$ are shown in the Figures 25-27. To get knowledge of the distribution of the the components of $\mathbf{D}_0$ we plot them as well. Furthermore, the von Mises stress distributions are depicted.

It can be observed, that for a fibre reinforcement in the direction of $[1\ 1\ 1]^{\mathrm{I}}$ the membrane bends into positive $\mathbf{e}_3$-direction. If $\mathbf{a}_0 = [1\ 0\ 0]^{\mathrm{T}}$ there is in total less deflection and the cranking of the lower right corner does not appear.

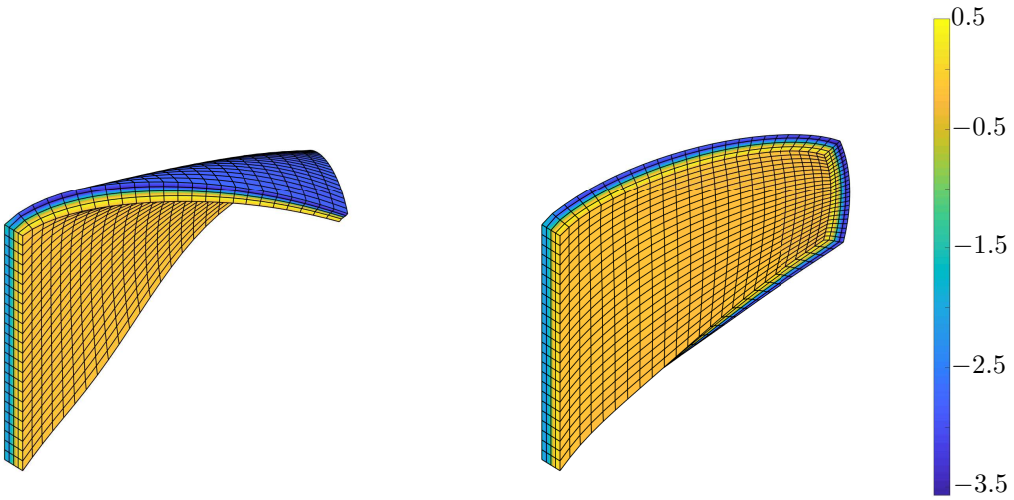

Figure 25: $D_{03}\,[10^{-3}\,C/m^2]$ for $\mathbf{a}_0 = [1\ 0\ 0]^{\mathrm{T}}$ (left) and $\mathbf{a}_0 = [1\ 1\ 1]^{\mathrm{T}}$ (right)

[I]For the cases in which the fibre direction may be given in an unnormed representation of $\mathbf{a}_0$, the standardisation prescription $\mathbf{a}_0 \leftarrow ||\mathbf{a}_0||^{-1}\mathbf{a}_0$ has to be taken into account as the considered material model requires an unit vector expression.

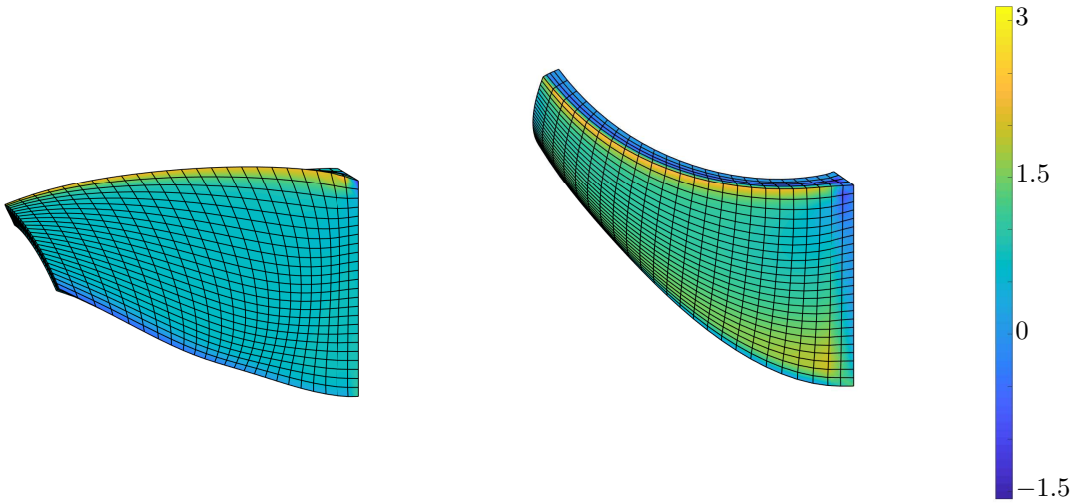

Figure 26: $D_{02}\,[10^{-4}\,C/m^2]$ for $\mathbf{a}_0 = [1\ 0\ 0]^{\mathrm{T}}$ (left) and $\mathbf{a}_0 = [1\ 1\ 1]^{\mathrm{T}}$ (right)

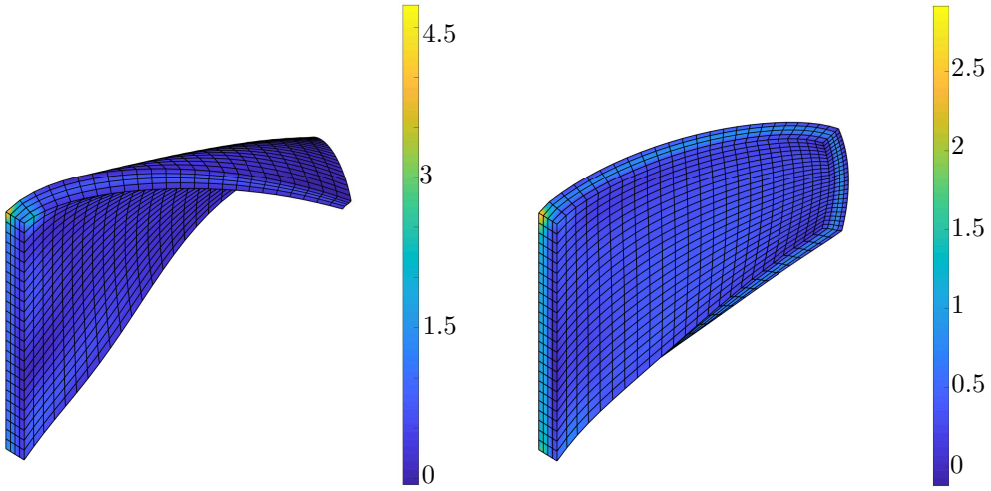

Figure 27: $\sigma_{vM}\,[10^5\,Pa]$ for $\mathbf{a}_0 = [1\ 0\ 0]^{\mathrm{T}}$ (left) and $\mathbf{a}_0 = [1\ 1\ 1]^{\mathrm{T}}$ (right)

Then several discretizations were tested and the convergence of the displacement of point C with $\mathbf{X}^C = [48\ 60\ 4]^{\mathrm{T}}$ into $\mathbf{e}_3$-direction is plotted over the number of elements used (see Figure 28) . Therefore, the difference between the achieved displacement U_3^D and the displacement for the finest FE mesh $(U_3^D)_{ref}$ is plotted over the total amount of global DOFs. It can be derived via the amount of nodes multiplied by 4, as there are 3 components of $\boldsymbol{\varphi}$ and one scalar value of ϕ. For this case the non-zero electric potential has been reduced to $0.5 \cdot 10^8\,V$ and the fibre direction vector was chosen as $\mathbf{a}_0 = [1\ 1\ 1]^{\mathrm{T}}$. The corresponding amounts of elements are given in Table 6.

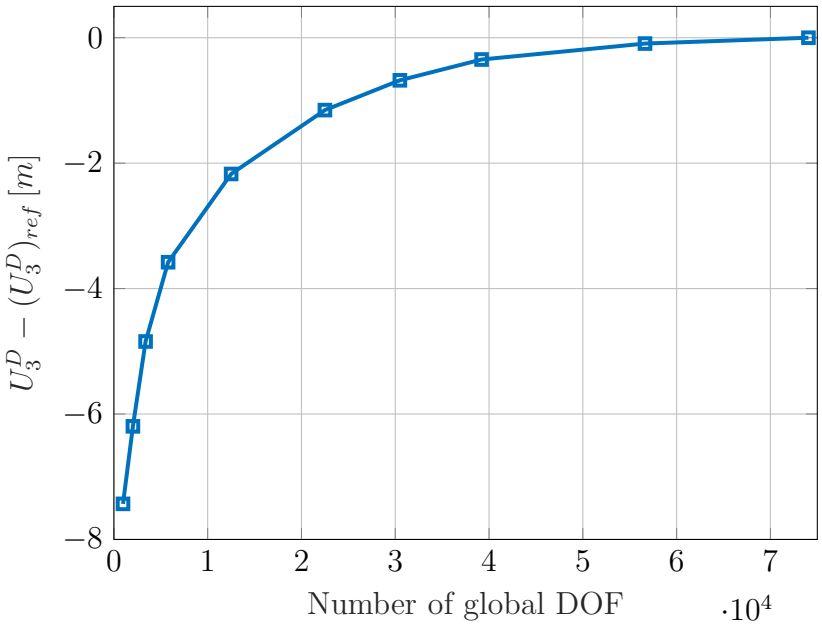

Figure 28: Convergence during h-refinement

	Number of global DOF	Elements in $\mathbf{e}_1$-$\mathbf{e}_2$-plane	Elements in $\mathbf{e}_3$-direction
1	972	8×8	2
2	2028	12×12	2
3	3380	12×12	4
4	5780	16×16	4
5	12500	24×24	4
6	22500	24×24	8
7	30492	32×32	6
8	39204	32×32	8
9	56628	32×32	12
10	74052	32×32	16

Table 6: Discretizations of h-refinement test of Cook's membrane

It can be observed, that for an increasing number of finite elements the system tends to the valid solution. The finer one discretizes the body, the more exact is the obtained solution. The used element formulation accomplishes this first investigation.

Eventually, the locally quadratic convergence of Newton's method in each load iteration step as claimed in the chapter concerning Newton's method in equation (2.106) could be observed. One splendid iteration is shown in Figure 29. $\mathbf{R}$ represents the whole column vector from (4.101). The correct computational implementation is consequently confirmed.

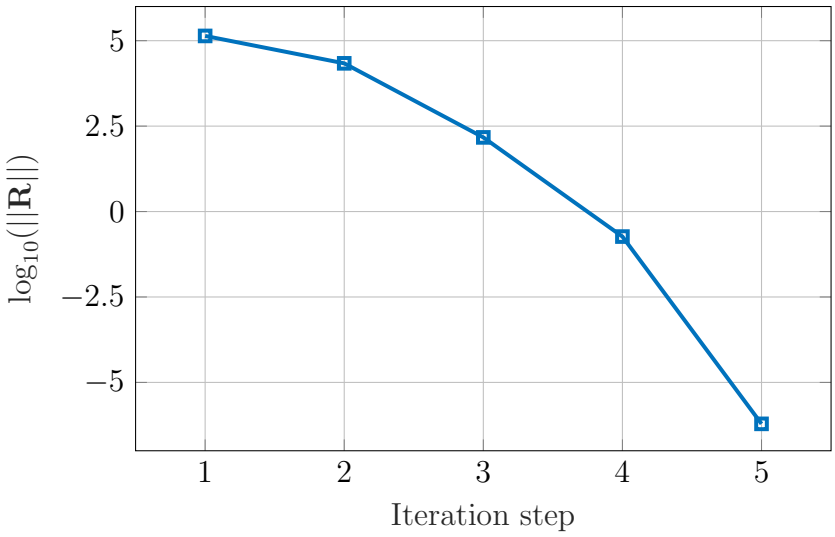

Figure 29: Residual development over Newton iteration steps

5.4 Twisting Actuator

The next example shown here is a twisting actuator exposed to electric influences. Thereby the formulation's ability to perform under very large deformations is tested. Furthermore, the materials sensitivity towards small changes of $\mathbf{a}_0$ can be evaluated.

The structure of the actuator is as follows: a cuboid block with the length $L = 10$, width $B = 2$ and thickness $t = 1$ (also see Table 7) is clamped on one of the short sides similarly to the cantilever beam in section 5.1 as

$$\mathbf{U}(X_1 = 0) = \mathbf{0} \tag{5.17}$$

This time deformation is indirectly induced via electric BCs, so that

$$\phi(X_3 = 0) = 0 \tag{5.18}$$

$$\omega_0^e(X_3 = 0.5) = 3 \cdot 10^{-2} \, \frac{C}{m^2} \tag{5.19}$$

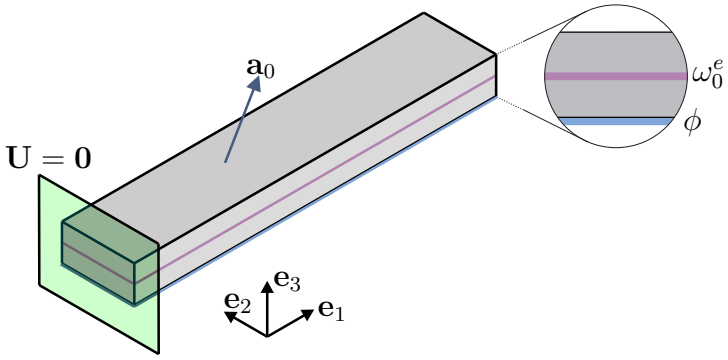

Figure 30: BCs for the twisting actuator

Anisotropic parameters	g_0	$3 \cdot 10^5$	Pa	Geometry:
	$g_\mathbf{C}$	4		
	$g_\mathbf{G}$	8		$t = 1m$, $2m$, $10m$
	g_C	1		
Electric parameters	ε_0	$8.854 \cdot 10^{-12}$	Pa	
	ε_r	4		

Table 7: Simulation parameters for the twisting actuator tests.

Expressed in words: The lower surfaces electric potential ϕ is constantly held zero via a Dirichlet BC. In the centre plane of this actuator an electric areal charge ω_0^e is applied,

so that the electric potential at this surface, in contrast to the Cook's membrane test, becomes negative (also see Figure 31). However, the sign of the electric potential is not relevant in contrast to the resulting potential difference between the two planes. Analogously to the Cook's membrane test, the different transverse strain of the two layers evoke bending of the actuator. The following figures of computed deformations make the gradient of ϕ obvious. Figure 30 comprises the BCs and Table 7 shows the incorporated material parameters. The discretisation has been done with $20 \times 4 \times 2$ finite elements.

The initial configuration and final configurations with $\mathbf{a}_0 = [1\ 0\ 0]^{\mathrm{T}}$ and $[0\ 0\ 1]^{\mathrm{T}}$ respectively (see Figure 31) show that there are bending processes in both possible directions. They can be controlled via the choice of $\mathbf{a}_0$ in the $\mathbf{e}_1$-$\mathbf{e}_3$-plane. As long as the fibre direction vectors $\mathbf{e}_2$-component remains zero, the actuator stays in that plane as well.

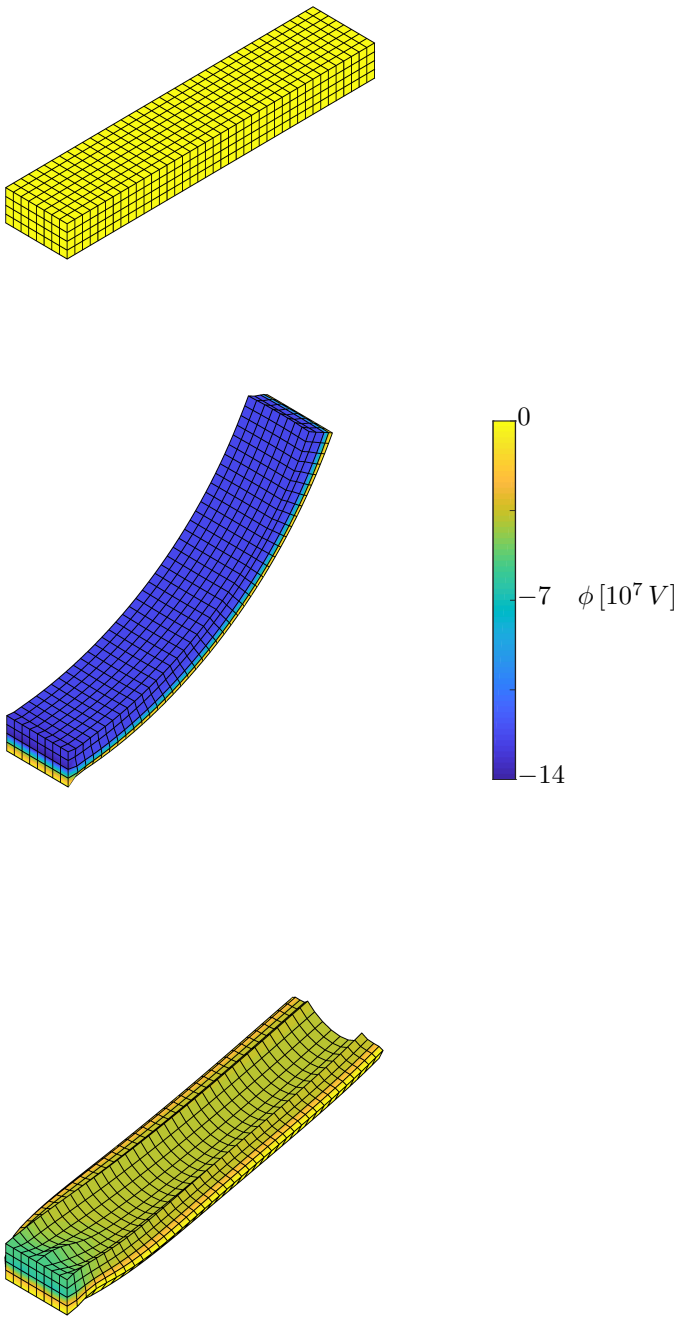

Figure 31: Reference configuration (top) and final configurations with potential distribution for $\mathbf{a}_0 = [0\ 0\ 1]^{\mathrm{T}}$ (centre) and $\mathbf{a}_0 = [1\ 0\ 0]^{\mathrm{T}}$ with half the prescribed electric load (bottom)

If an $\mathbf{e}_2$-direction is incorporated, the actuator starts to twist and screw-shaped deformations become visible (see Figure 32).

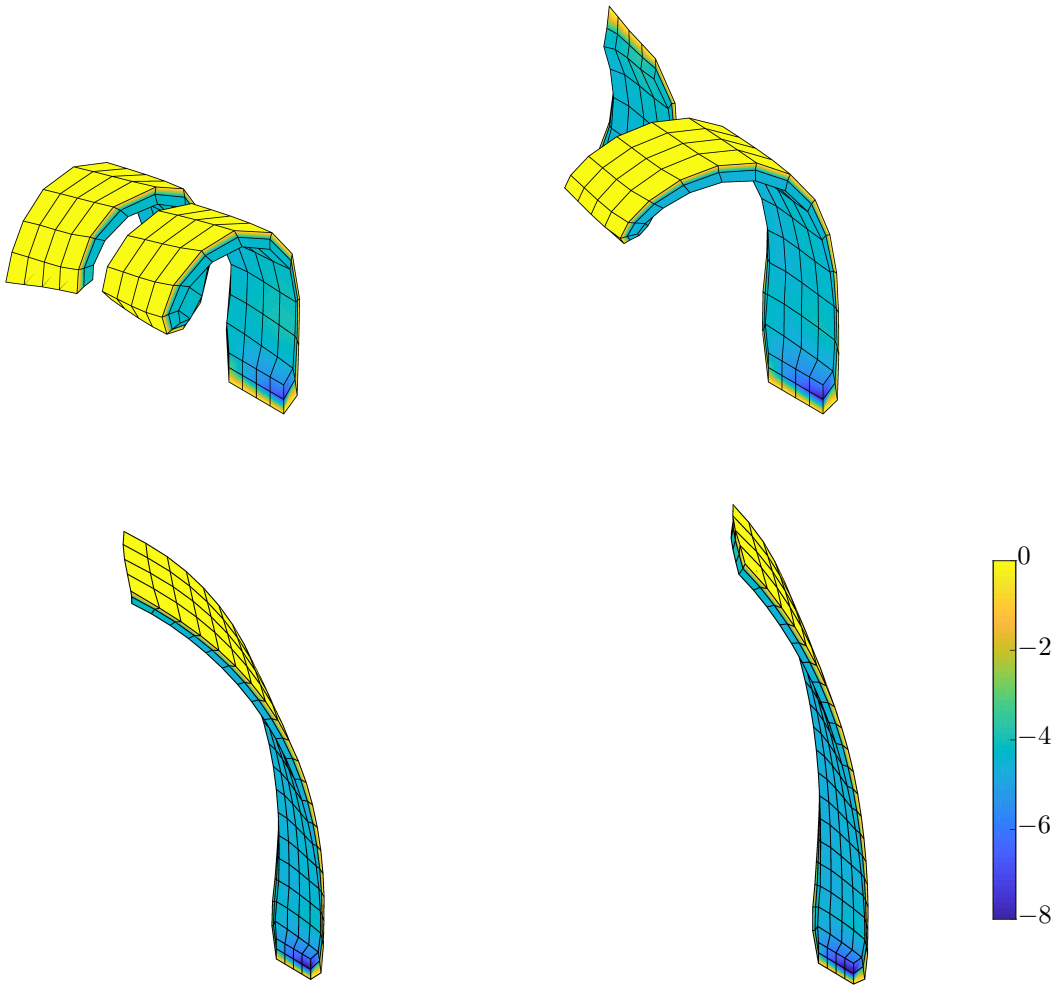

Figure 32: Final configurations for $\mathbf{a}_0 = [0.4\ -1\ 0.4]^{\mathrm{T}}$ (top left), $\mathbf{a}_0 = [0.5\ -1\ 0.5]^{\mathrm{T}}$ (top right), $\mathbf{a}_0 = [0.6\ -1\ 0.6]^{\mathrm{T}}$ (bottom left) and $\mathbf{a}_0 = [0.7\ -1\ 0.7]^{\mathrm{T}}$ (bottom right) with electric potential distribution $[10^7\, V]$

The bigger the ratio between $\mathbf{e}_2$- and $\mathbf{e}_1$-/$\mathbf{e}_3$-component of $\mathbf{a}_0$ is, the more bending of the actuator can be observed and the less twisting along its longitudinal axis is evoked. For particular choices of $\mathbf{a}_0$ a highly distincted sensitivity towards the $\mathbf{e}_2$-component were examined (see Figure 33).

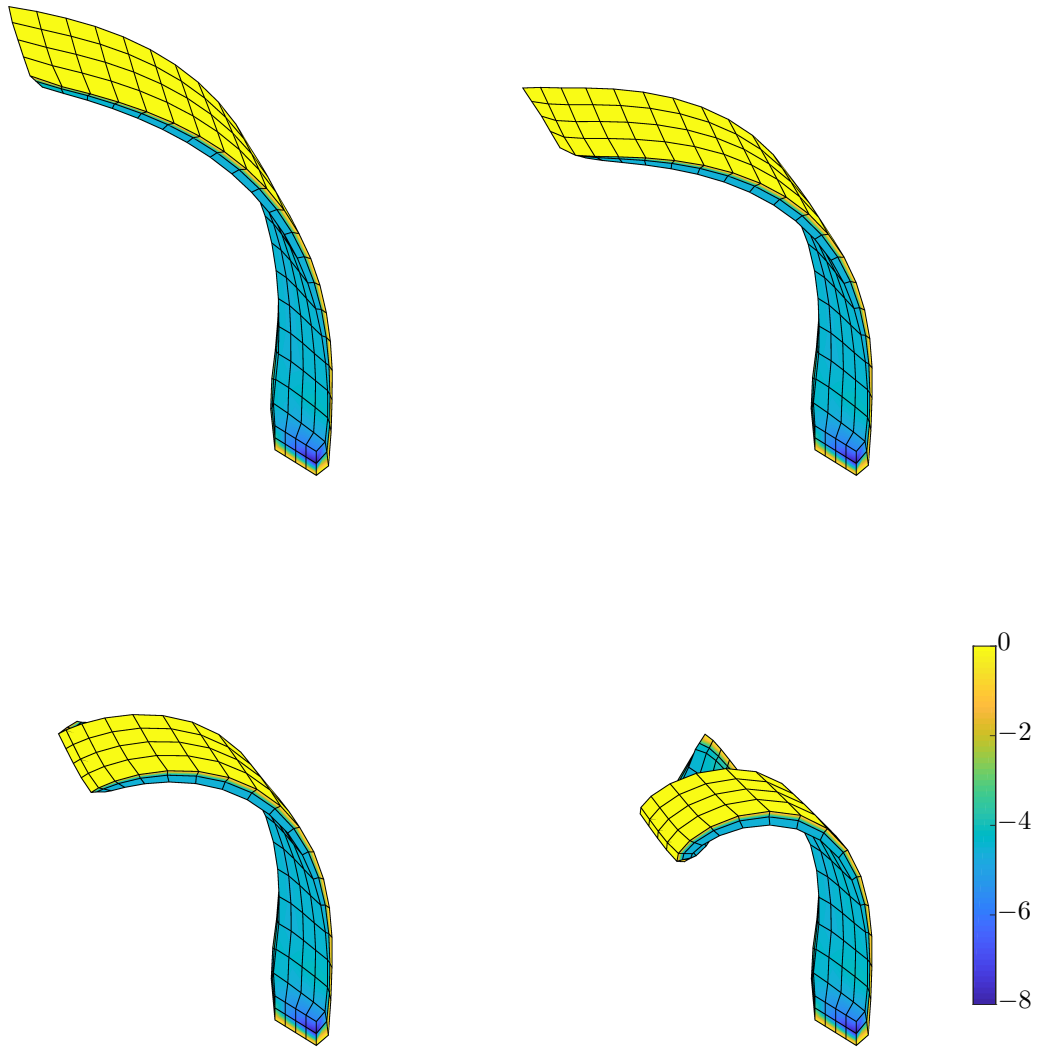

Figure 33: Final configurations for $\mathbf{a}_0 = [0.5\ -0.92\ 0.5]^{\mathrm{T}}$ (top left), $\mathbf{a}_0 = [0.5\ -0.96\ 0.5]^{\mathrm{T}}$ (top right), $\mathbf{a}_0 = [0.5\ -0.97\ 0.5]^{\mathrm{T}}$ (bottom left) and $\mathbf{a}_0 = [0.5\ -0.98\ 0.5]^{\mathrm{T}}$ (bottom right) with electric potential distribution $\varphi\,[10^7\,V]$

Let us now investigate the impact of the Neumann BC on the deformation behaviour of the actuator. Therefore, we raise the applied areal electric charge by making use of a scaling factor Λ as

$$\omega_0^e = \Lambda \cdot 3 \cdot 10^{-2}\,\frac{C}{m^2} \tag{5.20}$$

The fibre direction vector has been chosen as $\mathbf{a}_0 = [0.5\ \ -1\ 0.5]^{\mathrm{T}}$. As it can be seen in the following Figures the observed screw-like twisting occurs directly proportional to the applied load. The process of deformation becomes obvious. The electric potential

distribution $\phi\,[10^7\,V]$ is shown. It is worth noting that for the different load levels from $\Lambda = 0.4$ on predominantly equal potential distributions are achieved although the applied ω_0^e is not the same. Only around the clamping, ϕ increases further.

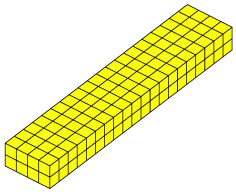

$\Lambda = 0$

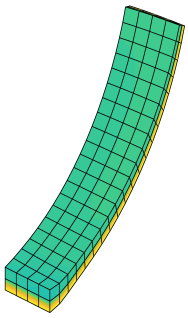

$\Lambda = 0.2$

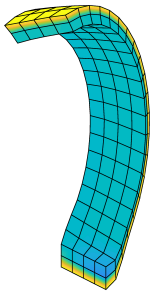

$\Lambda = 0.4$

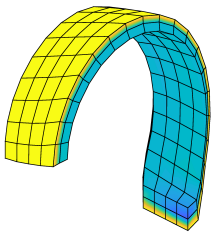

$\Lambda = 0.6$

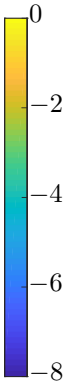

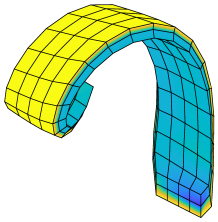

$\Lambda = 0.8$

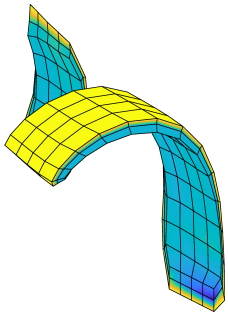

$\Lambda = 1$

5.5 Simplified Artificial Muscle Model

As mentioned earlier in the motivation chapter of this work, one technical realisation of EAPs investigated in this work are artificial muscles. To not miss this mind, the last conducted example shall be a deeply simplified model of such a muscle. It has cylindric shape with a length of $l_0 = 0.3m$ and a diameter of $d = 0.05m$ (see Figure 35) and includes similarly to the ones proposed in [SL16] multiple electrodes perpendicular to the muscle's longitudinal axis with alternating signs. These electrodes dictate a particular electric potential, e.g. via electric voltages, as

$$\phi(X_1 = X_{e1}) = 2.5 \cdot 10^6\, V =: \phi_1 \tag{5.21}$$

$$\phi(X_1 = X_{e2}) = -2.5 \cdot 10^6\, V = -\phi_1 =: \phi_2 \tag{5.22}$$

where $X_{e1} \in \{0,\ 0.1m,\ 0.2m,\ 0.3m\}$ and $X_{e2} \in \{0.05m,\ 0.15m,\ 0.25m\}$. These electrodes are modeled as Dirichlet boundaries without any size along the longitudinal axis of the muscle. The fibre reinforcement was chosen along the longitudinal axis of the model as $\mathbf{a}_0 = [0\ 0\ 1]^{\mathrm{T}}$. The important facts about this investigation are comprised in Figure 34 and the conducted material parameters are shown in Table 8. Mechanical BCs were applied on the three symmetry planes of the model. The FE discretization used 32 elements in the $\mathbf{e}_2$-$\mathbf{e}_3$-plane, as shown in Figure 36, and 30 elements along the $\mathbf{e}_1$-axis.

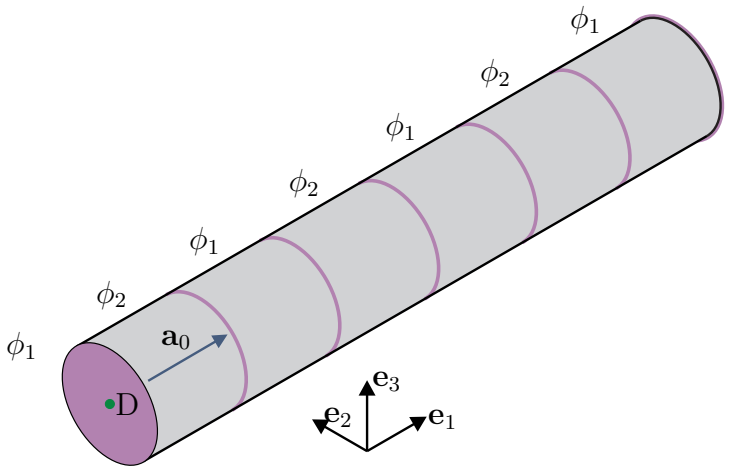

Figure 34: BCs of the artificial muscle tests

Anisotropic parameters	g_0	$3 \cdot 10^3$	Pa
	$g_{\mathbf{C}}$	4	
	$g_{\mathbf{G}}$	8	
	g_C	1	
Electric parameters	ε_0	$8.854 \cdot 10^{-12}$	Pa
	ε_r	4	

Table 8: Simulation parameters for the artificial muscle tests

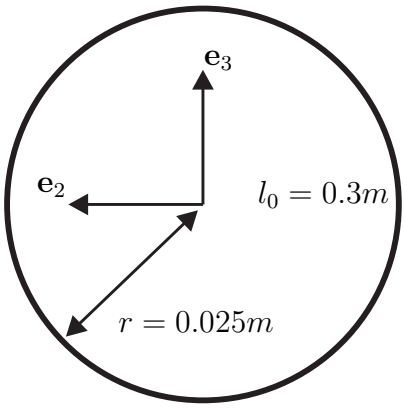

Figure 35: geometry of muscle model

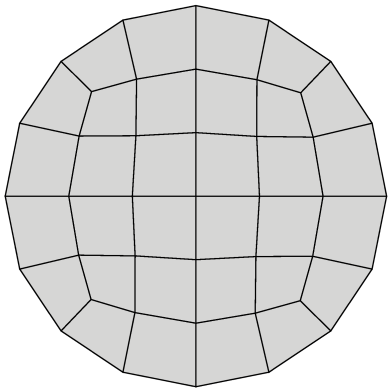

Figure 36: meshing in the y-z-plane

As can be seen in the Figure 37 the potential oscillates periodically between the prescribed values at the electrodes. We now have a look at the resulting compression in dependence

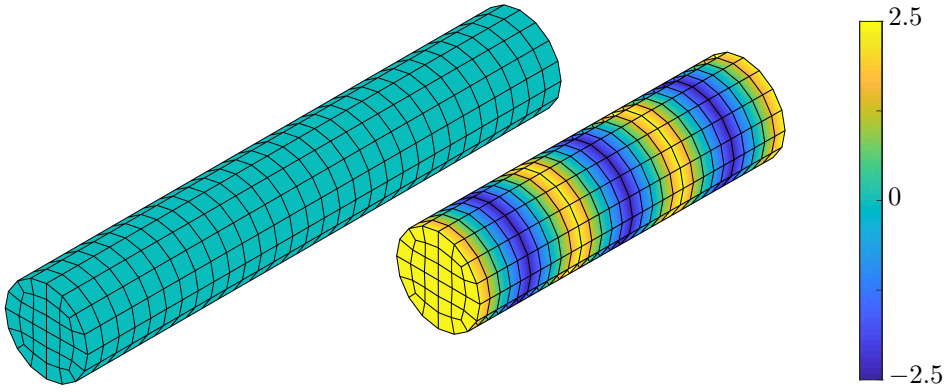

Figure 37: Final configuration and electric potential distribution $\phi\,[10^6\,V]$ of the artificial muscle model

of the relative permittivity of the EAP the muscle model is made of. As values around 4 are typical for the investigated type of material, ε_r between 2 and 6 are investigated. For this purpose the prescribed electric potentials were chosen as $\phi_1 = -\phi_2 = 2 \cdot 10^6\,V$. The resulting longitudinal one-dimensional strain measure $\Delta l / l_0$ which is globally defined has

been investigated. Note that this quantity must not be confused with the first component of the linear strain tensor $\boldsymbol{\varepsilon}$ as this would be defined locally. The change of length Δl is simply the difference between l_0 and l_{end}, which denotes the length of the model in the final configuration. The evaluation was executed in the point D at $[0\ 0\ 0]^{\mathrm{T}}$, that is depicted in Figure 34. We observe a nearly linear relation (see Figure 38). This result goes perfectly with the linear relationship introduced in equation 3.35. A first validation has been accomplished.

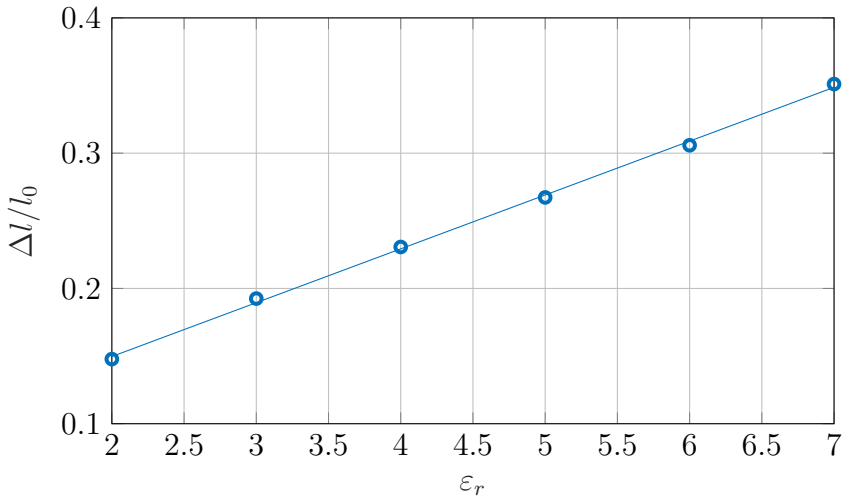

Figure 38: compression κ over relative permittivity ε_r

To further validate the element formulation used, two further tests have been carried out. First, the resulting compression is again examined. This time, the prescribed electric potentials are varied. As compression is limited due to compressibility properties of the material, loads could only be investigated until $\phi_1 = 2.5 \cdot 10^6\, V$. The first choice turned out to be very lucky. A similar study has already been conducted by [SL16] and hence the results presented in this work are to be validated. The achieved relationship between ϕ_1 and $\Delta l/l_0$ can be eventually seen in Figure 39.

The results withstand the comparison as perfectly similar graphs can be seen. For very low potentials a nonlinear behaviour can be observed. As deformations become larger, a linear relationship can be observed. This linearity is determined by the structure of equation (2.70).

In the end, a possibly evoked force of the artificial muscle has been investigated. Therefore, the short surfaces of the model were prevented from moving (see Figure 40). A Dirichlet constraint

$$U_1(X_1 = 0) = U_1(X_1 = l_0) = 0 \tag{5.23}$$

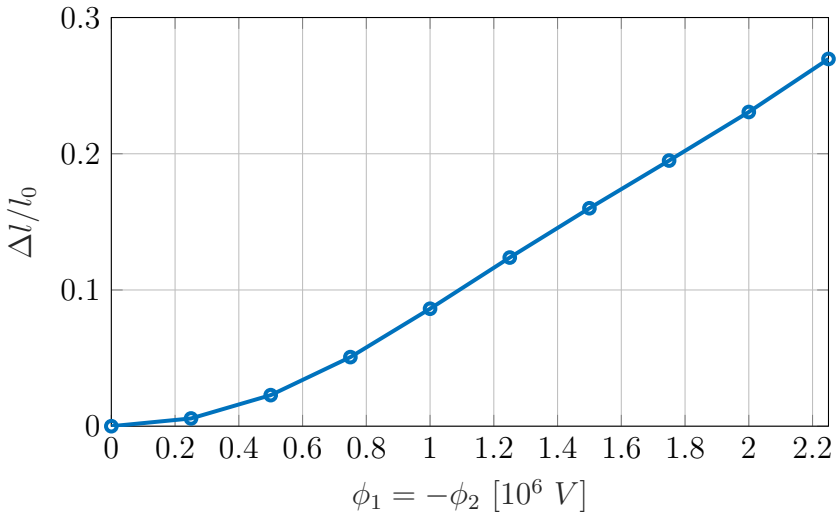

Figure 39: compression over prescribed potential in the electrodes

is applied and the nodal forces of the surfaces are summed up to achieve a resultant force of the magnitude F^{total}. Again, this test was conducted for several ϕ_1 and the outcome is depicted in Figure 41.

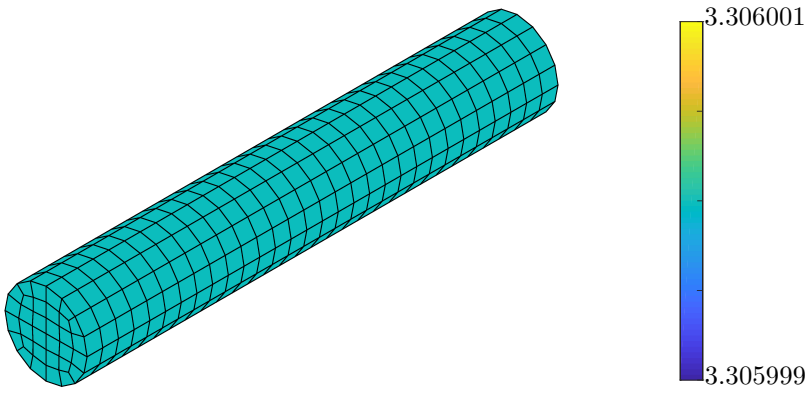

Figure 40: Final configuration with distribution of σ_{vM} [10^5 Pa]

A perfectly quadratic relation can be noted. This relation does not only fit irrevocably the test results by [SL16], but also represents the quadratic nature of the force on dielectric capacitors

$$F^{total} = \varepsilon_0 \varepsilon_r A \left|\mathbf{E}_0\right|^2 \tag{5.24}$$

The last equation can be found in standard physics teaching books, such as [GK11]. A denotes the overall area of the dielectric and F represents the magnitude of force on the capacitors surfaces.

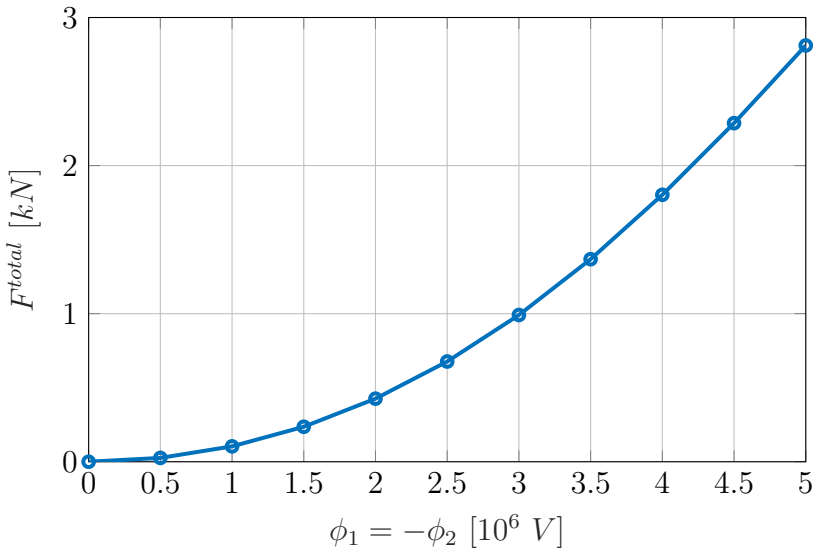

Figure 41: resultant force over prescribed potential in the electrodes

The idea for this investigation has been taken from [SL16] as well. Hence, a final validation of the element formulation and the model's implementation itself has been gained. The results achieved on the account of transversely isotropy are covered by general physical laws and coincide with isotropic investigations.

6 Conclusion and outlook

In this thesis, the theory of transversely isotropic materials has been included into an electromechanical framework. For this purpose, a corresponding strain energy function was considered to extend an existing formulation additively. The resulting function is inspired by the concept of polyconvexity and is formulated in symmetric strain measures which are computed in a cascade algorithm. On that account a FE formulation was derived based on a three-field variational principle, in which the mechanical displacement field as well as the electric displacement field and the electric potential field represent independent variables. By making use of variational calculus the weak form of the BVP has been gained and was then discretised with the FEM. In doing so, the isoparametric concept has been considered which made it possible to execute the computations elementwise based on standard Lagrange shape functions. The final algebraic set of nonlinear equations could be further modified by employing the procedure of static condensation. Hence, the electric displacement field represents an internal variable of the final formulation.

The established formulation was investigated in numerical examples. Meaningful results promoted the comprehension of the considered material behaviour:

Due to the increased stiffness in the direction of fibre reinforcement, the deformation patterns changed significantly. The deflection of bending bodies can be more reduced, the more the fibre direction vector lies within the direction of evoked normal stresses. A plate subjected to tension escapes the direction of loading in the opposite direction of the fibres. A crucial impact of the stiffness of the fibres on the motion could be observed and the symmetry of the probed material model was validated. The distributions of several field variables have been shown and numerical properties of the FE formulation could be outlined by investigating the deformation of an electric Cook's membrane. Large twisting deformations could be evoked for an actuator very sensitive towards small differences of the fibre direction. Eventually, a simplified muscle model could take account of the fibroid structure and possible usages within the field of robotics were motivated. Moreover, the correctness of the considered formulation was validated, such as the force-potential relation or the quadratical convergence of Newton's method.

However, it is worth noting, that several simplifications have been made throughout the theoretical deviation of the strain energy function, such as neglecting dynamics both for the mechanical fields and the electric ones. On that account, terms of inertia were neglected, which would lead to taking account of the mass of certain models. During the work on this thesis [OFJ+] expandet the FE formulation to electro-elastodynamics and also included the transversely isotropic material model. Moreover, the time-dependence

of the electric field was still omitted. Further research should aim at overcoming this simplification. If electro-dynamic assumptions were considered, taking account of magnetic fields would be inevitable as well.

The relation between the electric field and the electric displacement field within the solid was considered to be isotropic. Obtaining deeper knowledge about the transversal isotropy of EAPs with respect to the electric field theory would be target-aimed. Perhaps a more general - such as tensorial - approach or consideration of the polarisation density as presented in Section 3.3 would allow more realistic models.

An interesting point to pay more attention to would be the counter-intuitive observations in the second example with low fibre stiffnesses. It has been observed, that for certain choices of the direction vector the plate moved in the direction of the fibres and not into the opposite direction. The impact of transverse deformation on the displacement's magnitude perpendicular to the load's direction has been shown. However, the effect did remain and it's reasons are still to be investigated.

Nevertheless, the presented material model and FE formulation served well to get a thoroughly knowledge of the theory of transversely isotropic material behaviour. It constitutes a solid basis for further developments of mixed variational principles and electromechanically coupled strain energy functions. Eventually, modeling and simulating eletro-active polymers could provide benefits for the realisation of artificial muscle-structures in the fields of applied engineering.

References

[BDO09] R. Bustamante, A. Dorfmann, and R.W. Ogden. Nonlinear electroelastostatics: a variational framework. *Z. Angew. Math. Phys.*, 60:154–177, 2009.

[Bet13] P. Betsch. *Finite-Elemente-Methoden, Scriptum zur Vorlesung (Institute of Mechanics, KIT, German).* 2013.

[BGO15] J. Bonet, A.J. Gil, and R. Ortigosa. A computational framework for polyconvex large strain elasticity. *Comput. Methods Appl. Mech. Engrg.*, 283:1061–1094, 2015.

[BGO16] J. Bonet, A.J. Gil, and R. Ortigosa. On a tensor cross product based formulation of large strain solid mechanics. *Int. J. Solids Structures*, 84:49–63, 2016.

[BJH17] P. Betsch, A. Janz, and C. Hesch. A mixed variational framework for the design of energy-momentum schemes relying on polyconvex stored energy functions. *Submitted for publication in Comput. Methods Appl. Mech. Engrg.*, 2017.

[Coo74] R.D. Cook. Improved two-dimensional finite element. *ASCE J. Struct. Div.*, 100:1851–1863, 1974.

[dB82] R. de Boer. *Vektor- und Tensorrechnung für Ingenieure (German).* Springer-Verlag, Berlin, 1982.

[DO05] L.A. Dorfmann and R.W. Ogden. Nonlinear electroelasticity. *Acta Mechanica*, 174:167–183, 2005.

[DO14] L.A. Dorfmann and R.W. Ogden. *Nonlinear Theory of Electroelastic and Magnetoelastic Interactions.* Springer Science+Business Media, 2014.

[dSNPO08] E.A. de Souza Neto, D. Peri, and D.R.J. Owen. *Computational methods for plasticity : theory and applications.* Wiley, Chichester, 2008.

[FJSB] M. Franke, A. Janz, M. Schiebl, and P. Betsch. An energy-momentum consistent integration scheme using a polyconvexity-based framework for non-linear thermo-elastodynamics. *Submitted to Int. J. Numer. Meth. Engng.*

[Fra14] M. Franke. *Discretisation techniques for large deformation computational contact elastodynamics.* KIT Scientific Publishing, Karlsruhe, 2014.

[GHW11] D. Gross, W. Hauger, and P. Wriggers. *Technische Mechanik 4 (German).* Springer-Verlag, 2011.

[GK11] J. Grehn and J. Krause. *Metzler Physik (German)*. Bildungshaus Schulbuchverlage, 2011.

[GO16] A.J. Gil and R. Ortigosa. A new framework for large strain electromechanics based on convex multi-variable strain energies: Variational formulation and material characterisation. *Computer Methods in Applied Mechanics and Engineering*, 302:293 – 328, 2016.

[Gov07] S. Govindjee. *Lecture notes for Nonlinear Continuum Mechanics (Institute for Mechanical Systems, ETH Zürich)*. 2006/07.

[HGO+17] C. Hesch, A.J. Gil, R. Ortigosa, M. Dittmann, C. Bilgen, P. Betsch, M. Franke, A. Janz, and K. Weinberg. A framework for polyconvex large strain phase-field methods to fracture. *Comput. Methods Appl. Mech. Engrg.*, 317:649–683, 2017.

[Hol00] G.A. Holzapfel. *Nonlinear solid mechanics. A continuum approach for engineering*. John Wiley & Sons, Ltd, 2000.

[Hug00] T.J.R. Hughes. *The Finite Element Method*. Dover Publications, 2000.

[LL60] L.D. Landau and E.M. Lific. *Course of theoretical physics*, volume 8: Electrodynamics of continuous media. Pergamon Pr., Oxford [u.a.], 1960.

[OFJ+] R. Ortigosa, M. Franke, A. Janz, A.J. Gil, and P. Betsch. An energy-momentum integration scheme based on a convex multi-variable framework for non-linear electro-elastodynamics. *Submitted to Comput. Methods Appl. Mech. Engrg.*

[OG16] R. Ortigosa and A.J. Gil. A new framework for large strain electromechanics based on convex multi-variable strain energies: Finite element discretisation and computational implementation. *Computer Methods in Applied Mechanics and Engineering*, 302:329 – 360, 2016.

[Rug17] J. Ruge. *Entwicklung eines viskoplastischen Werkstoffmodells für gummimodifizierte thermoplastische Kunststoffe (Master's thesis, German)*. 2017.

[SL16] T. Schlögl and S. Leyendecker. Electrostatic-viscoelastic finite element model of dielectric actuators. *Computer Methods in Applied Mechanics and Engineering*, 299:421 – 439, 2016.

[SSG17] K.B. Subramani, R.J. Spontak, and T.K. Ghosh. Influence of fiber characteristics on directed electroactuation of anisotropic electroactive polymers with tunability. *Composites Science and Technology*, 154:187–193, 2017.

[SWB11] J. Schröder, P. Wriggers, and D. Balzani. A new mixed finite element based on different approximations of the minors of deformation tensors. *Comput. Methods Appl. Mech. Engrg.*, 200(49-52):3583–3600, 2011.

[VSP07] D.K. Vu, P. Steinmann, and G. Possart. Numerical modelling of non-linear electroelasticity. *Int. J. Numer. Methods Eng.*, 70:685–704, 2007.

[Wri01] P. Wriggers. *Nichtlineare Finite-Element-Methoden (German)*. Springer-Verlag, 2001.

[www16] www.ders.org. Researchers create 3d printed robotic muscles using electroactive polymer [www.3ders.org]. http://www.3ders.org/articles/20160618-researchers-create-3d-printed-robotic-muscles-using-electroactive-polymer.html (3.12.17,15:23), 2016.

A Appendix

A.1 Tensor Analysis

For the sake of completeness the incorporated differential operators are shortly presented here. A well overview and further consequences can be found in [Hol00]. In order to define derivative operators a very concise way approach is to work with the so-called nabla operator. It comprises the partial derivative operations. For the case of a three dimensional Euklidean space it is defined as

$$\nabla = \frac{\partial}{\partial X_i}\,\mathbf{e}_i = \begin{bmatrix} \frac{\partial}{\partial X_1} & \frac{\partial}{\partial X_2} & \frac{\partial}{\partial X_3} \end{bmatrix}^{\mathrm{T}} \tag{A.1}$$

The gradient of a vector field $\mathbf{U} = U_j \mathbf{e}_j$ is defined to be a second order tensor field. Hence, the gradient operator increases the tensor order by one. It can be written under the use of the dyad of the vector field with the nabla operator as

$$\mathrm{Grad}(\mathbf{U}) = \nabla \otimes \mathbf{U} = \frac{\partial U_i}{\partial X_j}\,\mathbf{e}_i \otimes \mathbf{e}_j \tag{A.2}$$

If the gradient of a scalar is to computed, the last equation still holds. Therefore, there is only one component U_1. The operations yields a vector field. The gradient with respect to spatial coordinates is denoted by grad$(\bullet)$. The divergence of a vector field is a scalar field. It is defined as the single contraction of the nabla operator with the vector field. Hence, applying divergence reduces the tensor order by one

$$\mathrm{Div}(\mathbf{U}) = \nabla \cdot \mathbf{U} = \frac{\partial U_j}{\partial X_i}\,\mathbf{e}_j \cdot \mathbf{e}_i = \frac{\partial U_j}{\partial X_i}\,\delta_{ij} = \frac{\partial U_i}{\partial X_i} \tag{A.3}$$

where the well-known Kronecker delta δ_{ij} has been taken into account. The divergence of quantities of a second order tensor $\mathbf{A} = A_{ik}\,\mathbf{e}_i \otimes \mathbf{e}_k$ is executed analogously via

$$\mathrm{Div}(\mathbf{A}) = \nabla \cdot \mathbf{A} = \frac{\partial A_{ik}}{\partial X_j}\,(\mathbf{e}_i \otimes \mathbf{e}_k) \cdot \mathbf{e}_j = \frac{\partial A_{ik}}{\partial X_j}\delta_{kj}\,\mathbf{e}_i = \frac{\partial A_{ij}}{\partial X_j}\,\mathbf{e}_i \tag{A.4}$$

The divergence operation with respect to spatial coordinates is denoted by div$(\bullet)$. The Curl of a vector field in Lagrangian description is given by the cross product of the nabla operator with the regarded vector

$$\mathrm{Curl}(\mathbf{U}) = \nabla \times \mathbf{U} = \frac{\partial U_j}{\partial X_i}\,\mathbf{e}_i \times \mathbf{e}_j = \frac{\partial U_j}{\partial X_i}\varepsilon_{ijk}\,\mathbf{e}_k \tag{A.5}$$

The Eulerian counterpart is symbolised by curl(•). The total differential of an arbitrarily valued quantity $\mathbf{A}(\mathbf{B})$ is defined by the first order Taylor's expansion as

$$\mathrm{d}\mathbf{A} = \frac{\partial \mathbf{A}(\mathbf{B})}{\partial \mathbf{B}} : \mathrm{d}\mathbf{B} \tag{A.6}$$

The kind of multiplication depends on the tensor order of the argument $\mathbf{B}$. In the last equation $\mathbf{B}$ needed to be of order two. If $\mathbf{B}$ is a vector valued quantity, only single contraction is to be applied. If $\mathbf{A}$ and $\mathbf{B}$ are both of order two, the partial derivative $\partial \mathbf{A}(\mathbf{B})/\partial \mathbf{B}$ denotes a fourth order tensor.

Moreover, integral theorems are essential in the field of continuum mechanics. Thus, the most important ones are introduced in the following. The divergence theorem or sometimes referred to as Gauss' theorem allows to rewrite an area integral as a volume integral with the relation

$$\int_{\partial \mathcal{B}_0} \mathbf{U} \cdot \mathbf{N} \, \mathrm{dA} = \int_{\mathcal{B}_0} \mathrm{Div}(\mathbf{U}) \, \mathrm{d}V \tag{A.7}$$

where $\partial \mathcal{B}_0$ denotes the boundary surface corresponding the volume $\mathcal{B}_0$ and $\mathbf{N}$ characterises the outward unit normal vector on each infinitesimal surface element $\mathrm{d}\mathbf{A}$. One special case in which the vector field can be expressed as $\mathbf{U} = g\,\mathbf{W}$, with a scalar function f and $\mathbf{W}$ being vector valued makes use of the product rule and reads

$$\int_{\partial \mathcal{B}_0} (g\mathbf{W}) \cdot \mathbf{N} \, \mathrm{dA} = \int_{\mathcal{B}_0} [\mathbf{W} \cdot \mathrm{Grad}(g) + g \cdot \mathrm{Div}(\mathbf{W})] \, \mathrm{d}V \tag{A.8}$$

Stokes' theorem enables the transformation of curve integrals into area integrals in the form of

$$\oint_{\mathcal{C}_0} \mathbf{U} \cdot \mathrm{d}\mathbf{x} = \int_{\partial \mathcal{B}_0} \mathrm{Curl}(\mathbf{U}) \cdot \mathbf{N} \, \mathrm{d}\mathbf{A} \tag{A.9}$$

with $\mathcal{C}_0$ symbolising the boundary curve and $\mathbf{N}$ denoting the outward unit normal vector of the surface $\partial \mathcal{B}_0$.

A.2 Lagrange shape functions

For the case of linear approximation in three dimensions, there are in total 8 nodes in each element and by that, 8 trilinear shape functions in total which read:

$$N_1(\xi,\eta,\zeta) = \frac{1}{8}(1-\xi)(1-\eta)(1-\zeta) \tag{A.10}$$

$$N_2(\xi,\eta,\zeta) = \frac{1}{8}(1+\xi)(1-\eta)(1-\zeta) \tag{A.11}$$

$$N_3(\xi,\eta,\zeta) = \frac{1}{8}(1+\xi)(1+\eta)(1-\zeta) \tag{A.12}$$

$$N_4(\xi,\eta,\zeta) = \frac{1}{8}(1-\xi)(1+\eta)(1-\zeta) \tag{A.13}$$

$$N_5(\xi,\eta,\zeta) = \frac{1}{8}(1-\xi)(1-\eta)(1+\zeta) \tag{A.14}$$

$$N_6(\xi,\eta,\zeta) = \frac{1}{8}(1+\xi)(1-\eta)(1+\zeta) \tag{A.15}$$

$$N_7(\xi,\eta,\zeta) = \frac{1}{8}(1+\xi)(1+\eta)(1+\zeta) \tag{A.16}$$

$$N_8(\xi,\eta,\zeta) = \frac{1}{8}(1-\xi)(1+\eta)(1+\zeta) \tag{A.17}$$

Others can be found in standard FE books, such as [Hug00, Wri01].

A.3 Derivatives of the strain energy function

Differentiation of (3.41) with respect to the strain measures and the electric displacement field can be derived as

$$\frac{\partial \Psi}{\partial \mathbf{C}} = a\,\mathbf{I} + g_0\,\mathrm{tr}(\mathbf{C}\,\mathbf{M})^{g_\mathbf{C}}\,\mathbf{M} + \frac{1}{2\varepsilon_0\varepsilon_r C^{1/2}}\,\mathbf{D}_0 \otimes \mathbf{D}_0 \tag{A.18}$$

$$\frac{\partial \Psi}{\partial \mathbf{G}} = b\,\mathbf{I} + g_0\,\mathrm{tr}(\mathbf{G}\,\mathbf{M})^{g_\mathbf{G}}\,\mathbf{M} \tag{A.19}$$

$$\frac{\partial \Psi}{\partial C} = c\,(1 - C^{-1/2}) - \frac{d}{2}\,C^{-1} - g_0\,C^{-g_C-1} - \frac{1}{4\varepsilon_0\varepsilon_r C^{3/2}}\,\mathbf{D}_0 \cdot \mathbf{C}\,\mathbf{D}_0 \tag{A.20}$$

$$\frac{\partial \Psi}{\partial \mathbf{D}_0} = \frac{1}{\varepsilon_0\varepsilon_r C^{1/2}}\,\mathbf{C}\,\mathbf{D}_0 \tag{A.21}$$

The non-zero second derivatives are as follows and can be refound in the stiffness matrices of the FE formulation:

$$\frac{\partial^2 \Psi}{\partial \mathbf{C}^2} = g_0 g_\mathbf{C}\,\mathrm{tr}(\mathbf{C}\,\mathbf{M})^{g_\mathbf{C}-1}\,\mathbf{M} \otimes \mathbf{M} \tag{A.22}$$

$$\frac{\partial^2 \Psi}{\partial \mathbf{G}^2} = g_0 g_\mathbf{G}\,\mathrm{tr}(\mathbf{G}\mathbf{M})^{g_\mathbf{G}-1}\,\mathbf{M} \otimes \mathbf{M} \tag{A.23}$$

$$\frac{\partial^2 \Psi}{\partial C^2} = \frac{c}{2}\,C^{-3/2} + \frac{d}{2}\,C^{-2} + g_0(g_C+1)\,C^{-g_C-2} - \frac{3}{8\varepsilon_0\varepsilon_r C^{5/2}}\,\mathbf{D}_0 \cdot \mathbf{C}\,\mathbf{D}_0 \tag{A.24}$$

$$\frac{\partial^2 \Psi}{\partial \mathbf{D}_0^2} = -\frac{1}{\varepsilon_0\varepsilon_r C^{1/2}}\,\mathbf{C} \tag{A.25}$$

$$\frac{\partial^2 \Psi}{\partial C\,\partial \mathbf{D}_0} = \frac{\partial^2 \Psi}{\partial \mathbf{D}_0\,\partial C} = -\frac{1}{2\varepsilon_0\varepsilon_r C^{3/2}}\,\mathbf{C}\,\mathbf{D}_0 \tag{A.26}$$

$$\frac{\partial^2 \Psi}{\partial \mathbf{C}\,\partial \mathbf{D}_0} = \frac{\partial^2 \Psi}{\partial \mathbf{D}_0\,\partial \mathbf{C}} = \frac{1}{\varepsilon_0\varepsilon_r C^{1/2}}\,(\mathbf{I} \otimes \mathbf{D}_0 + \mathbf{D}_0 \otimes \mathbf{I}) \tag{A.27}$$

The last two terms vividly demonstrate Schwarz's theorem.

A.4 Voigt Notation

The Voigt notation transfers tensor valued variables that are symmetric to column vectors and thereby facilitates the computational implementation. In general the transformation of stress-type quantities $\mathbf{A} \in \mathbb{R}^{3\times3}$ is

$$[\mathbf{A}] = \begin{bmatrix} A_{11} & A_{12} & A_{13} \\ A_{21} & A_{22} & A_{23} \\ A_{31} & A_{32} & A_{33} \end{bmatrix} \quad \rightarrow \quad [\mathbf{A}^{\mathrm{V}}] = \begin{bmatrix} A_{11} \\ A_{22} \\ A_{33} \\ A_{12} \\ A_{23} \\ A_{13} \end{bmatrix} \tag{A.28}$$

with $\mathbf{A}^{\mathrm{V}} \in \mathbb{R}^6$. The Voigt notation $\hat{\mathbf{A}}^{\mathrm{V}} \in \mathbb{R}^6$ of strain-type quantities $\hat{\mathbf{A}} \in \mathbb{R}^{3\times3}$ reads

$$[\hat{\mathbf{A}}] = \begin{bmatrix} \hat{A}_{11} & \hat{A}_{12} & \hat{A}_{13} \\ \hat{A}_{21} & \hat{A}_{22} & \hat{A}_{23} \\ \hat{A}_{31} & \hat{A}_{32} & \hat{A}_{33} \end{bmatrix} \quad \rightarrow \quad [\hat{\mathbf{A}}^{\mathrm{V}}] = \begin{bmatrix} \hat{A}_{11} \\ \hat{A}_{22} \\ \hat{A}_{33} \\ 2\hat{A}_{12} \\ 2\hat{A}_{23} \\ 2\hat{A}_{13} \end{bmatrix} \tag{A.29}$$

On that account, work-conjugate pairings in the form of double contraction can be written in Voigt notation as

$$\mathbf{A} : \hat{\mathbf{A}} = (\hat{\mathbf{A}}^{\mathrm{V}})^{\mathrm{T}}\, \mathbf{A}^{\mathrm{V}} \tag{A.30}$$

This explanation is based on the description in [BJH17].

A.5 Parts of the tangent matrix $\mathbf{K}_{\varphi\varphi}$

The material parts of the tangential matrix related to $\boldsymbol{\varphi}$ in equation (4.87) read

$$\mathbf{K}_{IJ}^{mat,e,1} = \int_{\Omega_e} \mathbf{B}_I^{\mathrm{T}}\, 2 \left(\frac{\partial^2 W_{sym}}{\partial \mathbf{C}\, \partial C} \otimes \mathbf{G} \right)^{\mathrm{V}} \mathbf{B}_J \, \mathrm{d}V \tag{A.31}$$

$$\mathbf{K}_{IJ}^{mat,e,2} = \int_{\Omega_e} \mathbf{B}_I^{\mathrm{T}}\, \mathcal{D}(\boldsymbol{\Sigma}_{\mathbf{G}})\, \mathbf{B}_J \, \mathrm{d}V \tag{A.32}$$

$$\mathbf{K}_{IJ}^{mat,e,3} = \int_{\Omega_e} \mathbf{B}_I^{\mathrm{T}}\, \Sigma_C\, \mathcal{D}(\mathbf{C})\, \mathbf{B}_J \, \mathrm{d}V \tag{A.33}$$

$$\mathbf{K}_{IJ}^{mat,e,4} = \int_{\Omega_e} \mathbf{B}_I^{\mathrm{T}}\, 2\, \frac{\partial^2 W_{sym}}{\partial C^2}\, (\mathbf{G} \otimes \mathbf{G})^{\mathrm{V}}\, \mathbf{B}_J \, \mathrm{d}V \tag{A.34}$$

$$\mathbf{K}_{IJ}^{mat,e,5} = \int_{\Omega_e} \mathbf{B}_I^{\mathrm{T}}\, 2 \left(\mathbf{G} \otimes \frac{\partial^2 W_{sym}}{\partial \mathbf{C}\, \partial C} \right)^{\mathrm{V}} \mathbf{B}_J \, \mathrm{d}V \tag{A.35}$$

$$\mathbf{K}_{IJ}^{mat,e,6} = \int_{\Omega_e} \mathbf{B}_I^{\mathrm{T}}\, 2 \left(\frac{\partial^2 \Psi_{sym}}{\partial \mathbf{C}^2} \right)^{\mathrm{V}} \mathbf{B}_J \, \mathrm{d}V \tag{A.36}$$

$$\mathbf{K}_{IJ}^{mat,e,7} = \int_{\Omega_e} \mathbf{B}_I^{\mathrm{T}}\, 2\, \left[(\mathbf{M} \diamondsuit \mathbf{C}) \otimes (\mathbf{M} \diamondsuit \mathbf{C}) \right]^{\mathrm{V}}\, \mathbf{B}_J \, \mathrm{d}V \tag{A.37}$$

where the operator matrix $\mathcal{D}$ has been introduced. It conveys $\mathbf{A} : \mathbf{B} \diamondsuit \mathbf{C}$ into Voigt notation $(\mathbf{B}^{\mathrm{V}})^{\mathrm{T}}\, \mathcal{D}(\mathbf{A})\, \mathbf{C}^{\mathrm{V}}$ and its matrix notation is built up of the components of $\mathbf{A}$ as

$$\mathcal{D}(\mathbf{A}) = \begin{bmatrix} 0 & 2\,A_{33} & 2\,A_{22} & 0 & -2\,A_{23} & 0 \\ 2\,A_{33} & 0 & 2\,A_{11} & 0 & 0 & -2\,A_{13} \\ 2\,A_{22} & 2\,A_{11} & 0 & -2\,A_{12} & 0 & 0 \\ 0 & 0 & -2\,A_{12} & -A_{33} & A_{13} & A_{23} \\ -2\,A_{23} & 0 & 0 & A_{13} & -A_{11} & A_{12} \\ 0 & -2A_{13} & 0 & A_{23} & A_{12} & -A_{22} \end{bmatrix} = \mathcal{D}(\mathbf{A})^{\mathrm{T}}$$

B List of Abbreviations

Abbreviation	Meaning
EAP	electroactive polymer
FEM	finite element method
FE	finite element
BVP	boundary value problem
BC	boundary condition
1st PK	first Piola-Kirchhoff stress tensor
2nd PK	second Piola-Kirchhoff stress tensor
DOF	degree of freedom